
Ji Yeong Lee

Korea Institute of Science and Technology (KIST)
Seoul, Korea
jiyeongl@andrew.cmu.edu

Howie Choset

Carnegie Mellon University
Pittsburgh, PA 15213, USA

Sensor-based Planning for a Rod-shaped Robot in Three Dimensions: Piecewise Retracts of $\mathbb{R}^3 \times S^2$

Abstract

We present a new roadmap for a rod-shaped robot operating in a three-dimensional workspace, whose configuration space is diffeomorphic to $\mathbb{R}^3 \times S^2$. This roadmap is called the rod hierarchical generalized Voronoi graph (rod-HGVG) and can be used to find a path between any two points in an unknown configuration space using only the sensor data. More importantly, the rod-HGVG serves as a basis for an algorithm to explore an unknown configuration space without explicitly constructing it. Once the rod-HGVG is constructed, the planner can use it to plan a path between any two configurations. One of the challenges in defining the roadmap revolves around a homotopy theory result, which asserts that there cannot be a one-dimensional deformation retract of a non-contractible space with dimension greater than two. Instead, we define an exact cellular decomposition on the free configuration space and a deformation retract in each cell (each cell is contractible). Next, we “connect” the deformation retracts of each of the cells using a roadmap of the workspace. We call this roadmap a piecewise retract because it comprises many deformation retracts. Exploiting the fact that the rod-HGVG is defined in terms of workspace distance measurements, we prescribe an incremental procedure to construct the rod-HGVG that uses the distance information that can be obtained from conventional range sensors.

KEY WORDS—motion planning, sensor-based planning, rod-shaped robot, Voronoi diagram, roadmap, exploration, retract, piece-wise retract

1. Introduction

In this paper, we present a new structure for sensor-based planning for a rod-shaped robot (i.e., a line segment with a

notion of direction) operating in a three-dimensional space. Unlike robots that can be modeled as a point, rod-shaped robots have rotational degrees of freedom in addition to translational degrees of freedom. This problem is challenging because the robot is operating in a three-dimensional workspace, thus making the configuration space a five-dimensional non-Euclidean space. More specifically, the configuration space is diffeomorphic to $\mathbb{R}^3 \times S^2$.

Our approach is based on a structure called a “roadmap”. We interpret from the work of Canny (1988) that a roadmap is a one-dimensional subset of the configuration space that satisfies the following properties: (i) accessibility, (ii) connectivity, and (iii) departability. This means that if there exists a path between two configurations, we can determine a path by first finding a path to the roadmap from the start configuration, then following the roadmap, and then finding a path from the roadmap to the destination. If a planner can construct a roadmap in a given environment with sensor data, then the planner has in essence explored the configuration space because the planner can then use the roadmap to find a path between any two configurations.

In this paper, we introduce a new roadmap for a rod in an unknown three-dimensional workspace, called the *rod hierarchical generalized Voronoi graph* (rod-HGVG) (Figure 1). As its name suggests, the rod-HGVG is one of the roadmaps derived from the generalized Voronoi diagram (GVD; Aurenhammer 1991). As shown in Figure 2, the work in this paper represents a step toward the ultimate goal of motion planning for highly articulated robots (such as snake robots). Previous work in this line of research extended the GVD method in two directions: the point-HGVG (Choset and Burdick 2000a, 2000b), which is a roadmap for a point in a three-dimensional workspace, and the rod-HGVG (Choset and Lee 2001), which is a roadmap for a rod in the plane. Naively one could view the work in this paper as a combination of these two roadmaps to define a new roadmap for the rod operating in a three-dimensional space.

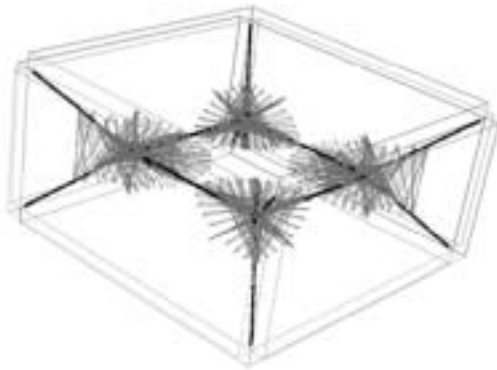


Fig. 1. Samples from the swept volume of the rod-HGVG in a rectangular environment. The walls are removed to show the inside of the box. The dark “lines” represent the configurations that are three-way equidistant, and the gray regions represent the configurations that are four-way equidistant. For this example, the set of three-way and four-way equidistant configurations form a roadmap of this environment.

We seek to define the rod-HGVG in terms of a deformation retract (Bredon 1995). One of the challenges in defining the rod-HGVG is due to a homotopy theory result (Bredon 1995), which asserts that there cannot be a one-dimensional deformation retract of a non-contractible space with dimension greater than two. Instead of defining the roadmap as a deformation retract of the entire configuration space, we first define an exact cellular decomposition on the free configuration space so that each cell is contractible. Then, we connect the deformation retracts of each of the cells using a roadmap of the workspace. We call this roadmap a piecewise retract because it comprises many deformation retracts.

It is important to note, however, when the planner uses the rod-HGVG to either navigate or explore, it does not explicitly define or construct a decomposition. The decomposition itself is just used to prove the roadmap properties of the rod-HGVG.

The outline of this paper is as follows. In Section 2, we discuss the prior work on which this work is based. In Section 3, we define the rod-HGVG in \mathbb{R}^3 , and, in Section 4, we show that the rod-HGVG indeed satisfies the roadmap conditions (Canny 1988) under the assumption that the point-GVG is connected in a given environment. In Section 5, we briefly show how to construct the rod-HGVG incrementally. Then, in Section 6, we extend the rod-HGVG so that the rod-HGVG is connected if the point-HGVG (Choset and Burdick 2000a) is connected. The point-HGVG is an extension of the point-GVG, which is connected in a wider range of environments than the point-GVG. Finally, in Section 7, we summarize this work and consider some future directions in which the current work can be extended.

2. Relation to Prior Work

2.1. Robot Motion Planning

Motion planning algorithms can be classified into classical methods and sensor-based methods according to what information is assumed or used by each of the algorithms. The classical methods assume complete knowledge about the environment, or even the configuration space, while the sensor-based methods perform the planning using only the sensor-provided information. The classical methods can generate more efficient paths compared to the sensor-based methods since they can use information that the sensor-based methods cannot.

Motion planning methods—classical and sensor-based—include the potential field methods, cell decompositions (Latombe 1991) and roadmaps. The potential field methods (Khatib 1986; Khosla and Volpe 1988; Koren and Borenstein 1991; Borenstein and Koren 1998; Chuang and Ahuja 1998) use an artificial vector field defined on the free space, which pulls the robot toward the goal position and pushes the robot away from the obstacle boundaries. Then, a path between two configurations can be found by solving a differential equation defined by the vector field. In general, potential field methods are not complete since there can be local minima

	Workspace : \mathbb{R}^2	Workspace : \mathbb{R}^3
Point	<p>GVD</p> <p>Ó'Dúnlaing & Yap [35] Choset & Burdick [12]</p>	<p>HGVG: DP31</p> <p>Choset & Burdick [12] Keerthi [17]</p>
Rod	<p>Rod-HGVG: DR21 DR22</p> <p>Ó'Dúnlaing & Yap [34] Brooks [8] Choset & Burdick [13]</p>	<p>Rod-HGVG: Definitions & Incremental Construction</p>
Convex ⋮	<p>Near Term Future Work</p> <p>Pisula et al. [37]</p>	
Highly Articulated Robot	<p>Long Term Goal</p>	

Fig. 2. The overview of roadmaps derived from the GVD. The references indicate work related to each of the environments and the robots, and are not necessarily derived from the GVD.

where the robot may become trapped. The cell decomposition methods (Brooks 1983; Brooks and Lozano-Pérez 1983; Kuan, Zamiska, and Brooks 1985; Noborio, Haniwa, and Arimoto 1989) first decompose the free space into cells such that, in each of the cells, the motion planning is simple, and then represent the adjacency relation between cells using a connectivity graph, which is used to find a path between the cells. A roadmap is a one-dimensional subset of the space, which is accessible to and from any point in the space and has a connected component in each connected component of the free space. The visibility graph (Nilsson 1969) is an example of a roadmap.

Recently, there have been active developments in the random or probabilistic methods (Overmars 1992). Specifically, the probabilistic community (Kavraki and Latombe 1994; Kavraki et al. 1996; Latombe et al. 1996; Kavraki 1997; LaValle 1998; Wilmarth, Amato, and Stiller 1999; Kuffner and LaValle 2000) has successfully demonstrated the capabilities of probabilistic roadmaps for highly articulated robots. These probabilistic roadmaps are, in general, relatively easy to implement and can solve planning problems in high dimensions quickly compared to other methods by trading off the notion of completeness with probabilistic completeness. This means that the probabilistic roadmaps may not be connected even when the workspace is connected. Many probabilistic methods do not construct the configuration space prior to planning, but still require prior knowledge about the workspace, which implies that they cannot be implemented in a sensor-based way. However, recently, Yu and Gupta (1999) developed an algorithm that can construct a roadmap in a sensor-based way using probabilistic technique.

2.2. Related Roadmap Approaches

As we have noted before, the rod-HGVG is based on the roadmap approach. Canny (1988) developed a roadmap algorithm that can be used in any configuration space that can be represented as a semi-algebraic set. More specifically, in a configuration space represented using n polynomials of maximum degree d for some positive d , Canny showed that any motion planning problem can be solved in $n^k (\log n) d^{O(k^4)}$ time using his roadmap algorithm, where k is the number of degrees of freedom (Sharir 1997).

Ó'Dúnlaing and Yap (1985) first applied the GVD (see Figure 3) to define a roadmap for a disk-shaped robot operating in plane. The GVD is the set of points equidistant to two obstacles, and can be defined using line-of-sight sensor data. In the plane, the GVD is a collection of one-dimensional sets. Ó'Dúnlaing and Yap (1985) showed that the GVD is a deformation retract of the free space and thus can be used as a roadmap for the point robot in the plane. Later, motivated by the sensor-based construction method of Rimón (1997), Choset and Burdick (2000a) developed a method to incrementally construct the GVD in \mathbb{R}^2 .

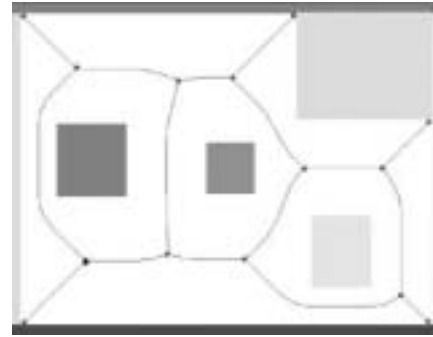


Fig. 3. The point-GVD or the GVD is the set of points equidistant to two obstacles in the plane.

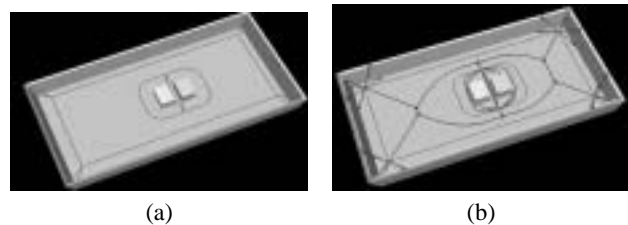


Fig. 4. (a) The GVG is shown with dark lines. In this example, there are two disconnected components of the GVG. (b) The HGVG, the GVG with the higher-order GVG edges forms a connected set.

In a three-dimensional workspace, the GVD is two-dimensional and therefore cannot be used as a roadmap. The generalized Voronoi graph (GVG) is the three-dimensional analog of the GVD and is defined as the set of points equidistant to three obstacles. The GVG is one-dimensional in \mathbb{R}^3 , but, unfortunately, the GVG does not form a connected set. Choset and Burdick (2000a) defined additional structures to connect the disconnected components of GVG, resulting in the hierarchical generalized Voronoi graph (point-HGVG; see Figure 4). They also provided an incremental construction algorithm for the point-HGVG that uses only range-sensor information (Choset and Burdick 2000b). We review the point-HGVG in more detail in Section 6 when we extend the rod-HGVG using the point-HGVG. Also Pisula et al. (2000) considered motion planning for an arbitrary body operating in the three-dimensional space, using the point-GVG. However, the robot was restricted to performing translational motions only.

Finally, it is worth noting that one of the approaches to improve the connectivity of the probabilistic roadmap is to use the GVD. For example, Foskey et al. (2000) developed a hybrid algorithm, which constructs a path for an arbitrarily shaped-robot in three-dimensional space using a randomized planner along with the GVD.

2.3. Rod-related Work

The work of Ó'Dúnlaing, Sharir, and Yap (1986) motivates our approach in that they use workspace distance measurements to define their roadmap. They extended their disk result (Ó'Dúnlaing and Yap 1985) to rod-shaped robots in a planar environment, using a concept called a “racetrack”, which is the set of the points whose distance to the robot is smaller than some fixed value. The backbone of their roadmap is the set of configurations where three or more obstacles are tangent to the racetrack, i.e., triple or more equidistant in the workspace. Cox and Yap (1991) developed an “on-line” strategy for rod path-planning, which can be used for a start-goal problem, but does not construct a roadmap at all; this method is just a navigation algorithm.

Choset and Burdick (1996) and Choset and Lee (2001) developed a roadmap called the rod-HGVG in the plane (Figure 5). This structure provides the groundwork for the roadmap for the rod-shaped robot in three dimensions, which is the prime contribution of this paper. The planar rod-HGVG consists of two types of components: the first are the rod-GVG edges, which are the sets of configurations equidistant to three-obstacles; the second are the one-tangent edges,¹ which are tangent to the point-GVG edges. In essence, they define a cellular decomposition of the free configuration space, such that a deformation retract (the rod-GVG edge) can be defined in each cell, and connect up these deformation retracts using another structure (the one-tangent edge) derived from the connectivity of the workspace (the point-GVG). Both the rod-GVG edge and the one-tangent edges are defined in terms of the workspace distance function, and therefore the rod-HGVG can be constructed using only sensor-provided information.

3. Rod Hierarchical Generalized Voronoi Graph in \mathbb{R}^3

Using distance measurements in workspace, we define the rod-HGVG in a three-dimensional space, i.e., a five-dimensional configuration space. Throughout this section, we assume that the point-GVG is connected in the workspace, and we define the rod-HGVG which is connected under this assumption.

3.1. Piecewise Retracts

The rod operating in \mathbb{R}^3 has five degrees of freedom (i.e., three translational and two rotational degrees of freedom) and hence lives in a five-dimensional configuration space diffeomorphic to $\mathbb{R}^3 \times S^2$. As we mentioned above, the definition of the rod-HGVG is inspired by a structure called a “deformation retract” (Munkres 2000). For a given space, a deformation retract of a space is a lower-dimensional subset of the space to which the space itself can be continuously contracted. By definition, a

1. In Choset and Burdick (1996) and Choset and Lee (2001), the one-tangent edges are called R -edges.

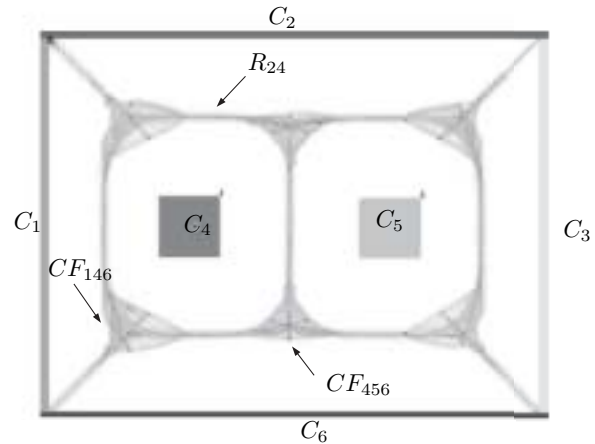


Fig. 5. Swept volumes (sampled placements) of the rod in a planar workspace. CF_{146} and CF_{456} are the rod-GVG edges defined by the three obstacles with the corresponding indices. R_{24} is the one-tangent edge defined by C_2 and C_4 .

deformation retract is connected for a connected space. Hence, if one can find a one-dimensional deformation retract of the free configuration space, then one can use the deformation retract as a roadmap. For example, as we mentioned above, the GVD can be shown to be a deformation retract of the free space in the plane (Ó'Dúnlaing and Yap 1985), and thus it can be used as a roadmap for a point operating in the plane.

However, it is not generally possible to define a one-dimensional deformation retract in a space with dimension greater than two (Bredon 1995). Since the dimensions of the configuration space for the rod in three dimensions is five, we cannot define a roadmap that is a one-dimensional deformation retract of the entire free configuration space of the rod. Instead, our approach is to decompose the free configuration space into contractable regions, and then to define deformation retracts in each cell. These deformation retracts are defined so that the robot can access and trace the deformation retract of each cell without computing the decomposition explicitly.

In general, these deformation retracts are not connected to each other and thus do not form a roadmap. To connect the disconnected deformation retracts, we define new structures using the point-GVG, which, in some sense, represents the topology of the workspace. Note that, in general, the point-GVG is not connected in a three-dimensional space populated by obstacles. In this section, we assume that the point-GVG is connected in a given environment, and show that the rod-HGVG (the deformation retracts and the additional structures defined using the point-GVG) forms a connected set, and thus can be used as a roadmap. We call this collection of deformation retracts a piecewise retract. It is interesting to note that since the deformation retracts of the cells are connected using

the point-GVG, the planner is inferring the topology of the configuration space from the topology of the workspace.

3.2. Overview of the Rod-HGVG Structures

Since the rod's configuration space has five dimensions, it is natural to first define a five-way equidistant structure, which we call the "rod-GVG edges". As in the planar rod-HGVG, the rod-GVG edges are not connected to each other, and do not form a roadmap themselves. So, just like the planar rod-GVG, it seems natural to use the point-GVG edges in \mathbb{R}^3 to connect the rod-GVG edges. Here, we define the one-tangent edges, which are tangent to the point-GVG in \mathbb{R}^3 just as the one-tangent edges for the planar rod-HGVG are tangent to the point-GVG in the plane. That is, the one-tangent edges are the set of configurations equidistant to three obstacles and tangent to the point-GVG.

Alas, there is still a problem: to transition from a five-way equidistant structure to a three-way equidistant structure, it would stand to reason that we would need an additional four-way equidistant structure. Moreover, there is a bigger problem: there are environments where the rod-GVG edges do not exist at all. This is due to the fact that the rod operates in a three-dimensional workspace, in which, in general, no five-way equidistant configurations necessarily exist. Thus, if the rod were not "long" or the environment were not cluttered, there would not be five-way equidistant configurations. Instead, the four-way equidistant configurations always exist for the rod with an arbitrary length in an arbitrary environment. This motivates us to use the four-way equidistant configurations as a building block for the rod-HGVG.

Actually, the sets of the four-way equidistant configurations, which are two-dimensional, are the first deformation retracts that we define for the rod-HGVG in a three-dimensional space. Like the rod-GVG edges of the planar rod-HGVG, the sets of four-way equidistant configurations induce a cellular decomposition of the free configuration space and can be shown to be deformation retracts of the cells.

For the moment, let us not worry about these deformation retracts being two-dimensional. We connect these two-dimensional four-way equidistant deformation retracts with the one-tangent edges and the rod-GVG edges. Here, we use the topology of the workspace to ensure connectivity of a structure, albeit not a roadmap yet, in configuration space.

One can view the rod four-way equidistant faces as the structure that links up the one-tangent edges. Recall that the point-GVG edges are connected together at the point-GVG meetpoints, which are the four-way equidistant points. That is, the point-GVG meetpoints are the places where the point robot can move from one point-GVG edge to another point-GVG edge. Likewise, the rod four-way equidistant faces can be seen as the set in which the rod travels from one one-tangent edge to another one-tangent edge.

In the final step, we recursively define a new decomposition on the two-dimensional deformation retracts and, within each

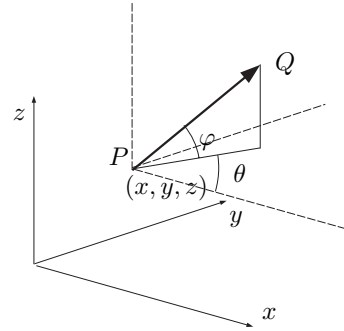


Fig. 6. Rod-shaped robot in three-dimensional workspace. The arrowhead is used to distinguish between two endpoints of the rod. It has five degrees of freedom in three dimensions, and can be parametrized by x, y, z, θ , and ϕ , where (x, y, z) are the coordinates of one of the endpoints of the rod and θ and ϕ define the orientation of the rod represented as Euler angles.

cell, we define one-dimensional deformation retracts called "two-tangent edges". These deformation retracts are called two-tangent edges because they are tangent to a point two-way equidistant face,² which is two-dimensional, whereas the one-tangent edges are tangent to a point three-way equidistant face (i.e., a point-GVG edge), which is one-dimensional. In summary, the rod-HGVG is defined as the union of these three components: rod-GVG edges, one-tangent edges, and two-tangent edges. In this section, we define each of the rod-HGVG components in detail, and we show that the rod-HGVG forms a roadmap in Section 4.

3.3. Rod and Distance Definitions

The definition of the rod and the distance function in three dimensions is analogous to that in plane.

DEFINITION 1. [Rod] A rod R is a line segment of length L with a notion of direction, which has two endpoints P and $Q \in \mathbb{R}^3$ and whose configuration can be parametrized by $q = (x, y, z, \theta, \phi)^T$ (Figure 6).

The coordinates (x, y, z) specify the position of the endpoint P , and θ and ϕ define the orientation of the rod at a given configuration q . The symbol $R(q)$ denotes the set of points in \mathbb{R}^3 occupied by the rod when the rod is at a configuration q . Also, we denote $P(q)$ and $Q(q)$ as the positions of the endpoints of the rod and $PQ(q)$ as the vector $P(q) - Q(q)$ when the rod is at the configuration q .

We assume that the rod operates in a bounded workspace populated by the convex obstacles, denoted by C_i . The concave obstacles can be modeled as a union of convex obstacles

2. The set of points in the workspace that are equidistant to two obstacles.

as discussed in Choset and Burdick (2000a). The free configuration space FCS is the set of rod configurations that do not intersect any obstacles. In other words

$$FCS = \{q \in \mathbb{R}^3 \times S^2 : R(q) \cap C_i = \emptyset \forall i\}. \quad (1)$$

As mentioned above, the rod-HGVG is defined using workspace distance measurements.

DEFINITION 2. [Rod–Distance Function] The rod distance function $D_i : FCS \rightarrow \mathbb{R}$ is defined as

$$D_i(q) = \min_{r \in R(q), c \in C_i} \|r - c\|. \quad (2)$$

We denote $r_i(q)$ as the closest point on the rod to the obstacle C_i , and $c_i(q)$ as the closest point on the obstacle C_i to the rod. The rod distance gradient is denoted by ∇D_i , and it is represented as a function of the vector $r_i - c_i$ and the point r_i (see Appendix A for the derivation of the rod distance gradient). This implies that the rod distance cannot be defined if r_i cannot be uniquely defined. For example, if the rod is parallel to one of the flat faces of an obstacle, then the closest point between the rod and the obstacle cannot be uniquely defined. In this paper, we assume that the walls of the obstacles are “slightly curved” so that the rod distance gradient can be always defined.³

Note that we measure the distance in the workspace, and this distance can be easily provided by the range sensors placed along the length of the rod. This distance function can be measured using a series of range sensors along the length of the rod (see Figure 7). Each range sensor registers a distance measurement, and then one can find the location of the range sensor where the distance measurement is smaller than those of the adjacent range sensors. Each of these local minima of the sensor readings corresponds to the distance to an obstacle visible from the current rod configuration. That is, the number of local minima of the sensor reading represents the number of obstacles visible from the current configuration, and the point r_i is the point where one of the local minima of the sensor reading is attained. Likewise, the closest point on the obstacle c_i , which is needed to trace the one-tangent edges and the two-tangent edges, can also be computed from the position of r_i and the value of the sensor reading. This model requires an infinite number of sensors along the length of the rod, but it can be reasonably approximated by a finite number of range sensors. We delay investigating the issues of sensor quantization until future work.

3.4. Rod Four-way Equidistant Faces (Deformation Retract)

Now we define the rod four-way equidistant faces, which are, as the name suggests, the sets of four-way equidistant

3. In simulation, where we have obstacles with flat faces, we can have infinitely many closest points on the rod to the obstacle, lying on a closed interval on the rod. In this case, we take the middle point as the closest point r_i . For c_i , we also use the same approach.

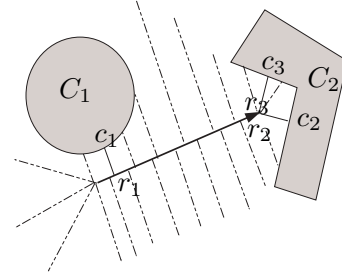


Fig. 7. The obstacles are identified using the local minima of the sensor reading along the length of the rod. In this example, the rod “sees” three obstacles since there are three local minima of the sensor reading at r_1 , r_2 , and r_3 . Note that even if C_2 is a single concave obstacle, the robot sees it as two obstacles. The locations of c_1 , c_2 , and c_3 can also be computed from r_i and the values of the sensor reading.

configurations. The rod four-way equidistant faces are two-dimensional and thus are not components of the rod-HGVG. However, they are important in our discussion, since they are the first deformation retracts used in defining the rod-HGVG. Even if the rod in three dimensions has five degrees of freedom, we do not consider the five-way equidistant configurations as deformation retracts, which, as we see later, may not even exist at all. In contrast, the rod four-way equidistant faces are guaranteed to exist because of the boundedness assumption.

We define the rod four-way equidistant faces by intersecting the rod two-way equidistant faces, which are defined as

$$CF_{ij} = \{q \in FS : 0 \leq D_i(q) = D_j(q) \leq D_h(q) \forall h \neq i, j \text{ and } \nabla D_i(q) \neq \nabla D_j(q)\}. \quad (3)$$

The last condition $\nabla D_i(q) \neq \nabla D_j(q)$ guarantees that CF_{ij} is a four-dimensional structure under the pre-image theorem (Abraham, Marsden, and Raitu 1988).

Then, the rod three-way equidistant face is defined as

$$CF_{ijk} = CF_{ij} \cap CF_{jk} \cap CF_{ik}. \quad (4)$$

Note that for a rod operating in a three-dimensional workspace, the rod three-way equidistant face is a three-dimensional structure. Continuing this process, we define the rod four-way equidistant face as follows.

DEFINITION 3. [Rod Four-way Equidistant Face]

$$CF_{ijkl} = CF_{ijk} \cap CF_{ikl} \cap CF_{jkl} \cap CF_{ijl}. \quad (5)$$

Later, we show that the rod four-way equidistant faces are deformation retracts of the subsets of the free configuration space by defining a deformation retraction which is derived

from fixed-orientation gradient ascent. Since the configuration space for the rod with a fixed orientation is essentially just the three-dimensional Euclidean space, one can easily see that an arbitrary rod configuration can access a rod four-way equidistant configuration.

If the rod were “short”, CF_{ijkl} would be homeomorphic to S^2 , the two-dimensional sphere. This can be easily shown as follows. Let q be an arbitrary rod configuration in the free space with orientation $(\theta, \phi) \in S^2$. Consider a configuration space of the rod with fixed orientation of (θ, ϕ) . This configuration space is a three-dimensional Euclidean space bounded by convex obstacles, and thus we can find a four-way equidistant point in this configuration space, i.e., the four-way equidistant configuration of the rod with the orientation $(\theta, \phi) \in S^2$, which implies that the rod four-way equidistant face CF_{ijkl} is homeomorphic to S^2 . Also, if the rod were short, there would be a one-to-one correspondence between the point-GVG meetpoints F_{ijkl} in a given workspace and CF_{ijkl} in the configuration space derived from the given workspace. This can easily be seen; if the rod has zero length, then for any given point-GVG meetpoint F_{ijkl} , there is a four-way equidistant face which is just $CF_{ijkl} = \{q \in FCS : (x(q), y(q), z(q)) = F_{ijkl}, (\theta(q), \phi(q)) \in S^2\}$.

If the rod were short, the rod four-way equidistant faces would be disconnected from each other. From the observation above about the relation between the rod four-way equidistant faces and the point-GVG meetpoints, it is natural to connect the rod four-way equidistant faces using point-GVG edges. Just as for the planar rod-HGVG, these structures are called one-tangent edges and are defined as the set of three-way equidistant rod configurations, which are tangent to the point-GVG. We discuss the one-tangent edges in more detail later.

If the rod were long, two of the rod four-way equidistant faces CF_{ijkl} and CF_{iklm} would intersect each other, and the intersection is a set of five-way equidistant configurations, or a rod-GVG edge CF_{ijklm} , which we discuss later in more detail. Note that, by definition, CF_{ijklm} also contains the elements of CF_{ijlm} , CF_{iklm} , and CF_{jklm} , as well as the elements of CF_{ijkl} and CF_{ijkm} . These CF_{ijlm} , CF_{iklm} , and CF_{jklm} are the four-way equidistant faces, which do not have the corresponding point-GVG meetpoints and would not exist if the rod were short. In other words, even if there was no point in the workspace equidistant to the obstacles C_i , C_j , C_l , and C_m , there could be at least one rod configuration that is equidistant to these four obstacles if the rod were “long”. Later, we need to consider this fact in proving the connectivity of the rod-HGVG.

The rod-GVG edge is one of the boundary components of the rod four-way equidistant face. The other is the boundary edges, which are the set of rod configurations that have zero distance to the four obstacles.

DEFINITION 4. [Boundary edge]

$$B_{ijkl} = \{q \in \text{cl}(CF_{ijkl}) : D_i(q) = D_j(q) = D_k(q) = D_l(q) = 0\}, \quad (6)$$

where $\text{cl}(\cdot)$ denotes the closure of a set. Again, the boundary edges may not exist always. Recall that the boundary edge (i.e., $\{p \in \mathbb{R}^3 : d_i(p) = d_j(p) = 0\}$) is considered as a component of the point-HGVG. However, we do not consider the boundary edges as components of the rod-HGVG. The motivation for this will be clear in Section 4.2, but essentially we use the boundary edges as links that connect disconnected components of the rod-HGVG, rather than a formal component of the rod-HGVG, and we trace them only when necessary.

3.5. Rod-GVG Edges

The rod-GVG edges are the first component of the rod-HGVG which we formally define. As discussed above, the rod-GVG edge is defined as the set of five-way equidistant rod configurations, which also can be represented as the intersection of the rod four-way equidistant faces.

DEFINITION 5. [Rod-GVG edges]

$$CF_{ijklm} = CF_{ijkl} \cap CF_{iklm} \cap CF_{jklm} \cap CF_{ijkm} \cap CF_{ijlm}. \quad (7)$$

In the rod configuration space $\mathbb{R}^3 \times S^2$, the collection of rod-GVG edges is not necessarily connected. The rod-GVG edges are homeomorphic to S^1 if there are no boundary edges and none of the rod-GVG edges intersects each other. Otherwise, the rod-GVG edges would be homeomorphic to the union of open intervals of \mathbb{R} . If the rod were long enough so that two rod-GVG edges intersect each other, a *rod-meet configuration* CF_{ijklmn} is formed, which is a zero-dimensional set of rod configurations that are six-way equidistant.

In many environments, the rod-GVG edges may not even exist at all. Figure 8 shows a rectangular environment, where $L > W$, $L > H$, and CF_{12345} and CF_{12346} are the rod-GVG edges. If L were substantially larger than the length of the rod, there could not be any six-way equidistant configurations, so these two components cannot be connected. Now, if W were also substantially larger than the length of the rod, then no five-way equidistant configuration could exist either (Figure 9). Figure 1 also shows an example of a workspace where no rod-GVG edges exist. Figure 10 shows all of the rod GVG-edges in a simple environment similar to that in Figure 8, where there are four disconnected components of rod-GVG edges. (Only two distinct components are identifiable in the figure, since for each of the identifiable components, there is another rod-GVG edge component that occupies same workspace volume but “points” in the opposite direction.)

Unlike the rod-GVG edges for the planar rod-HGVG, the rod-GVG edges in three dimensions are not considered to be the deformation retracts of the subsets of the free configuration space. Rather, the rod-GVG edges are the boundary components of the deformation retracts, which are the rod four-way equidistant faces. Since a rod-GVG edge is the intersection

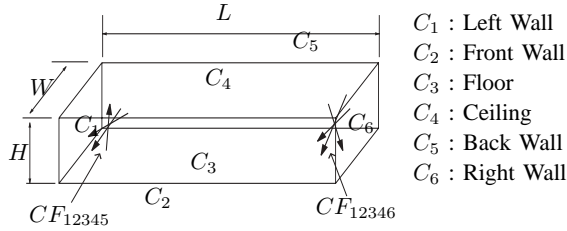


Fig. 8. Here, there are two sets of rod configurations that are five-way equidistant. The configurations in CF_{12345} are equidistant to $C_1, C_2, C_3, C_4,$ and C_5 , and the configurations in CF_{12346} are equidistant to $C_1, C_2, C_3, C_4,$ and C_6 . Note that they are not connected to each other.

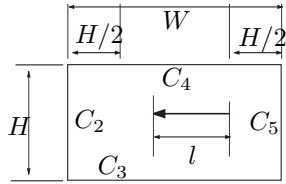


Fig. 9. Side view of Figure 8 with $L > W, L > H$, but here the length of the rod is smaller than $W - H$, and thus the rod cannot be four-way equidistant to $C_2, C_3, C_4,$ and C_5 . Therefore, five-way equidistant configurations do not exist either.

of two rod four-way equidistant faces, in some sense, the rod-GVG edges connect the disconnected rod four-way equidistant faces. Actually, we see later that the rod-GVG edges and the one-tangent edges perform a dual role in connecting the rod four-way equidistant faces.

3.6. One-tangent Edges

The second component of the rod-HGVG that we define is the one-tangent edge. As we noted, the one-tangent edges connect the disconnected rod four-way equidistant faces. The one-tangent edges are essentially identical to the one-tangent edges of the planar rod-HGVG edges, where the rod is “tangent” to the point-GVG edge (Figure 11).

Just as there is a close relationship between the point-GVG meetpoints and the rod four-way equidistant faces, there is a close relationship between the point-GVG edges and the one-tangent edges. If the rod were “short”, for any given point-GVG edge F_{ijk} , we could find two connected components (disconnected from each other) of the one-tangent edge R_{ijk} due to the symmetry of the rod. That is, there are two compo-

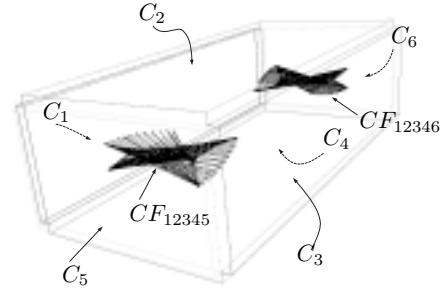


Fig. 10. The rod-GVG in the above rectangular enclosure contains two connected components as depicted by the two swept volumes in the workspace. The environment is shown with transparent walls so we can see inside. The rod-GVG edge CF_{12345} consists of the configurations that are equidistant to the obstacles C_1 (left wall), C_2 (ceiling), C_3 (right wall), C_4 (floor), and C_5 (front wall). The other rod-GVG edge CF_{12346} is defined by the obstacles $C_1, C_2, C_3, C_4,$ and C_6 (back wall).

nents of R_{ijk} which occupy the same workspace volume, but “point” in opposite directions. Moreover, if the point-GVG edge F_{ijk} terminates on two point-GVG meetpoints F_{ijkl} and F_{ijkm} , then the one-tangent edge R_{ijk} , if it exists, would terminate on the rod four-way equidistant faces CF_{ijkl} and CF_{ijkm} . If one of the endpoints of the F_{ijk} is the obstacle boundary, then the one-tangent edge R_{ijk} also has an endpoint on the obstacle boundary.

If the rod were long, there might not be an R_{ijk} for a given point-GVG edge F_{ijk} . However, as we show later, in that case there must be a rod-GVG edge connecting the two rod four-way equidistant faces, which would have been connected by the one-tangent edge. So, either a one-tangent edge or a rod-GVG edge connect two neighboring rod four-way equidistant faces, but not both.

Now we define the one-tangent edge more precisely. When $C_i, C_j,$ and C_k define a point-GVG edge F_{ijk} , we presume that:

- $D_i(q) = D_j(q) = D_k(q)$;
- the rod is “tangent” to F_{ijk} at a point r .

From these two conditions, the following can be easily shown:

- r is the closest point on the rod to the obstacles $C_i, C_j,$ and C_k , i.e., for $n = i, j, k, d_n(r) \leq d_n(r_o) \forall r_o \in R(q)$.

That is, the point r where the rod $R(q)$ intersects the point-GVG edge is also the closest point on the rod to all of the three closest obstacles. The proof is similar to the case of the planar rod-HGVG (Choset and Burdick 1996), where the point of intersection between the rod and the point-GVG edge is the closest point on the rod to the two closest obstacles.

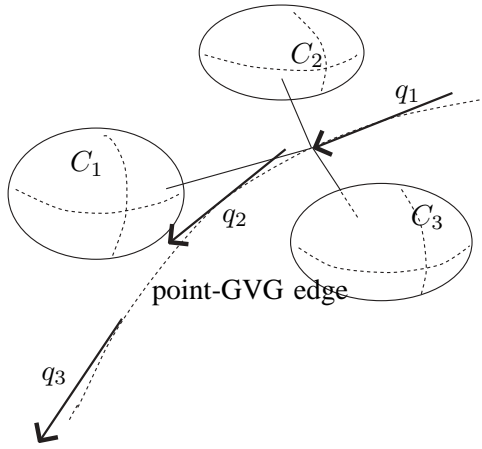


Fig. 11. The one-tangent edge where q_1 , q_2 , and q_3 are configurations on a one-tangent edge associated with obstacles C_1 , C_2 , and C_3 . The rod intersects the point-GVG at either of its endpoints (q_1 , q_3) except where the distance attains a local minima, where the rod can “slide” along q_2 .

This asserts that $r_i = r_j = r_k$, where r_i , r_j , and r_k are the closest points on the rod to each obstacle, and the rod must intersect the point-GVG edge at point r_i . Moreover, it can be shown that the point of contact r_i on the rod is uniquely defined and must be one of the endpoints of the rod except at the local minima or local maxima of distance to the closest workspace obstacle along the one-tangent edge. At the local minima and local maxima, the point of contact can be at any point on the rod. More precisely, at the local maxima or local minima of the distance to the closest obstacle, the point of contact is the point p on the point-GVG edge where the distance to the closest obstacle attains a local maximum or a local minimum along the point-GVG edge. Then, the rod slides through this point p as it traces the one-tangent edge, thus changing the point of the contact from one endpoint to another.⁴ Since the tangent direction of the point-GVG is normal to the plane spanned by the vectors $c_i - c_j$ and $c_i - c_k$, we have the following definition for the one-tangent edge.

DEFINITION 6. [One-tangent edge] A one-tangent edge R_{ijk} is defined as

$$R_{ijk} = \{q \in CF_{ijk} : \langle PQ(q), c_i(q) - c_j(q) \rangle = 0 \text{ and } \langle PQ(q), c_i(q) - c_k(q) \rangle = 0\}. \quad (8)$$

4. In general, there are no local maxima of the distance along the point-GVG edge, but if there is an isolated point-GVG edge, homeomorphic to S^1 (such a point-GVG edge is called a “cycle” in Choset and Burdick 2000a), there are local maxima of the distance along the point-GVG edge. However, as noted later, since we assume that the point-GVG is connected in this paper, there can be no point-GVG cycles, and hence no local maxima.

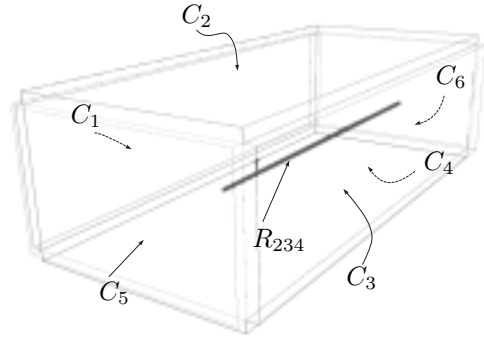


Fig. 12. The swept volume of a single one-tangent edge. The one-tangent edge R_{234} is defined by the obstacles C_2 (ceiling), C_3 (right wall), and C_4 (floor), and connects two junction regions.

The conditions $\langle PQ(q), c_i(q) - c_j(q) \rangle = 0$ and $\langle PQ(q), c_i(q) - c_k(q) \rangle = 0$ prescribe that the rod be tangent to the point two-way equidistant faces F_{ij} and F_{ik} , respectively. From these two conditions, it follows that the rod is tangent to the point-GVG edge F_{ijk} , which is intersection of F_{ij} and F_{ik} . Note that it also follows that the rod is tangent to F_{jk} as well.

The rod finishes the tracing of a one-tangent edge when (i) it reaches a four-way equidistant configuration, (ii) it reaches an obstacle boundary, or (iii) it detects a cycle. A cycle in the point-GVG is a disconnected point-GVG edge diffeomorphic to S^1 , and if there is a cycle in the point-GVG, there can be a one-tangent edge cycle in the rod-HGVG also. However, since we consider only environments where the point-GVG is connected, there is no one-tangent edge cycle in the context of the current work. Therefore, we can ignore condition (iii). Figure 12 shows the swept volume of a one-tangent edge along the side of a rectangular enclosure and Figure 13 shows the swept volume of all of the one-tangent edges in the same environment. Note that the one-tangent edges do not intersect each other, i.e., the union of the one-tangent edges does not form a connected set.

3.7. Two-tangent Edges

Thus far, we have defined the rod-GVG edge, a five-way equidistant structure, and the one-tangent edge, a three-way equidistant structure. As mentioned above, neither the union of the rod-GVG edges nor the union of the one-tangent edges forms a connected set. Moreover, the union of the rod-GVG edges and the one-tangent edges does not form a connected set either. Instead, they connect the disconnected rod four-way equidistant faces, which are two-dimensional. Later we formally show that the union of the rod four-way equidistant

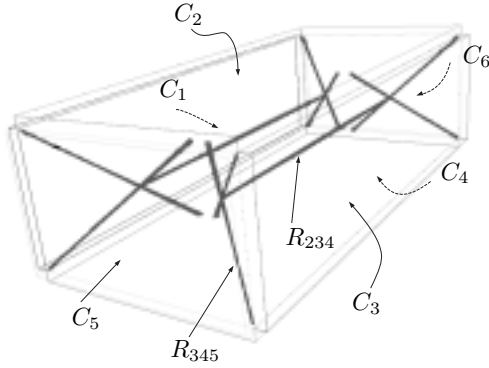


Fig. 13. The swept volume of all of the one-tangent edges in the same environment as Figures 10 and 12. Each one-tangent edge terminates either on the obstacle boundary or on a four-way equidistant configuration. For example, both of the end configurations of the one-tangent edge R_{234} are four-way equidistant configurations, but only one of the end configurations of the one-tangent edge R_{345} is a four-way equidistant configuration and the other is a boundary configuration. Note that the one-tangent edges are disconnected from each other.

faces, the one-tangent edges, and the rod-GVG edges forms a connected set. However, since the rod four-way equidistant faces are two-dimensional, we still need to define a one-dimensional structure on the rod four-way equidistant face to obtain a one-dimensional roadmap.

As already mentioned, in addition to being one-dimensional, this new four-way equidistant structure must have the following properties. First, this one-dimensional four-way equidistant structure must form a connected set on a single rod four-way equidistant face. Otherwise we would need additional structures to connect them. Secondly, this new four-way equidistant structure must intersect the one-tangent edges terminating on the four-way equidistant face or the rod-GVG edges on the four-way equidistant face. This second condition gives us the motivation to define the one-dimensional four-way equidistant structure.

Consider the rod four-way equidistant face CF_{ijkl} with one-tangent edges R_{ijk} and R_{ijl} each terminating at configurations in CF_{ijkl} (boundedness of the workspace ensures this can happen). For R_{ijk} , the rod lies in the tangent space associated with the point-GVG edges F_{ijk} . Recall that the F_{ijk} is the intersection of the three point two-way equidistant faces. A point two-way equidistant face F_{ij} is the set of points that are equidistant to two obstacles, C_i and C_j , and has two dimensions. Therefore, if the rod is in the tangent space of F_{ijk} , this implies that the rod lies in the tangent spaces of F_{ij} , F_{jk} , and F_{ik} at the same time. Likewise, for the configurations in R_{ijl} , the rod lies in tangent spaces F_{ij} , F_{il} , and F_{jl} . Note that, in both cases, the rod

lies in the tangent space associated with F_{ij} . Therefore, as our additional constraint, to travel from R_{ijk} to R_{ijl} along CF_{ijkl} , we presume that the rod must remain in the tangent space of F_{ij} . The edge formed on CF_{ijkl} with the additional constraint of staying in the tangent space of F_{ij} is called a “two-tangent edge” because the rod lies in a two-dimensional tangent space (as opposed to a one-dimensional tangent space with the one-tangent edge). We denote a two-tangent edge as $R_{ij/kl}$, where the rod is equidistant to C_i , C_j , C_k , and C_l and is in the tangent space of F_{ij} . Note that for a rod four-way equidistant face CF_{ijkl} , there are four one-tangent edges that terminate on the set, and there can be six different two-tangent edges on this face. If the rod were “short” and CF_{ijkl} homeomorphic to S^2 , then a two-tangent edge $R_{ij/kl}$ would be homeomorphic to S^1 . If the rod were long and CF_{ijkl} had “holes”, $R_{ij/kl}$ would be a union of sets, each homeomorphic to a closed interval of \mathbb{R} whose boundary point is a configuration on either a boundary edge or a rod-GVG edge.

Figure 14 shows an example where a point two-way equidistant face is homeomorphic to a bounded subset of the plane. Here, the rod is “tangent” to $F_{ceiling, floor}$ when the rod is moving from q_2 to q_3 , and “tangent” to $F_{front, floor}$ when moving from q_1 to q_2 . Figure 15 shows a single two-tangent edge in an environment and Figures 16 and 17 show all of the two-tangent edges in the same environment.

DEFINITION 7. [Two-tangent Edge] The two-tangent edge is formally defined as follows:

$$R_{ij/kl} = \{q \in CF_{ijkl} \mid \langle PQ(q), (c_i(q) - c_j(q)) \rangle = 0\}. \quad (9)$$

It can be shown that a two-tangent edge $R_{ij/kl}$ is a one-dimensional manifold (Appendix F). Since sensors can easily provide distance information and the planner can determine the closest points on the rod to the closest obstacles from the sensor information, the two-tangent edge can be readily constructed using only sensor-provided information.

Now we have defined all of the necessary components of the rod-HGVG, which comprises rod-GVG edges, one-tangent edges, and two-tangent edges.

DEFINITION 8. [Rod Hierarchical Generalized Voronoi Graph] The collection of rod-GVG edges, one-tangent edges, and two-tangent edges forms the rod-HGVG, i.e.

$$\text{Rod-HGVG} = \left(\bigcup_{i,j,k,l,m} CF_{ijklm} \right) \cup \left(\bigcup_{i,j,k} R_{ijk} \right) \cup \left(\bigcup_{i,j,k,l} R_{ij/kl} \right)$$

Table 1 shows the rough correspondence between the components of the point-HGVG, the rod-HGVG in the plane, and the rod-HGVG in three dimensions. Note that we do not include the boundary edges as components of the rod-HGVG because, as discussed in the next section, we do not try to trace all of the boundary edges, but instead use them as links that connect the disconnected components of the rod-HGVG.

Figure 18 shows the edges of the rod-HGVG near a corner of the environment, where the two-tangent edges connect

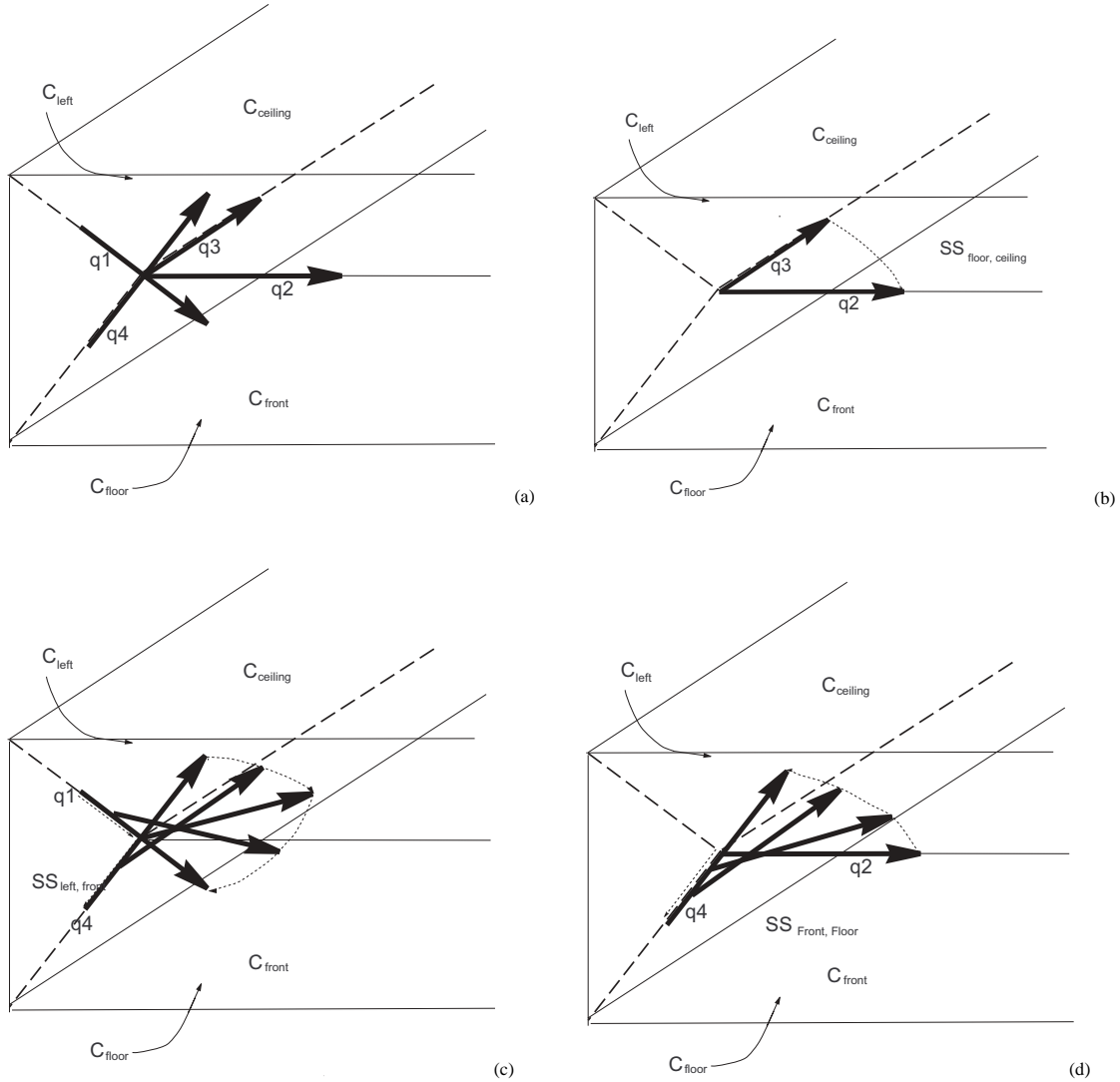


Fig. 14. (a) $q_1, q_2, q_3,$ and q_4 represent four-way equidistant configurations. They are also terminal configurations of different one-tangent edges. (b), (c), and (d) show two-tangent edges that connect some pairs of one-tangent edges. The figures do not show the complete two-tangent edges in each case. In these cases, each of the two-tangent edges are diffeomorphic to S^1 , i.e., on each of the two-tangent edges, the rod can fully rotate until it reaches the original configuration.

a GVG-edge and one-tangent edges, and also connect one-tangent edges to other one-tangent edges. Figure 19 shows all of the edges in the same environment. Figure 20 shows an example of a “large” environment with a “short” rod (see also Extension 1). Here all of the CF_{ijkl} are homeomorphic to S^2 , and thus there are no rod-GVG edges. Figure 20 shows four one-tangent-edges connected by six two-tangent-edges, forming a connected set. In other words, it is possible for the rod to travel from the endpoint of a one-tangent-edge to the endpoint of any other one-tangent-edge using only one two-tangent-edge. Figure 21 shows all of the edges in the

same environment. Note that, in this example, the rod-HGVG forms a connected set without the rod-GVG edges. Figure 22 shows another example of the rod-HGVG in a rectangular environment with a block in the middle of the room (see also Extension 2).

4. Roadmap Properties of the Rod-HGVG in \mathbb{R}^3

In this section, we discuss the roadmap properties of the rod-HGVG. We recall that the roadmap is a union of one-

Table 1. Comparison Between the Components of the Point-GVG, Rod-HGVG in Plane, and Rod-HGVG in \mathbb{R}^3

Point-GVG	Rod-HGVG in the Plane	Rod-HGVG in Three Dimensions
Point-GVG Meetpoints	Rod-GVG edges	CF_{ijkl} (which lead to two-tangent edges) Two-tan-edges
Point-GVG edges	One-tan-edges	One-tan-edges Rod-GVG edges
	Junction regions retract to CF_{ijk} (rod-GVG edge) (three-way equidistant)	Junction regions retract to CF_{ijkl} (four-way equidistant)

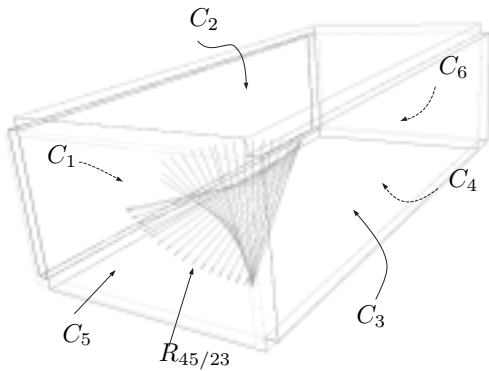


Fig. 15. A single two-tangent edge $R_{45/23}$, equidistant to the C_2 (ceiling), C_3 (right wall), C_4 (floor), and C_5 (front wall), and “tangent” to the point two-way equidistant face defined by the obstacles C_4 (floor) and C_5 (front wall) in the same environment as Figure 10. This two-tangent edge is not diffeomorphic to S^1 since there is a rod-GVG edge, at which the two-tangent edge terminates.

dimensional subsets of the free configuration space, which has the following properties: (i) accessibility, (ii) departability, and (iii) connectivity. In Section 4.1, we discuss accessibility in detail, and connectivity is discussed in Sections 4.2–4.6. Departability can be shown using accessibility applied in the reverse direction.

4.1. Accessibility

The rod accesses the rod-HGVG via four gradient ascent operations: the first three use a fixed orientation gradient $\tilde{\nabla}D_i(x)$ that directs the rod to increase distance to the closest obstacles while maintaining its orientation; the last gradient ascent operation uses the full gradient $\nabla D_i(x)$. The sequence of the first

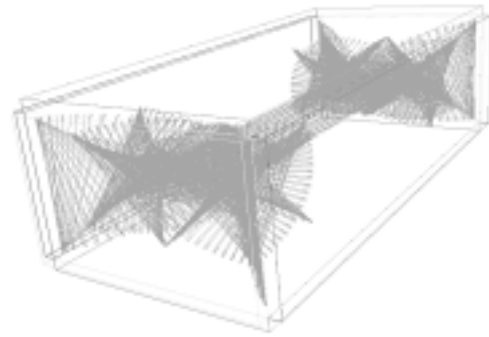


Fig. 16. All of the two-tangent edges in the same environment as Figure 10.

three gradient ascent operations implicitly defines a function $H : FS \times [0, 1] \rightarrow \cup CF_{ijkl}$. More specifically, H is defined as follows. First, while maintaining a fixed orientation, the rod moves away from its closest obstacle, i.e., the rod traces the solution of

$$\dot{c}(t) = \tilde{\nabla}D_i(c(t)), \tag{10}$$

until it reaches a configuration equidistant to two obstacles C_i and C_j . Then, while maintaining double equidistance and a fixed orientation, the rod moves away from the two closest obstacles until it reaches a configuration equidistant to three obstacles C_i , C_j , and C_k . That is, the rod traces the solution of

$$\dot{c}(t) = \pi_{T_{c(t)}CF_{ij}} \tilde{\nabla}D_i(c(t)), \tag{11}$$

where $T_{c(t)}CF_{ij}$ denotes the tangent space of CF_{ij} at the configuration $c(t)$ and $\pi_{T_{c(t)}CF_{ij}}$ is the projection operator onto the tangent space $T_{c(t)}CF_{ij}$. Finally, while maintaining triple equidistance and a fixed orientation, the rod moves away from

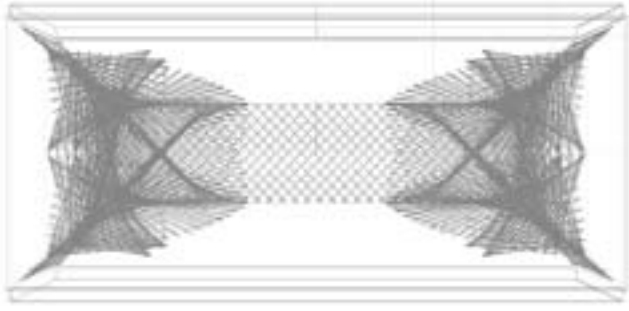


Fig. 17. Top view of all of the two-tangent edges in the same environment as Figure 16.

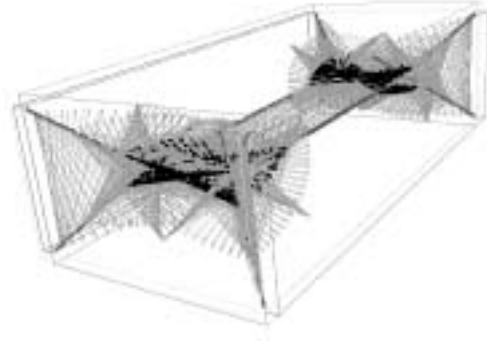


Fig. 19. Swept volume of all of the edges of the rod-HGVG.

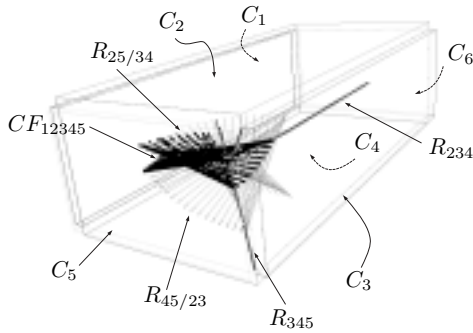


Fig. 18. Swept volume of the edges of the rod-HGVG near a corner of an environment. The rod-GVG edge (CF_{12345}) and the one-tangent edges (R_{234} and R_{345}) are connected by two-tangent edges ($R_{25/34}$ and $R_{45/23}$).

the three closest obstacles until it reaches four-way equidistance. That is,

$$\dot{c}(t) = \pi_{T_{c(t)}CF_{ijkl}} \tilde{\nabla} D_i(c(t)). \quad (12)$$

where $T_{c(t)}CF_{ijkl}$ is the tangent space of CF_{ijkl} at the configuration $c(t)$. From the boundedness assumption, after this operation, the rod is guaranteed to terminate at a four-way equidistant configuration. This sequence of gradient ascent operations defines the mapping H . We assume that the parameter t is scaled appropriately so that $H(q, 0) = q$ and $H(q, 1) \in \cup CF_{ijkl}$. Note that $\theta(q) = \theta(H(q, t))$ and $\phi(q) = \phi(H(q, t))$ for all $t \in [0, 1]$.

The map H directs the rod to a four-way equidistant configuration, which may not be on the rod-HGVG. To bring the rod to the rod-HGVG, we define an additional mapping $HJ : \cup CF_{ijkl} \times [0, 1] \rightarrow R_{ij/kl} \cup CF_{ijklm}$ that moves the rod away from the four closest obstacles, using the full gradient

$$\dot{c}(t) = \pi_{T_{c(t)}CF_{ijkl}} \nabla D_i(c(t)). \quad (13)$$

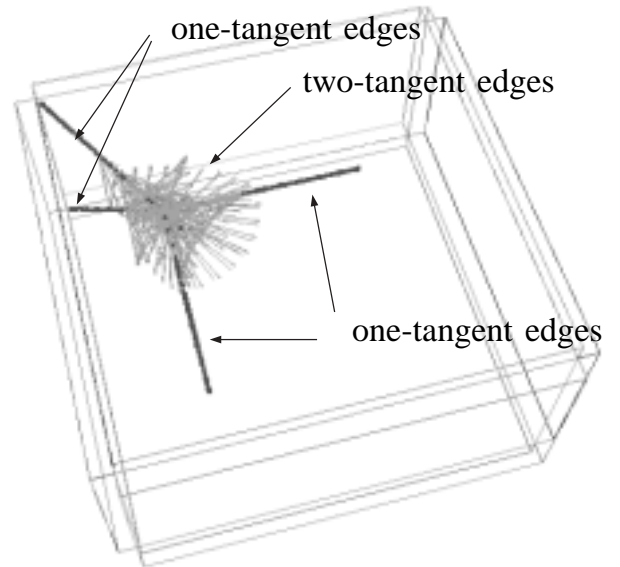


Fig. 20. A set of one-tangent edges connected by two-tangent edges in an environment. There are no rod-GVG edges in this environment and the union of the one-tangent edges and the two-tangent edges forms a connected set.

This step terminates at either of the following: (i) five-way equidistance (i.e., a rod-GVG edge) or (ii) a two-tangent edge.

In Appendix B, we show that once the rod achieves four-way equidistance, continued gradient ascent (full gradient ascent) brings the rod either to a two-tangent edge $R_{ij/kl}$ or to a rod-GVG edge CF_{ijklm} .

This shows that an arbitrary rod configuration can access a components of the rod-HGVG using a series of the distance gradient ascents. Once the rod has accessed the rod-HGVG, it can then begin incrementally constructing the rod-HGVG using the previously defined numerical techniques. If

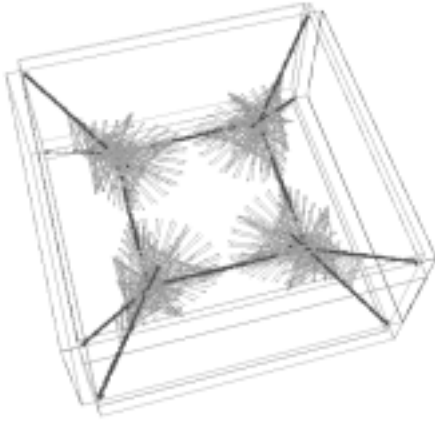


Fig. 21. All of the edges in an environment. There are no rod-GVG edges in this example. Note that this is the same environment as Figure 1.

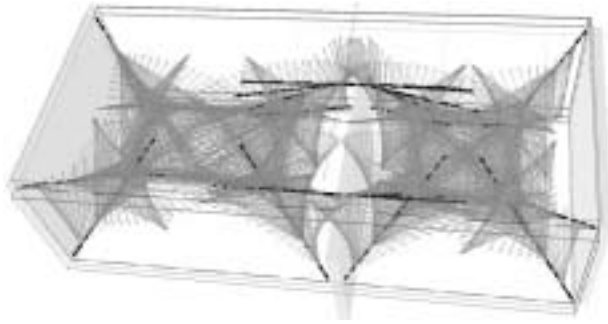


Fig. 22. The rod-HGVG in a rectangular box environment with a block in the middle. The one-tangent edges “connect” two regions of the environment.

the rod-HGVG is connected, numerically constructing it ensures complete exploration of a connected component of the rod’s configuration space.

4.2. Connectivity

Now we prove the connectivity of the rod-HGVG, i.e., that the rod-HGVG forms a connected set in a connected free configuration space if the point-GVG is connected. The main idea is to decompose the free configuration space into retractible sets, called “junction regions”. We define deformation retracts in each junction region and then use the point-GVG to connect up the deformation retracts of the junction regions. The connectivity is shown in two separate steps (Figure 23).

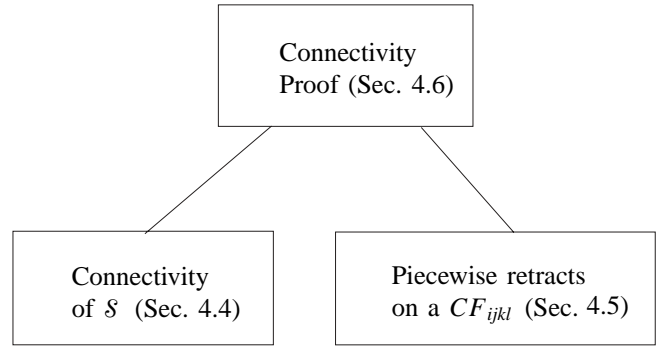


Fig. 23. Overview of the connectivity proof.

Step 1. We show that the structure

$$\mathcal{S} = \cup_{i,j,k,l} CF_{ijkl} \cup \cup_{i,j,k} R_{ijk} \cup \cup_{i,j,k,l,m} CF_{ijklm} \quad (14)$$

forms a connected set. Note that CF_{ijkl} is two-dimensional, and thus \mathcal{S} is not a roadmap, but it is a superset of the rod-HGVG. To prove this part of the connectivity, we use the assumption that the point-GVG is connected in a given environment.

Step 2. We show the connectivity of the union of the two-tangent edges and the rod-GVG edges on a single CF_{ijkl} . In this step, we also show that the union of the two-tangent edges and the rod-GVG edges contains the endpoints of the one-tangent edges terminating at CF_{ijkl} . We note that the union of the two-tangent edges and the rod-GVG edges on a single CF_{ijkl} by themselves may not be connected in some environments. However, in these environments, it is shown that the disconnected components of the rod-HGVG can be connected using the boundary edges.

From these two steps, we conclude that the rod-HGVG is connected. Before we proceed to the proof of the connectivity, we define and discuss the junction regions and their deformation retracts in Section 4.3.

4.3. Junction Regions

In this section we formally define the junction regions. There are two types of junction regions for the rod-HGVG in three dimensions. The first are the junction regions under mapping H , and the union of these junction regions is the free configuration space, i.e., this induces a cellular decomposition of the free configuration space. The deformation retracts of the junction regions under the mapping H are the rod four-way equidistant faces which are two-dimensional, and are connected together by the rod-GVG edges and the one-tangent edges, which we prove in Section 4.4. The second type of junction region is the subjunction region under the mapping

HJ , which induces the cellular decomposition of a rod four-way equidistant face CF_{ijkl} . The deformation retracts of the junction regions under the mapping HJ are the two-tangent edges or rod-GVG edges.

The junction region under the mapping H is defined formally as follows.

DEFINITION 9. [Junction region] A junction region J_{ijkl} is the pre-image of CF_{ijkl} under $H : FS \times [0, 1] \rightarrow CF_{ijkl}$, i.e.

$$J_{ijkl} = \{q \in FS : H(q, 1) \in CF_{ijkl}\}. \quad (15)$$

Using a similar approach as in Choset and Burdick (1996), H can be shown to be continuous in each of the connected components of a junction region J_{ijkl} (see Appendix C), and moreover $H(CF_{ijkl}, 1) = CF_{ijkl}$. Therefore, the rod four-way equidistant face CF_{ijkl} is a deformation retract of the junction region J_{ijkl} .

Next, we define the subjunction region, which decomposes CF_{ijkl} . Recall that there are two one-dimensional structures defined on the rod four-way equidistant face CF_{ijkl} : the rod-GVG edges and two-tangent edges. Therefore, there are two types of subjunction region under the mapping HJ , defined as follows.

DEFINITION 10. [Subjunction region]

$$J_{ij/kl} = \{q \in CF_{ijkl} : HJ(q, 1) \in R_{ij/kl}\} \quad (16)$$

and

$$J_{ijklm} = \{q \in CF_{ijkl} : HJ(q, 1) \in CF_{ijklm}\}. \quad (17)$$

In each cell $J_{ij/kl}$, HJ is continuous on $J_{ij/kl}$ (for proof, see Appendix D) and $HJ(R_{ij/kl}, 1) = R_{ij/kl}$. Therefore, $R_{ij/kl}$ is a one-dimensional deformation retract of $J_{ij/kl}$. Similarly, HJ is continuous on J_{ijklm} and $HJ(CF_{ijklm}, 1) = CF_{ijklm}$. Therefore, CF_{ijklm} is a one-dimensional deformation retract of J_{ijklm} .

If the rod were “short” enough so that no four-way equidistant faces intersect each other and there are no rod-GVG edges on CF_{ijkl} , then the union of $J_{ij/kl}$ is equal to CF_{ijkl} . However, if there is a rod-GVG edge CF_{ijklm} on CF_{ijkl} , we have the subjunction J_{ijklm} related to the rod-GVG CF_{ijklm} , which is the set of configurations that access the rod-GVG edges under the mapping HJ .

Finally, we note that even if there are boundary edges B_{ijkl} , we do not need to define subjunction regions for them. No configuration would access the boundary edge under the mapping HJ since HJ is a gradient ascent operation.

4.4. Connectivity of \mathcal{S}

In this section, we show the connectivity of the set

$$\mathcal{S} = (\cup_{i,j,k,l} CF_{ijkl}) \cup (\cup_{i,j,k} R_{ijk}) \cup (\cup_{i,j,k,l,m} CF_{ijklm}).$$

To show this we use the connectivity of the point-GVG and the relationship between the structures of the point-GVG and the structures of the rod-HGVG. Then, just like the point-GVG edges connect the point-GVG meetpoints, we can show the one-tangent edges and the rod-GVG edges connect the rod four-way equidistant faces. For this we first need to show the following.

LEMMA 1. Let J_{ijkl} and J_{ijkm} be two adjacent junction regions. If the one-tangent edge $R_{ijk} = \emptyset$, then CF_{ijkl} and CF_{ijlm} intersect each other, and it follows that the rod-GVG edge $CF_{ijklm} \neq \emptyset$.

The two junction regions are said to be adjacent if they share a common boundary. The proof of this lemma can be found in Appendix D. From this, we can also show the following.

LEMMA 2. Given two adjacent rod four-way equidistant faces CF_{ijkl} and CF_{ijkm} , for which $CF_{ijkl} \cup CF_{ijklm} \cup R_{ijk} \cup CF_{ijklm}$ is a connected set, we have

$$R_{ijk} \neq \emptyset \Leftrightarrow CF_{ijklm} = \emptyset$$

which is equivalent to

$$CF_{ijklm} \neq \emptyset \Leftrightarrow R_{ijk} = \emptyset.$$

The proof of this lemma can be found in Appendix E. Essentially, this lemma states that the one-tangent edge and the rod-GVG edges perform a dual role in connecting the two rod four-way equidistant faces. That is, the two adjacent two rod four-way equidistant faces are connected either by a one-tangent edge or a rod-GVG edge, but not by both.

Before we prove the connectivity of the set \mathcal{S} , we introduce some notations. In the following, f_i and t_i denote the index sets of the obstacles with four and three elements, respectively. For example, J_{f_2} denotes a junction region where f_2 is an index set of size four, e.g., $f_2 = \{3, 4, 6, 7\}$, and R_{t_1} denotes a one-tangent edge with, for example, $t_1 = \{1, 2, 5\}$.

The proof relies on the fact that there is a close relationship between the components of the point-GVG and the components of the rod-HGVG. Recall that, in this section, we assume that the point-GVG is connected in the workspace. If the point-GVG is connected, given two point-GVG meetpoints, we can find a series of point-GVG meetpoints and the point-GVG edges which form a connected set themselves. Then using the close relationship between the point-GVG structures and the rod-HGVG structures discussed in the previous section, we find a connected series of the rod four-way equidistant faces, the one-tangent edges and the rod-GVG edges.

If the rod were “short”, then there would be no rod-GVG edges and we could find a one-to-one correspondence between the CF_{f_i} and point-GVG meetpoints, and between the one-tangent edges and the point-GVG edges. In other words, for a given point-GVG edge F_{ijk} , there exists a one-tangent edge

R_{ijk} defined by the same three obstacles, and for a given point-GVG meetpoint F_{ijkl} , there exists a rod four-way equidistant face CF_{ijkl} defined by the same four obstacles. If the rod were “long”, then there would exist rod-GVG edges that connect adjacent CF_{fi} , i.e., we do not need to use the one-tangent edges to connect them (Figure 24). In actuality, as shown in Lemma 2, the one-tangent edges do not exist at all between two rod four-way equidistant configurations if they intersect each other.

Finally, recall that if the rod-GVG edge exists, then there are rod-GVG structures which do not have corresponding point-GVG structures, as depicted above. In other words, CF_{fi} can exist without F_{fi} existing. However, note that such a CF_{fi} can only exist when there is a rod-GVG edge. For example, if CF_{1234} and CF_{1235} intersect, the intersection formed is CF_{12345} , and by definition CF_{12345} is also a subset of CF_{1245} , CF_{1345} , etc., which does not have corresponding point-GVG meetpoints. However, clearly, these CF_{fi} intersect a rod-GVG edge and, in turn, intersect some CF_{fi} that have corresponding point-GVG meetpoints. This implies that we need to consider only those CF_{ijkl} that have corresponding point-GVG meetpoints in the following proof.

Now we prove the connectivity of S .

LEMMA 3. In a given environment, if the point-GVG is connected and the configuration space is connected, the set

$$S = (\cup_{i,j,k,l} CF_{ijkl}) \cup (\cup_{i,j,k} R_{ijk}) \cup (\cup_{i,j,k,l,m} CF_{ijklm})$$

forms a connected set.

Proof. Note that to show the connectivity of the set S is equivalent to showing that given two arbitrary configuration q_s and q_g on S , there exists a path between them that lies completely on the set S . Since any rod configuration can access a rod four-way equidistant configuration, we can, without loss of generality, assume that the start and the goal configurations are on some rod four-way equidistant faces CF_{f_s} and CF_{f_g} , respectively. Then, it suffices to show that there is a connected series of rod four-way equidistant faces, one-tangent edges, and rod-GVG edges that contain CF_{f_s} and CF_{f_g} to show the connectivity.

From the discussion above, given CF_{f_s} and CF_{f_g} , we can find point-GVG meetpoints F_{f_s} and F_{f_g} , which are defined by the same set of respective obstacles. Then, since the point-GVG is connected, there is a sequence of index sets $f_1 (= f_s)$, t_1 , f_2 , t_2 , \dots , t_{n-1} , $f_n (= f_g)$, such that $(\cup F_{f_i}) \cup (\cup F_{t_i})$ is a connected set. Note that using our convention, F_{f_i} is a point-GVG meetpoint, and F_{t_i} is a point-GVG edge and we have the relation $t_i = f_i \cap f_{i+1}$. We also define the sequence $v_i = f_i \cup f_{i+1}$. Then, since F_{f_i} and $F_{f_{i+1}}$ share the three closest obstacles between them, v_i is an index set with five obstacles.

From the index sets f_i found above, we find a sequence of the rod four-way equidistant faces $CF_{f_1}, \dots, CF_{f_n}$. Then, if we show that the union of two adjacent rod four-way equidistant faces CF_{f_i} and $CF_{f_{i+1}}$ with either the one-tangent edge

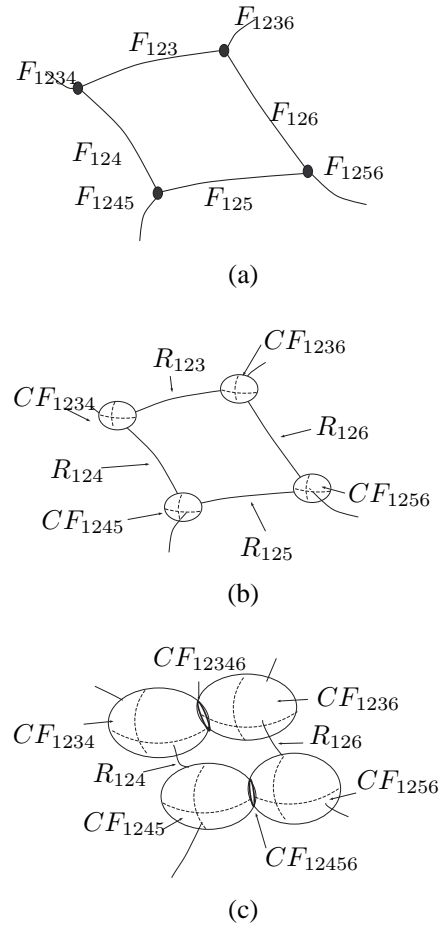


Fig. 24. (a) shows a portion of the point-GVG in an environment (not all the edges shown are labelled). (b) and (c) show the rod-HGVG in the same environment. If the rod were short (b), then there would be a one-to-one mapping between the point-GVG edges and the one-tangent edges. Also there would be a one-to-one mapping between the point-GVG meetpoints and the rod four-way equidistant faces, and the rod four-way equidistant faces would be connected by the one-tangent edges exactly in the same manner as the point-GVG meetpoints are connected by the point-GVG edges. If the rod were long, some of the rod four-way equidistant faces would intersect each other, and form the rod-GVG edges between them. Also note that, in this case, there would be some rod four-way equidistant faces that do not have corresponding point-GVG meetpoints. Such rod four-way equidistant faces are not shown in (c).

R_{t_i} or the rod-GVG edge CF_{v_i} , forms a connected set, we can conclude that \mathcal{S} is a connected set, using induction.

If $CF_{f_i} \cap CF_{f_{i+1}} \neq \emptyset$, then the intersection of these two sets is actually a rod-GVG edge CF_{v_i} . Thus, it follows that $CF_{f_i} \cup CF_{v_i} \cup CF_{f_{i+1}}$ forms a connected set. If $CF_{f_i} \cap CF_{f_{i+1}} = \emptyset$, then, by definition, $CF_{v_i} = \emptyset$, and we need to show that the set $CF_{f_i} \cup CF_{f_{i+1}} \cup R_{t_i}$ forms a connected set. If $CF_{v_i} = \emptyset$, from Lemma 1, we have $R_{t_i} \neq \emptyset$. Since the point-GVG edge F_{t_i} terminates at the two meetpoints F_{f_i} and $F_{f_{i+1}}$, the one-tangent edge R_{t_i} has endpoints on both of CF_{f_i} and $CF_{f_{i+1}}$. This implies that the set $CF_{f_i} \cup CF_{f_{i+1}} \cup R_{t_i}$ is a connected set.

This completes the proof that the set $(\cup CF_{f_i}) \cup (\cup R_{t_i}) \cup (\cup CF_{v_i})$ forms a connected set, for a sequence of f_i and t_i found as above and the rod-GVG edges CF_{v_i} formed between any adjacent CF_{f_i} in the sequence. Since q_s and q_g are chosen arbitrarily from any junction regions, this implies that $(\cup_{f_i \in \mathcal{F}} CF_{f_i}) \cup (\cup_{t_i \in \mathcal{T}} R_{t_i}) \cup (\cup_{v_i \in \mathcal{V}} CF_{v_i})$ (where \mathcal{F} , \mathcal{T} and \mathcal{V} are the set of index sets of three, four, and five indices, respectively). \square

4.5. Connectivity of Two-tangent Edges and Rod-GVG Edges on a Single CF_{ijkl}

This is the second (and final) step in proving the connectivity of the rod-HGVG under the assumption that the point-GVG is connected in a given environment. More specifically, we show that the union of $R_{ij/kl}$ and CF_{ijklm} on a single CF_{ijkl} forms a connected set, and we also show that the network of two-tangent edges $R_{ij/kl}$ contains the endpoints of the one-tangent edges (if they exist) terminating on the given CF_{ijkl} . In addition, if there are holes on CF_{ijkl} , it is shown that the union of the two-tangent edges and the boundary elements of CF_{ijkl} forms a connected set. We consider this problem in two subproblems (Figure 25): (i) CF_{ijkl} is homeomorphic to S^2 , and (ii) CF_{ijkl} is not homeomorphic to S^2 , i.e., CF_{ijkl} has boundaries.

4.5.1. CF_{ijkl} is homeomorphic to S^2

This corresponds to the case where the rod is “short” or the environment is not cluttered. Note that if CF_{ijkl} is homeomorphic to S^2 , there are no rod-GVG edges on CF_{ijkl} since rod-GVG edges are boundary components of CF_{ijkl} . Therefore, we need to show that the union of two-tangent edges, by themselves, forms a connected set. Also we need to show that this union contains the endpoints of the one-tangent edges.

To prove the connectivity of the union of the two-tangent edges, we need the following results whose proofs can be found in Appendices F and G.

LEMMA 4. A two-tangent edge $R_{ij/kl}$ is a one-dimensional manifold.

LEMMA 5. A two-tangent edge $R_{ij/kl}$ has one connected component on CF_{ijkl} , which is homeomorphic to S^2 .

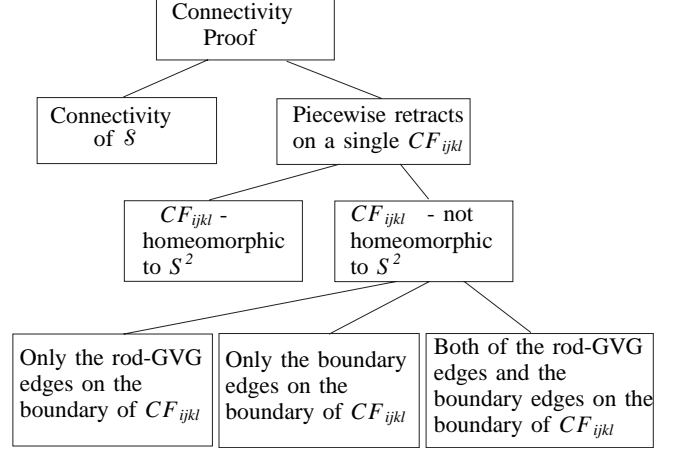


Fig. 25. Overview of the connectivity proof.

Now, we prove the connectivity of the two-tangent edges and rod-GVG edges on a single CF_{ijkl} , which is homeomorphic to S^2 .

LEMMA 6. If CF_{ijkl} is homeomorphic to S^2 , then the union of the two-tangent edges on CF_{ijkl} forms a connected set. Moreover, the two-tangent edges on CF_{ijkl} contain the endpoints of the one-tangent edges terminating on CF_{ijkl} .

Proof. Before we show that the union of the two-tangent edges forms a connected set, we make some observations. Recall that there are six two-tangent edges on a CF_{ijkl} . Also, recall that there are four one-tangent edges, each terminating at some points in CF_{ijkl} . In fact, the endpoints of one-tangent edges are, by definition, the intersection of three two-tangent edges. For example, the endpoints of R_{ijk} on CF_{ijkl} are the intersection of $R_{ij/kl}$, $R_{ik/jl}$, and $R_{jk/il}$.

Now we show that the union of the two-tangent edges forms a connected set, which contains the endpoints of the one-tangent edges terminating on CF_{ijkl} . Recall that, by definition, there are six two-tangent edges on a CF_{ijkl} . Without loss of generality, we first consider one of the two-tangent edges, say, $R_{ij/kl}$. Since $R_{ij/kl}$ has one connected component, it contains the endpoints of R_{ijk} and R_{ijl} . Since the endpoints of R_{ijk} are also elements of $R_{ik/jl}$ and $R_{jk/il}$, and, by assumption, each two-tangent edge has one connected component, we can trivially conclude that the union of $R_{ij/kl}$, $R_{ik/jl}$, and $R_{jk/il}$ forms a connected set. Continuing this argument, we can show that the union of six two-tangent edges on CF_{ijkl} forms a connected set and contains all of the endpoints of the one-tangent edges. \square

This completes the proof of the connectivity of the two-tangent edges on a rod four-way equidistant face CF_{ijkl} . Note that if CF_{ijkl} is homeomorphic to S^2 , the endpoints of the

one-tangent edges are also elements of two-tangent edges, i.e., the one-tangent edges terminate on the two-tangent edges. If all of CF_{ijkl} are homeomorphic to S^2 , the rod-HGVG is connected since we have already established that the union of CF_{ijkl} , R_{ijk} , and CF_{ijklm} (which does not exist in this case) forms a connected set.

4.5.2. CF_{ijkl} is not homeomorphic to S^2

Note that if CF_{ijkl} is not homeomorphic to S^2 , CF_{ijkl} may have boundaries on it. There can be two types of boundaries for CF_{ijkl} : (a) the rod-GVG edges (i.e., five-way equidistant configurations); (b) the boundary edges (i.e., $B_{ijkl} = \{q \in CF_{ijkl} : D_i(q) = 0\}$). Note that a connected component of the boundary of CF_{ijkl} can contain both a rod-GVG edge and a boundary edge. Also note that CF_{ijkl} can have multiple disconnected components, where each connected component contains a rod-GVG edge or a boundary edge or both in its boundary.⁵ However, if a rod four-way equidistant face CF_{ijkl} has multiple disconnected components, this implies that the junction region itself is disconnected also because CF_{ijkl} is a two-dimensional deformation retract of the junction region. Therefore, we only need to consider the connectivity of the rod-HGVG on a single connected component of CF_{ijkl} .

We first consider the case where the boundary of CF_{ijkl} consists only of the rod-GVG edge(s). Then we discuss the case where the boundary of CF_{ijkl} contains the boundary edge(s) and no rod-GVG edges. Finally, we discuss the case where the boundary of CF_{ijkl} contains both rod-GVG edges and boundary edges. We see that if there are boundary edges, the union of the rod-HGVG edges together with all of the boundary edges does not form a connected set. However, we show that by selectively using the boundary edges, we can connect the disconnected components of the rod-HGVG.

The Case of Rod-GVG Edge CF_{ijklm} . Note that there actually can be more than one rod-GVG edge on a given CF_{ijkl} . Initially, we assume that there is only one rod-GVG edge CF_{ijklm} on CF_{ijkl} . The case of multiple rod-GVG edges will be discussed later. Also note that here we assume that there are no boundary edges on CF_{ijkl} .

It is shown that, if CF_{ijklm} exists, the three of the six two-tangent edges on CF_{ijkl} ($R_{ij/kl}$, $R_{ik/jl}$, and $R_{jk/il}$) intersect CF_{ijklm} , and thus the union of CF_{ijklm} and the three two-tangent edges form a connected set. In this sense, the one-tangent edge R_{ijk} and the rod-GVG edge CF_{ijklm} perform a dual role in connecting the two-tangent edges on CF_{ijkl} . Note that to show the connectivity, we only need to show that a rod-GVG edge must intersect at least one two-tangent edge in a manner such that the union of the rod-GVG edge and the two-tangent edge it intersects is still a connected set.

Now we show that assuming CF_{ijklm} is the only boundary

component of CF_{ijkl} , the union of the two-tangent edges and CF_{ijklm} forms a connected set.

LEMMA 7. If the rod-GVG edge CF_{ijklm} is the only boundary component of CF_{ijkl} , then the union of the two-tangent edges on CF_{ijkl} and CF_{ijklm} forms a connected set.

Proof. First we consider a structure, denoted by $CF_{ijkl/m}$, which is

$$CF_{ijkl/m} = \{q \in FS \mid 0 < D_i(q) = D_j(q) = D_k(q) = D_l(q) \leq D_o(q), \\ o \neq m, i, j, k, l\}. \quad (18)$$

In other words, $CF_{ijkl/m}$ is the rod four-way equidistant face in a workspace where C_m is removed. Also, we can similarly define a “virtual” two-tangent edge $R_{ij/kl/m}$ on $CF_{ijkl/m}$, by ignoring C_m temporarily, i.e., $R_{ij/kl/m}$ is the two-tangent edge defined on $CF_{ijkl/m}$ rather than on CF_{ijkl} . Then $CF_{ijkl/m}$ is homeomorphic to S^2 , since we assume that CF_{ijklm} is the only rod-GVG edge on CF_{ijkl} and there are no boundary edges either. Therefore, there is a connected network of two-tangent edges $R_{ij/kl/m}$, $R_{ik/jl/m}$, etc., on $CF_{ijkl/m}$, using Lemma 6.

By definition, $CF_{ijkl/m}$ and the two-tangent edges $R_{ij/kl/m}$ on it contain CF_{ijkl} and the two-tangent edges $R_{ij/kl}$ on it, respectively. In other words, the rod-GVG edge partitions $CF_{ijkl/m}$ into CF_{ijkl} and $CF_{ijkl/m} \setminus CF_{ijkl}$, where CF_{ijklm} is the boundary of each set. Also, CF_{ijklm} partitions $\cup R_{ij/kl/m}$ into $\cup R_{ij/kl}$ and $\cup R_{ij/kl/m} \setminus \cup R_{ij/kl}$. Note that there is a possibility that $\cup R_{ij/kl}$ is empty if CF_{ijklm} exists, which implies that CF_{ijklm} is the only rod-HGVG component on CF_{ijkl} . Therefore, in this case, the connectivity of the rod-HGVG components on CF_{ijkl} is trivially satisfied. Thus, in the following, we assume that $\cup R_{ij/kl}$ is not-empty.

First we claim that, if CF_{ijklm} does not intersect $\cup R_{ij/kl}$, then $\cup R_{ij/kl} = \cup R_{ij/kl/m}$. This can be shown by contradiction. Assume $\cup R_{ij/kl} \neq \cup R_{ij/kl/m}$. This means $\cup R_{ij/kl/m} \setminus \cup R_{ij/kl} \neq \emptyset$. Let q be a point on $\cup R_{ij/kl/m} \setminus \cup R_{ij/kl}$. Then, by definition $D_m(q) < D_i(q)$,⁶ and, since $R_{ij/kl}$ is not an empty set, there is a configuration in q' in $\cup R_{ij/kl}$, where $D_i(q') < D_m(q')$, and obviously, $q' \in \cup R_{ij/kl/m}$. Since $\cup R_{ij/kl/m}$ is a connected set, there is a path between q and q' which lies on $\cup R_{ij/kl/m}$. Then there must be a configuration q'' on the path where $D_m(q'') = D_i(q'')$ from the continuity of the distance function. Then q'' is, by definition, on CF_{ijklm} and $R_{ij/kl}$, i.e., $CF_{ijklm} \cap R_{ij/kl} \neq \emptyset$, which is a contradiction. Therefore, we have $\cup R_{ij/kl} = \cup R_{ij/kl/m}$.

Next we show that CF_{ijklm} intersects the network of two-tangent edges, i.e., $\cup R_{ij/kl}$. We show this by contradiction. Assume that CF_{ijklm} does not intersect $\cup R_{ij/kl}$. Then, from the claim above, $\cup R_{ij/kl} = \cup R_{ij/kl/m}$, which forms a connected set. This means there is at least one (actually six) point where three of the two-tangent edges intersect, and one of these is

5. Note that the “boundary edge” and the “boundary” of CF_{ijk} (or of any structure) are two different things.

6. Of course, $D_i(q) = D_j(q) = D_k(q) = D_l(q)$, which we omit from the main text for simplicity.

the intersection of $R_{ij/kl}$, $R_{ik/jl}$, and $R_{jk/il}$. This point, by definition, belongs to R_{ijk} . That is, R_{ijk} is not an empty set, which contradicts Lemma 2. Thus, CF_{ijklm} must intersect $\cup R_{ij/kl}$.

Now we show that $CF_{ijklm} \cup (\cup R_{ij/kl})$ forms a connected set. Recall that CF_{ijklm} and $(\cup R_{ij/kl})$ are subsets of CF_{ijkl} . In other words, we need to show that given two arbitrary configurations q_1 and q_2 on $CF_{ijklm} \cup (\cup R_{ij/kl})$, there is a path between q_1 and q_2 that lies entirely on $CF_{ijklm} \cup (\cup R_{ij/kl})$. Recall that the rod-GVG edge CF_{ijklm} must intersect the two-tangent edges, and CF_{ijklm} is a connected set, because we assume that CF_{ijklm} is the only boundary component on CF_{ijkl} . Therefore, we can assume that q_1 and q_2 are the elements of $\cup R_{ij/kl}$.

Recall that CF_{ijklm} partitions $\cup R_{ij/kl/m}$ into $\cup R_{ij/kl}$ and $\cup R_{ij/kl/m} \setminus \cup R_{ij/kl}$, and $\cup R_{ij/kl/m}$ is a connected set. Now, given two configurations q_1 and q_2 on $\cup R_{ij/kl}$, note that there is a path $P(t)$ between q_1 and q_2 that entirely lies on $R_{ij/kl/m}$. This is obvious since $q_1, q_2 \in \cup R_{ij/kl} \subset \cup R_{ij/kl/m}$ and $\cup R_{ij/kl/m}$ is a connected set. Now, we should find a path between them which lies on $(CF_{ijklm}) \cup (\cup R_{ij/kl})$. If $P(t)$ lies entirely on $(\cup R_{ij/kl})$, we are done. Otherwise, we can find a sequence of t_i in $[0, 1]$ such that the path $P(t_i)$ lies on the boundary between $\cup R_{ij/kl}$ and $\cup R_{ij/kl/m} \setminus \cup R_{ij/kl}$, i.e., the rod-GVG edge CF_{ijklm} .

Since CF_{ijklm} is a connected set, there is a path between the consecutive $P(t_i)$ on CF_{ijklm} , which we denote by $S_i(t)$, i.e., $S_i(t)$ is a continuous mapping from $[0, 1]$ to CF_{ijklm} such that $S_i(0) = P(t_{2i})$, $S_i(1) = P(t_{2i+1})$. Then we construct a new path between q_1 and q_2 by concatenating the segments of $P(t)$, which lie on R_{ijkl} , and $S_i(t)$, which lie on CF_{ijklm} , and the resulting path, by construction, lies on $(CF_{ijklm}) \cup (\cup R_{ij/kl})$. Thus we have found a path between arbitrary configuration q_0 and q_1 on $(CF_{ijklm}) \cup (\cup R_{ij/kl})$, and thus we have shown that $(CF_{ijklm}) \cup (\cup R_{ij/kl})$ is a connected set.

In summary, we take the disconnected segments of the path $P(t)$ that lie on $\cup R_{ij/kl}$. Then, to construct a connected path, we connect them using the rod-GVG edge, which is a connected set if it is the only boundary component of CF_{ijk} . \square

Now we can prove the connectivity of the rod-HGVG on a single rod four-way equidistant face CF_{ijkl} with multiple rod-GVG edges.

LEMMA 8. If CF_{ijkl} is not homeomorphic to S^2 , but does not contain boundary edges, the union of the rod-GVG edges and the two-tangent edges on CF_{ijkl} is a connected set.

Proof. Assume that there are n rod-GVG edges, CF_{ijklm_1} , CF_{ijklm_2} , \dots , CF_{ijklm_n} . Now, define CF_{ijkl/m_1} (ignoring C_{m_1}), CF_{ijkl/m_1m_2} (ignoring C_{m_1} and C_{m_2}), $CF_{ijkl/\dots}$, etc., until we have $CF_{ijkl/\{m_1m_2\dots m_n\}}$, which is homeomorphic to S^2 . Now we consider $CF_{ijkl/\{m_1m_2\dots m_{n-1}\}}$, which has only one rod-GVG edge, i.e., CF_{ijklm_n} , on it. Then, it is obvious that the “virtual” CF_{ijklm_n} (defined by ignoring all the obstacles from C_{m_1} to $C_{m_{n-1}}$) and the “virtual” two-tangent edges on $CF_{ijkl/\{m_1m_2\dots m_{n-1}\}}$ form a

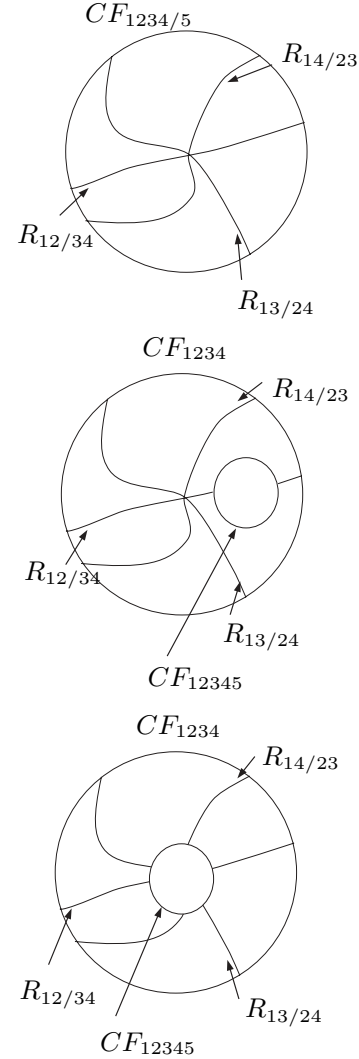


Fig. 26. The case of a rod-GVG edge CF_{12345} on CF_{1234} . We assume that CF_{12345} is the only boundary component on CF_{1234} . Then, if we ignore C_5 temporarily, and define $CF_{1234/5}$ as the four-way equidistant face, $CF_{1234/5}$ is homeomorphic to S^2 and the union of the two-tangent edges on $CF_{1234/5}$ form a connected set (top). Now we consider C_5 and thus CF_{12345} . Note that CF_{12345} is homeomorphic to S^1 because it is assumed that CF_{12345} is the only boundary components of CF_{1234} . Then if CF_{12345} intersects at least one of the two-tangent edges, the union of CF_{12345} and the union of the two-tangent edges form a connected set (center).

connected set, using the argument above. Let us call this set CX_{m_n} . Then, we consider $C_{m_{n-1}}$ (still ignoring C_1 to $C_{m_{n-2}}$) and $CF_{ijkl/(m_1m_2\dots m_{n-2})}$. Temporarily ignoring C_{m_n} also, we have a “virtual” $CF_{ijkl_{n-1}}$, which is homeomorphic to S^1 and partitions $CF_{ijkl/(m_1m_2\dots m_n)}$. This “virtual” $CF_{ijkl_{n-1}}$ also partitions CX_{m_n} into two sets, which we call “real” CX_{m_n} and “unreal” CX_{m_n} . For the points on “real” CX_{m_n} , the distance to $C_{m_{n-1}}$ is larger than the distance to C_i , and for the configurations on “unreal” CX_{m_n} , the distance to $C_{m_{n-1}}$ is smaller than the distance to C_i . Using a similar argument as above, we can show that the union of “real” CX_{m_n} and “virtual” $CF_{ijkl_{n-1}}$ forms a connected set. Now “real” $CF_{ijkl_{n-1}}$ is the same as “virtual” $CF_{ijkl_{n-1}}$, and we are done. (This case means that the two rod-GVG edges do not intersect each other.) Otherwise this implies that on some points on “virtual” $CF_{ijkl_{n-1}}$, the distance to $C_{m_{n-1}}$ must be smaller than C_{m_n} (since we are still ignoring all of the other obstacles). Using the continuity of the distance function, we can conclude that “real” $CF_{ijkl_{n-1}}$ and $CF_{ijkl_{m_n}}$ intersect, and the union of $CF_{ijkl_{n-1}}$ and $CF_{ijkl_{m_n}}$ forms a boundary of $CF_{ijkl/(m_1m_2\dots m_{n-2})}$. The union of $CF_{ijkl_{n-1}}$ and $CF_{ijkl_{m_n}}$ is also a boundary of $\cup R_{ij/kl}$ on $CF_{ijkl/(m_1m_2\dots m_{n-2})}$, and using a similar argument to that above, we can show the connectivity of the union of $CF_{ijkl_{n-1}}$ and $CF_{ijkl_{m_n}}$ and the two-tangent edges. Continuing in this way, considering one additional obstacle at a time, we can eventually conclude that the union of rod-GVG edges and the two-tangent edges forms a connected set. \square

The Case of the Boundary Edge B_{ijkl} . Here we consider the case where CF_{ijkl} is not homeomorphic to S^2 , and its only boundary components are the boundary edges. Unfortunately, if there is a boundary edge, there are examples where the union of the two-tangent edges and all of the boundary edges on CF_{ijkl} does not form a connected set. Therefore, we need to either introduce a new component to the rod-HGVG or provide a linking strategy to connect the disconnected components of the rod-HGVG.

Consider an environment where the free space is the interior of the regular tetrahedron. (Figure 28 and the figure on the left in Figure 27). In this example, the length of the rod is longer than the height of the tetrahedron, but shorter than the height of the triangular faces of the tetrahedron. Clearly, the point-GVG is connected. Also, with some reasoning, one can see that the configuration space is connected, i.e., the rod can move from any configuration to any other configuration. However, the rod-HGVG is not connected. First, since there are only four obstacles, there exist no rod-GVG edges. Also, since the length of the rod is larger than the height of the tetrahedron, there cannot be any one-tangent edges. However, there are two-tangent edges, which are disconnected from each other. (Recall that the two-tangent edges cannot be connected without one-tangent edges or rod-GVG edges.) That is, even if the configuration space is connected, the rod-HGVG is not connected.

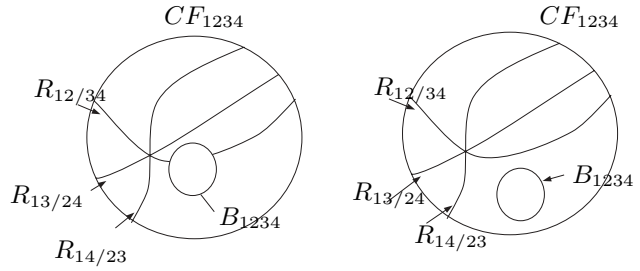


Fig. 27. The case of a boundary edge B_{1234} on CF_{1234} . Left: the boundary edge B_{1234} intersects the network of two-tangent edges. In this case, the union of the two-tangent edges and the boundary edge forms a connected set. Right: the boundary edge B_{1234} is isolated from other rod-HGVG components. In this case, the union of the two-tangent edges and the boundary edge does not form a connected set, but the union of the two-tangent edges themselves still forms a connected set. Therefore, we do not necessarily need to use the boundary edge.

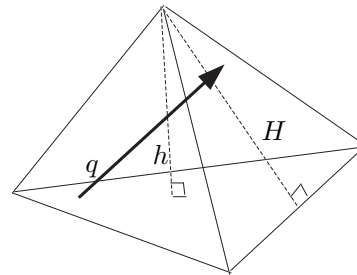


Fig. 28. In this example, the environment is the interior of a tetrahedron. If the length of the rod is less than the height of the triangular face of the tetrahedron, but larger than the height of the tetrahedron, the configuration space is connected. However, in this environment, there are only two-tangent edges disconnected from each other, and no GVG edges or one-tangent edges. This implies that the rod-HGVG is disconnected even if the configuration space is connected.

To amend this problem, one might consider the boundary edge as a component of the rod-HGVG. This is not surprising considering that the boundary edge is also a component of the point-HGVG in a three-dimensional space. However, this causes another problem to arise, as can be seen in the example shown in Figure 30 (and also the figure on the right in Figure 27). Here, we have an isolated boundary edge which does not intersect any rod-HGVG component. There are two

possible solutions to this problem. We can either define the boundary edge as a component of the rod-HGVG and try to devise a connecting scheme (and/or additional type(s) of edge, if necessary) for connecting isolated boundary edges, or we use boundary edges as links connecting disconnected rod-HGVG components, without considering them as components of the rod-HGVG. We take the latter approach, i.e., we will use the boundary edges only as links, and we do not try to trace all of the boundary edges.

This approach can be justified since the robot will never actually reach a configuration on an isolated boundary edge as the robot traces the rod-HGVG. Recall that to access the rod-HGVG from an arbitrary configuration, the robot uses distance gradient ascent. Thus, after the accessibility procedure, the robot will be at some configuration with distance greater than zero,⁷ and start tracing the first rod-HGVG component, which is not a boundary edge. As the robot traces the rod-HGVG, it will encounter some boundary edges, but cannot encounter an isolated component of a boundary edge (by definition). Therefore, the isolated boundary edges can be safely ignored.

In summary, the planner traces the boundary edge only if it encounters a configuration on the boundary edge while tracing one of the rod-HGVG edges and does not make an attempt to find all of the boundary edges. Finally, we note that the boundary edges can also be traced using the same technique described in Section 5.⁸ This discussion leads to the following lemma.

LEMMA 9. On a connected component of CF_{ijkl} , the union of the two-tangent edges on CF_{ijkl} and the boundary edges that intersect any of the two-tangent edges on CF_{ijkl} forms a connected set.

The Case Where Both Boundary Edges and Rod-GVG Edges Exist on CF_{ijkl} . Finally, we consider the case where boundary of CF_{ijkl} contains both rod-GVG edges and boundary edges.

LEMMA 10. On a connected component of CF_{ijkl} , the union of the two-tangent edges, the rod-GVG edges, and the boundary edges that intersect any of the two-tangent edges or the rod-GVG edges forms a connected set.

Proof. The proof for this case is essentially the same as the proof of Lemma 8. First, we consider the case in which there is only one rod-GVG edge CF_{ijklm} on CF_{ijkl} . As before, we temporarily ignore the obstacle C_m , and conclude that the union of the two-tangent edge and the boundary edge forms a connected set, denoted \mathcal{S} on $CF_{ijkl/m}$. Now if we consider

7. Actually, it may be the case that the distance is still zero after the gradient ascent, but this implies that the accessibility fails. In other words, the robot is initially “stuck” in a component of the configuration space which does not contain any configuration with distance greater than zero. In this case, the planner will trace the boundary edge (if possible) and then terminate.

8. In reality, we trace the set of configurations with the constant distance $\delta \approx 0$ rather than the boundary edge itself.

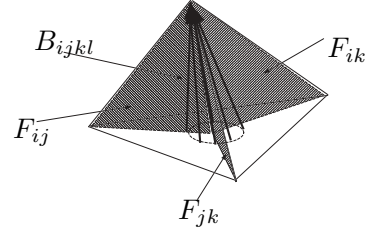


Fig. 29. The boundary edge B_{ijkl} (some of the configurations in B_{ijkl} are shown as a solid arrow) connects the three two-tangent edges $R_{ij/kl}$, $R_{ik/jl}$, and $R_{jk/il}$ (which are defined using F_{ij} , F_{ik} , and F_{jk} , respectively). The configurations in $R_{ij/kl}$, $R_{ik/jl}$, and $R_{jk/il}$ are not shown.

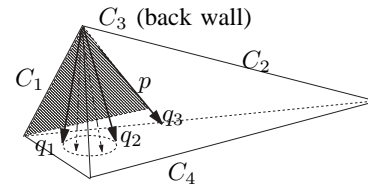


Fig. 30. Here, the boundary edge (double dotted arrows) connects two disconnected components of $R_{13/24}$. Note that q_1 , q_2 , and q_3 all belong to $R_{13/24}$, i.e., all of the configurations are on the plane p , but q_1 belongs to a different component of $R_{13/24}$. Note that q_3 also belongs to R_{123} .

the obstacle C_m , then CF_{ijklm} partitions $CF_{ijkl/m}$ into CF_{ijkl} and $CF_{ijkl/m} \setminus CF_{ijkl}$, and \mathcal{S} into $\mathcal{S} \cap CF_{ijkl}$ and $\mathcal{S} \cap (CF_{ijkl/m} \setminus CF_{ijkl})$. Then using a similar argument as before, we can conclude that the union of $\mathcal{S} \cap CF_{ijkl}$ and CF_{ijklm} forms a connected set. For the case where there are multiple rod-GVG edges, we can iterate the same argument on the union of $\mathcal{S} \cap CF_{ijkl}$ and CF_{ijklm} . \square

Figure 31 shows an example of an environment with boundary edges. The free space in the example is the interior of a regular tetrahedron, with the length of the rod longer than the height of the tetrahedron, but shorter than the height of the triangles which form the faces of the tetrahedron. Thus, the only components of the rod-HGVG in this environments are the two-tangent edges, which are disconnected from each other. In this case, it is not difficult to see that the configuration space is connected. There are six two-tangent edges which are not connected to each other, and actually each of the two-tangent edges also have multiple disconnected components. However, there are neither rod-GVG edges nor one-tangent edges in this environment. There are no rod-GVG edges, since

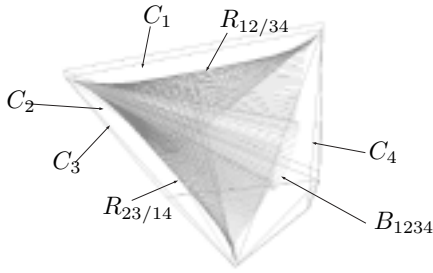


Fig. 31. The free space is the interior of a tetrahedron, defined by the obstacles C_1 , C_2 , C_3 , and C_4 . Here, two two-tangent edges, $R_{12/34}$ and $R_{23/14}$, are connected by a boundary edge component B_{1234} . (Not all of the two-tangent edges terminating on this boundary edge are shown.)

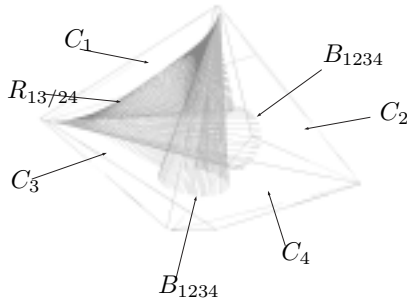


Fig. 32. A two-tangent edge component $R_{13/24}$ terminates at two disconnected boundary edge components B_{1234} . In other words, the two disconnected boundary edge components of the boundary edge B_{1234} are connected by two-tangent edge $R_{13/24}$.

there are only four obstacles, and there are no one-tangent edges, since for a rod configuration to be on a one-tangent edge, it must be tangent to a point-GVG edge, whose length is shorter than the length of the rod by design. Thus, there is no rod configuration that can be tangent to any point-GVG edge without intersecting any obstacles. This means that the union of the rod-HGVG components (i.e., two-tangent edges) does not form a connected set in this example. Thus, we need the boundary edges to connect those disconnected components. Figure 31 shows a boundary edge connecting two disconnected two-tangent edges, and Figure 32 shows a two-tangent edge terminating at two different boundary edges. Figure 33 shows all of the swept volume of all of the edges in the same environment.

This completes the proof of the connectivity of the rod-HGVG components on a four-way equidistant face CF_{ijkl} which is not homeomorphic to S^2 .

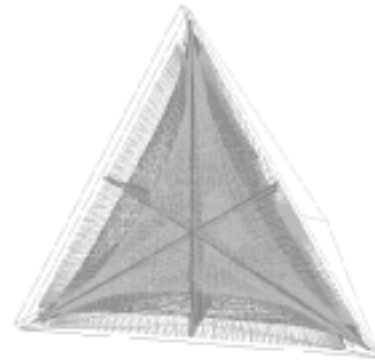


Fig. 33. The swept volume of the two-tangent edges and the boundary edges inside a regular tetrahedron.

4.6. Connectivity of the Rod-HGVG

We are now ready to prove the connectivity of the rod-HGVG under the assumption that the point-GVG is connected.

THEOREM 1. Assume that the point-GVG is connected and the configuration space is connected. Then the rod-HGVG, together with the boundary edge components that intersect at least one rod-HGVG component, forms a connected set.

Proof. The proof is just the straight application of Lemmas 3, 6, 7, 8, 9, and 10. □

5. Incremental Construction of the Rod-HGVG

In this section we discuss an incremental construction procedure for the components of the rod-HGVG. Figure 34 shows an overall flow of the construction procedure.

5.1. Accessing the Rod-HGVG

The incremental construction starts with a series of gradient ascents described in Section 4.1. As shown in Appendix B, after the gradient ascent, the robot is placed on a rod-GVG edge or a one-tangent edge. Depending on which edge the rod is placed on, the planner invokes an appropriate method to trace the current edge. The methods to trace each type of edges are described below.

5.2. Tracing the Rod-HGVG Edges

Recall that the components of the rod-HGVG are defined using the workspace distance function with some additional information. The additional information includes the points r_i , the closest point on the rod to each of the obstacles, c_i , the

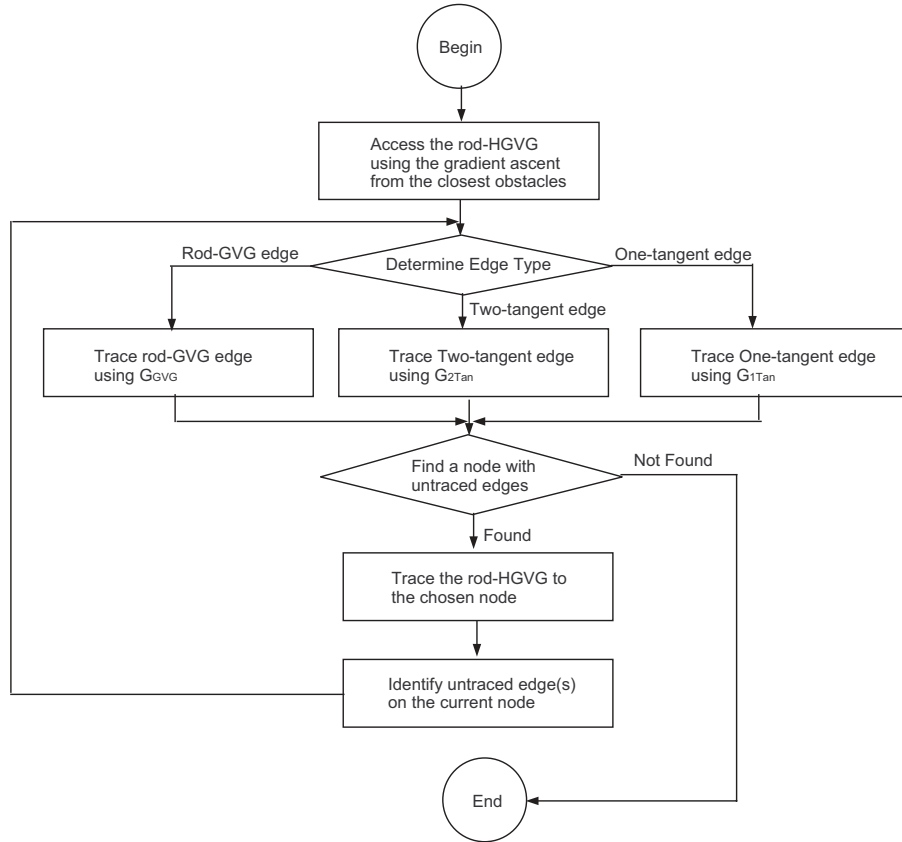


Fig. 34. Overall flow of the algorithm.

closest point on each of the the obstacles, and PQ , the vector parallel to the rod. Theoretically, all of this information can be easily obtained from a range sensor placed along the length of the robot, and computed from the configuration of the robot. This work does not consider the issues of sensor noise or the other problems that can arise in implementation.

To trace the edges of the rod-HGVG, we use the curve tracing technique described in Choset and Burdick (2000b). A detailed description of the technique can be found in Choset and Burdick (2000b) but, essentially, this method is a root tracing technique that consists of a predictor step and a corrector step. The predictor step moves the robot in the tangent direction of the curve it is tracing by a finite distance. This step usually takes the robot off the curve. The corrector step then brings the robot back onto the curve, using Newton's iterative root finder (Press et al. 2002).

More specifically a rod-GVG edge CF_{ijklm} , a two-tangent edge $R_{ij/kl}$, and a one-tangent edge R_{ijk} can be represented respectively as the zeros of

$$G_{GVG}(q) = \begin{pmatrix} (D_i - D_j)(q) \\ (D_i - D_k)(q) \\ (D_i - D_l)(q) \\ (D_i - D_m)(q) \end{pmatrix},$$

$$G_{2Tan}(q) = \begin{pmatrix} (D_i - D_j)(q) \\ (D_i - D_k)(q) \\ (D_i - D_l)(q) \\ (P(q) - Q(q)) \cdot (c_i - c_j)(q) \end{pmatrix},$$

and

$$G_{1Tan}(q) = \begin{pmatrix} (D_i - D_j)(q) \\ (D_i - D_k)(q) \\ (P(q) - Q(q)) \cdot (c_i - c_k)(q) \\ (P(q) - Q(q)) \cdot (c_i - c_j)(q) \end{pmatrix}.$$

The terms of the form $D_i - D_j$ represent the equidistant conditions and the terms of the form $PQ \cdot (c_i - c_j)$ represent the tangency condition that the rod be tangent to F_{ij} . Then, using a curve tracing method (Choset and Burdick 2000b), the planner can construct the edges of the rod-HGVG by tracing the root of the equations defined above depending on the type of the edge it is tracing. Note that the equidistant condition can be reliably checked up to the sensor accuracy, and it is not affected by the uncertainty in the localization since it is not explicitly defined using the coordinate of the robot. The tangency condition is not affected by localization error either, since, even if the coordinate of c_i must be known to check the

tangency condition, the coordinate of c_i is computed from the position of the local minima of the distance on the rod and the value of the sensor reading. In other words, the coordinate of c_i is computed relative to the coordinate of the rod configuration, and it also can be computed reliably up to the sensor accuracy. Finally, the differential of $G(q)$, which is required to compute the tangent direction and the correcting plane, can be also represented using only sensor-provided information. The detailed expression for the differential of $G(q)$ can be found in Appendix F.

5.3. Finding Edges to Explore

While tracing the rod-HGVG edges, the planner keeps track of the “nodes” it encounters, and stores them in the queue. The nodes include

- the “meet configurations” CF_{ijklmn} , i.e., the six-way equidistant configurations;
- the “boundary configurations”, i.e., the configuration where the distance to closest obstacles are zero;
- the configurations where a one-tangent edge and two-tangent edges intersect, i.e., $R_{ijk} \cap R_{ij/kl}$;
- the configurations where a two-tangent edge and a rod-GVG edge intersect, i.e., $CF_{ijklm} \cap R_{ij/kl}$.

Depending on the type of the node, we can identify what kinds of edges should be connected to the node. Table 2 summarizes the type of the path that can be connected to each type of node. Note that for the boundary configurations, no edges can be connected other than the edge terminating on it. At each node, the planner keeps track of the edges that are already traced. Then, given the type of node, and the list of edges that are connected, the planner can determine if there are more edges to be traced from the current node and, if so, what kind of edges should be traced.

Then, after the construction of the current edge, the planner finds a node in the queue which has untraced edges. Then the planner finds a path from the current node to the chosen node on the part of the rod-HGVG which is constructed up to that point. The planner moves the robot to the chosen node, and then begins tracing the untraced edges from the chosen node. By repeating this process until there is no node with untraced edges, the planner can completely construct the rod-HGVG in the given environment.

5.4. Notes on Complexity of the Rod-HGVG

We have implemented our exploration algorithm on a 3.2 GHz PC using C++. In a simple rectangular environment (as shown in Figure 20 and Extension 1), in which there are no rod-GVG edges, it took 3 min to completely construct the rod-HGVG. In a more complex environment, where there are rod-GVG edges (Figure 21 and Extension 2), it took 12 min to

construct the rod-HGVG. However, most of the CPU time was spent on computing the distance between the rod and the obstacles, as we did not try to optimize the distance computing function in the simulator. However, since we are considering sensor-based planning, in actuality, this distance information should be provided from the sensors, and the time spent on computing this information should not be counted as part of the run-time overhead of our method. Therefore, the run-time of the simulation does not provide appropriate measure of the performance of our method. A more meaningful measure would be the complexity of the rod-HGVG itself, i.e., the number of edges and the nodes of the rod-HGVG, represented as a function of the complexity of the environment, i.e., the number of the obstacles n .

Currently we are determining the exact complexity of the rod-HGVG in three dimensions. Since the rod-HGVG is defined using the point-GVG, naturally, the complexity of the rod-HGVG depends on the complexity of the point-GVG. First, we reason that the complexity of the planar rod-HGVG is the same as the complexity of the point-GVD, which is $O(n)$ where n is the number of obstacles.⁹ This is because there is a close relationship between the components of the point-GVD and the components of the planar rod-HGVG. For example, in an environment with no rod-HGVG meetpoints (i.e., the four-way equidistant configurations), there is a one-to-one correspondence between the rod-GVG edges and the point-GVD meetpoints, and a two-to-one correspondence between the one-tangent edges and the point-GVD edges. This implies that, in this simple case, the complexity of the point-GVD and the planar rod-HGVG is the same. If there are rod-HGVG meetpoints, then this simple relationship does not hold. However, since using the fact that the two rod-GVG edges are either connected by a one-tangent edge or rod-HGVG meetpoint, a similar relationship could be found.

Likewise, we try to compute the complexity of the rod-HGVG in three dimensions using the complexity of the point-GVG and the point-HGVG. Unfortunately, there is no result regarding the complexity of the point-GVG in three-dimensional space. If we assume all obstacles are isolated points, then the number of edges and nodes of the Voronoi diagram is $O(n^2)$, where n is the number of point obstacles (Aurenhammer and Klein 2000). In a d -dimensional space with point obstacles, the number of i -dimensional faces of the Voronoi diagram is $O(n^{\lfloor d/2 \rfloor})$ (Aurenhammer and Klein 2000). However, no general result is known when the obstacles are of general shape. Since the dimension of the configuration space is five, using the result for the point obstacles, the number of rod-GVG edges could naively be conjectured to be $O(n^{\lfloor 5/2 \rfloor})$. However, as we have seen, there is a close relationship between the number of components of the rod-HGVG

9. If we assume that the obstacles are polygonal, the complexity of the point-GVD also depends on the number of the vertices of the obstacles. However, here we do not make such assumptions.

Table 2. Rod-HGVG Nodes and the Types of Rod-HGVG Edges That are Connected to Them

Type of Node	Edges That are Connected to the Node
Meet configuration CF_{ijklmn}	Rod-GVG edges $CF_{ijklm}, CF_{ijkln}, CF_{ijkmn}, CF_{ijlmn}, CF_{iklmn}$ and CF_{jklmn}
Boundary configurations	(See text)
$R_{ijk} \cap R_{ij/kl}$	A one-tangent edge R_{ijk} and two-tangent edges $R_{ij/kl}, R_{ik/jl}$ and $R_{jk/il}$
$CF_{ijklm} \cap R_{ij/kl}$	A rod-GVG edge CF_{ijklm} and two-tangent edges $R_{ij/kl}, R_{ij/km}$ and $R_{ij/lm}$

and the number of components of the point-GVG. Thus, our conjecture is that there is a constant C so that the number of components of the rod-HGVG is bounded by C times the number of components of the point-GVG (i.e., the complexity of the rod-HGVG is also $O(n^2)$). This conjecture is based on the result for the point-GVG with point obstacles, which may not hold for the obstacles of general shape. Also, in Section 6, we extend the rod-HGVG using the point-HGVG so that the rod-HGVG is guaranteed to be connected in more general environment. To compute the complexity of the rod-HGVG with this extension, we need the complexity of the point-HGVG which is not known.

6. Extending the Rod-HGVG Using the Point-HGVG

In Section 3, we used the point-GVG to define the rod-HGVG and to ensure its connectivity. Alas, if the point-GVG were not connected, then the rod-HGVG might not be connected. In this section, we relax the assumption that the point-GVG be connected, and extend the rod-HGVG to the more general environment where the point-HGVG is connected. Since the rod-HGVG is based on the point-GVG, it is natural to define new structures based on the point-HGVG to connect the disconnected components of the rod-HGVG. That is, we define new structures in such a way that the rod-HGVG, with these new structures, is guaranteed to form a connected set in the environment where the point-HGVG is connected. Before we present the second-order structure of the rod-HGVG, we first review the components of the point-HGVG.

6.1. Point-HGVG in \mathbb{R}^3

Choset and Burdick (2000a, 2000b) extended the point-GVG into a three-dimensional space, resulting in the point hierarchical Voronoi graph (point-HGVG). As noted above, the point-GVG is, in general, not connected in \mathbb{R}^3 . To connect the point-GVG, they introduced new structures, called higher-order edges (Figure 4(b)). We consider an individual point two-way equidistant face F_{ij} , and we define new structures on it to connect the point-GVG edges, which are actually the boundary components of F_{ij} .

Here we need to consider obstacles other than the closest obstacles. For a point x in F_{ij} , the obstacles C_i and C_j are called the first closest obstacles and the obstacle with a distance smaller than the other obstacles, except C_i and C_j , is called the second closest obstacle. Since we consider the second closest obstacles as well as the first closest obstacles, we need to pay more careful attention to the definition of the distance function. Let $c_i(x)$ be the closest point on C_i from the point x , i.e., $c_i(x) = \operatorname{argmin}_{c \in C_i} \|x - c\|$. Note that, if there are multiple obstacles, the point $c_i(x)$ may not be “visible” from the point x . That is, the line segment connecting the points x and $c_i(x)$ may not lie completely in the free space. In this case, we define the distance between the point x and C_i to be infinity. This discussion leads us to use the “ V -distance function” $d_i^v(x)$, which is defined as

$$d_i^v(x) = \begin{cases} \min_{c \in C_i} \|x - c\| & \text{if } s(x, c_i(x)) \cap C_k = \emptyset \text{ for all } k \\ \infty & \text{otherwise} \end{cases} \quad (19)$$

where $s(x, c_i(x))$ is the line segment connecting the points x and $c_i(x)$.

There are four type of higher-order edges in \mathbb{R}^3 : (i) second-order point-GVG edges; (ii) occluding edges; (iii) boundary edges; (vi) floating boundary edges. The second-order point-GVG edge $F_{kl}|_{F_{ij}}$ is the subset of F_{ij} which contains the points satisfying $d_k^v(x) = d_l^v(x) < d_m^v(x)$ for all $m \neq i, j, k, l$. The intersection of two second-order point-GVG edges is called the second-order point-GVG meetpoint, denoted by $F_{klm}|_{F_{ij}}$. Second-order point-GVG edges can be used to find a disconnected point-GVG cycle, i.e., a point-GVG edge that is homeomorphic to S^1 and is not connected to any other point-GVG edges.

The occluding edge arises because of the use of the V -distance function. An occluding edge $V_{kl}|_{F_{ij}}$ is defined as the set of points on F_{ij} where the distance to the second closest obstacles C_k and C_l changes discontinuously.

The boundary edge is the set of points where the distances to two closest obstacles are zero, and the floating boundary edge is the set of points on F_{ij} where distance gradients to the two closest obstacles become the same, i.e., $\nabla d_i(x) = \nabla d_j(x)$. The boundary edge and floating boundary edge are required for completeness, but the simulation results from the

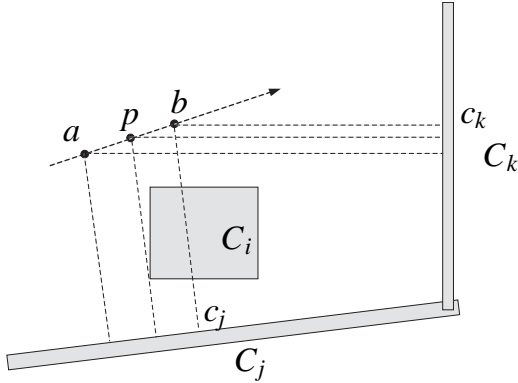


Fig. 35. The closest point on the obstacle C_j from the point b is the point c_j . However, if the line segment connecting x and c_j intersects the first closest obstacle C_i , the distance to the obstacle C_j is defined to be infinity for the V -distance function. As the robot moves from point a towards point b , the second closest obstacle changes from C_j to C_k at the point p , and the distance to the second closest obstacle changes discontinuously.

various environments seem to indicate that the point-HGVG forms a connected set without these higher-order edges.

Essentially, we are forming a cellular decomposition on F_{ij} (the cells are called second-order generalized Voronoi regions) and the higher-order edges are the boundary components of the cells. Unfortunately, in addition to these components, the point-HGVG also requires some linking strategies since these additional components do not guarantee that the point-HGVG is connected. Instead, these structures give clues about the “directions” to which the planner looks for the disconnected components of the point-HGVG components. A more detailed discussion on this subject can be found in Choset and burdick (2000a).

6.2. Second-order Components of the Rod-HGVG: Connecting the Rod-HGVG using the Point-HGVG

In this section, we define new components of the rod-HGVG, called higher-order edges, to connect the disconnected components of the rod-HGVG, and we discuss the construction methods for them. These new structures include (i) second-order one-tangent edges, (ii) second-order rod-GVG edges, and (iii) rod-occluding edges.

Since the rod-HGVG is defined using the point-GVG, it is natural to use the point-HGVG to define the components of the rod-HGVG. Just as the higher-order components of the point-HGVG are defined on a two-way equidistant-face F_{ij} , the higher-order components of the rod-HGVG are defined on a two-way equidistant structure. This two-way equidistant structure, denoted by RC_{ij} , is defined as

$$RC_{ij} = \{q \in CF_{ij} : \langle c_i(q) - c_j(q), PQ(q) \rangle = 0\}. \quad (20)$$

Essentially, RC_{ij} is the set of two-way equidistant configurations which are also tangent to the point two-way equidistant face F_{ij} . It can be shown that RC_{ij} is a three-dimensional manifold. Note that a two-tangent edge $R_{ij/kl}$ can be defined as the subset of RC_{ij} , i.e., $R_{ij/kl}$ is the set of configurations in RC_{ij} that are also four-way equidistant. Also, a one-tangent edge R_{ijk} can be viewed as the intersection of RC_{ij} and RC_{jk} . This produces a motivation to define the higher-order rod-HGVG structures on RC_{ij} , since we want the higher-order rod-HGVG structures to connect the disconnected components of the rod-HGVG. Just as the second-order point-GVG edges result in a planar GVD-like structure defined on the two-dimensional point two-way equidistant face F_{ij} , the second-order edges of the rod-HGVG result in a planar rod-HGVG-like structure defined on the three-dimensional manifold RC_{ij} . The rod-occluding edges are also defined on RC_{ij} , and allow the planner to find the disconnected component of the rod-HGVG, which is not “visible” from the current configuration.

Before we define the new components of the rod-HGVG, we briefly mention that if there is a point-GVG cycle, there can also be a one-tangent edge cycle, i.e., a one-tangent edge that is homeomorphic to S^1 and disconnected from any other components of the rod-HGVG. Then, from the continuity of the distance function, the one-tangent edge cycle has the same number of local maxima and local minima of the distance along it. This is a different situation from Section 3, where a one-tangent edge can have at most one local minimum of the distance on it and no local maxima. At the local minima of the distance, the rod can slide forwards along the length of the rod at the contact point between the rod and the point-GVG. At the local maxima, the rod also slides along the length of the rod, but here it moves backwards until the contact point changes from the one endpoint to the other, and then tracks the point-GVG.

6.3. Second-order One-tangent Edges

The second-order one-tangent edge is analogous to the second-order point-GVG edge, or, as its name suggests, analogous to the one-tangent edge of the planar rod-HGVG. This structure is not necessarily connected to the disconnected components of the rod-HGVG, but provides a “bridge” from which a link can be made to the disconnected components of the rod-HGVG.

The second-order one-tangent edges are defined as follows:

$$R_{kl} \mid_{RC_{ij}} = \{q \in RC_{ij} : \begin{aligned} & \text{(i)} D_k(q) = D_l(q), \\ & \text{(ii)} \nabla D_k(q) \neq \nabla D_l(q), \\ & \text{(iii)} \langle c_k(q) - c_l(q), PQ(q) \rangle = 0 \}. \quad (21) \end{aligned}$$

Essentially, the second-order one-tangent edge traces the

second-order point-GVG edge $F_{kl}|_{F_{ij}}$. Since $F_{kl}|_{F_{ij}}$ is the intersection of F_{ij} and SS_{kl} ,¹⁰ and the rod must be tangent to both of these planes to be an element of $R_{kl}|_{RC_{ij}}$, it follows that $r_i(q) = r_j(q) = r_k(q) = r_l(q)$ for all of the rod configurations in $R_{kl}|_{RC_{ij}}$.

The boundary component, i.e., the endpoint, of the second-order one-tangent edge is one of the following: (i) a boundary configuration (i.e., the distance to the closest obstacles becomes zero); (ii) a four-way equidistant configuration (i.e., a configuration on CF_{ijkl}); (iii) three-way equidistant to the second closest obstacles (i.e., a configuration q where $D_i(q) = D_j(q) < D_k(q) = D_l(q) = D_m(q)$ for an obstacle C_m – we call this configuration the second-order connect-configuration); (iv) a configuration on an occluding edge.

When the rod reaches a boundary configuration, it simply stops tracing the edge, and returns to the previous node with explored edges associated with it. When the rod reaches a four-way equidistant configuration, the rod is actually at a configuration in a two-tangent edge $R_{ij/kl}$, since the rod is at a configuration in RC_{ij} . Moreover, since $r_k(q) = r_l(q)$ at q , this is a configuration on $R_{kl/ij}$ as well.¹¹ If the rod reaches a configuration at which it is three-way equidistant to the second closest obstacles, as well as doubly equidistant to the first closest obstacles, then it is on a second-order rod-GVG edge, which is defined in the next section. The case of the occluding edge is discussed in more detail below.

Figure 37 shows an example of the second-order one-tangent edges in a rectangular enclosure with a box inside. Just as the one-tangent edges of the planar rod-HGVG do not form a connected set by themselves, the union of the second-order one-tangent edges does not form a connected set, even on a single RC_{ij} .

6.4. Second-order Rod-GVG Edges

The second-order rod-GVG edge is analogous to second-order point-GVG meetpoint, or to the rod-GVG edge for the planar rod-HGVG. Just as the rod-GVG edges connect the endpoints of the one-tangent edges for the planar rod-HGVG, the second-order rod-GVG edges connect the endpoints of the second-order one-tangent edges on RC_{ij} . The second-order rod-GVG edge is defined as

$$CF_{klm}|_{RC_{ij}} = \{q \in RC_{ij} : \begin{aligned} & \text{(i)} D_k(q) = D_l(q) = D_m(q), \\ & \text{(ii)} \nabla D_k(q) \neq \nabla D_l(q), \nabla D_l(q) \neq \nabla D_m(q), \\ & \nabla D_k(q) \neq \nabla D_m(q) \}. \end{aligned} \quad (22)$$

If the rod were small, $CF_{klm}|_{RC_{ij}}$ would be homeomorphic to S^1 , and there would be three second-order one-tangent edges emanating from it. If the rod were long, $CF_{klm}|_{RC_{ij}}$ would be homeomorphic to the union of the closed intervals of \mathbb{R} . In

10. $SS_{kl} = \{p \in \mathbb{R}^3 : 0 < d_k(p) = d_l(p), \nabla d_k(p) \neq \nabla d_l(p)\}$.

11. Note that this does not mean this configuration is on a one-tangent edge, since there is no guarantee that $\langle c_i - c_l, PQ(q) \rangle = 0$ at q .

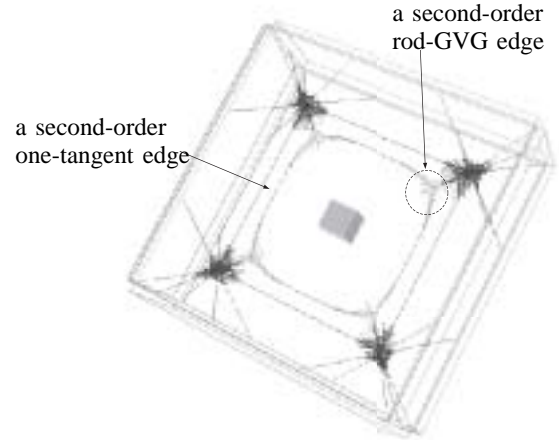


Fig. 36. The rod-HGVG with the second-order edges without the links. Note that there is a point-GVG edge (not shown) associated with the small box, the ceiling and the floor, and hence the one-tangent edge associated with the same set of obstacles. Without linking, just as the point GVG-cycle is disconnected from the other components of the point-HGVG, the one-tangent edge associated with the small box is disconnected from the rod-HGVG, even after the second-order edges are constructed.

this case, the boundary components of $CF_{klm}|_{RC_{ij}}$ are one of the following: (i) a configuration on a rod-GVG edge CF_{ijklm} ; (ii) a configuration on an occluding edge; (iii) a configuration that has the same distance to the four second closest obstacles (we call this the second-order rod-GVG meet-configuration).

In Figure 37, we can see that the second-order rod-GVG edges connect the second-order one-tangent edges that lie on the point two-way equidistant face defined by the top and bottom walls.

6.5. Connecting to a One-tangent Edge Cycle

Like the second-order point-GVG edges, the second-order one-tangent edges and the second-order rod-GVG edges do not actually connect two disconnected components of the rod-HGVG. Rather, from their structures, the planner can infer that there is a disconnected component of the rod-HGVG and make a connection to it. Here we describe how to make this connection.

For the point-HGVG, the existence of a set of second-order point-GVG edges, whose union is homeomorphic to S^1 , indicates that there could be a disconnected point-GVG cycle, i.e., a point-GVG edge that is homeomorphic to S^1 and disconnected from any other components of the point-GVG (Choset and Burdick 2000a). The planner accesses a disconnected point-GVG cycle using a gradient ascent restricted to

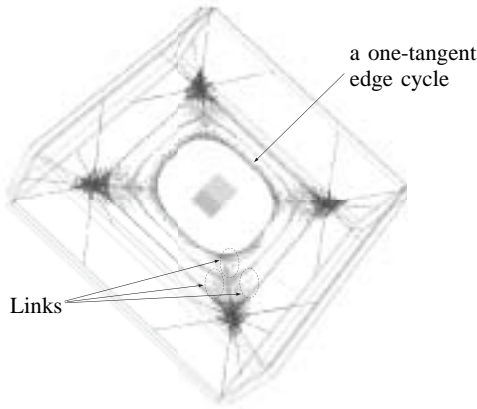


Fig. 37. The rod-HGVG in the same environment as Figure 36, but with the links. Using the links, the planner can access and trace the inner one-tangent edge cycle. There are links from each of the configurations where a second-order one-tangent edge and a second-order rod-GVG edge intersect each other.

F_{ij} from the second-point GVG meetpoints. In practice, it is computationally expensive to find a cycle in the point-GVG graph. Instead, the planner attempts to link to a point-GVG cycle at every second-order point-GVG meetpoint. This means that some redundant links are formed in the graph, while the time to search cycles is saved.

Now, note that if there is a point-GVG cycle, there can also be a one-tangent edge cycle, i.e., a one-tangent edge that is homeomorphic to S^1 and disconnected from any other components of the rod-HGVG. Just as the point-GVG cycle can be linked from the second-order point-GVG meetpoint, the one-tangent edge cycle can be linked from the second-order rod-GVG edge since the second-order rod-GVG edge is analogous to the second-order point-GVG meetpoint. Here, as in the point-HGVG, we try to connect to a one-tangent edge cycle from every second-order rod-GVG edge. Again, this will create some redundant links, while the time to search cycles is saved.

Since the second-order rod-GVG edge is a one-dimensional structure rather than a zero-dimensional structure, we need to choose specific configurations at which the connecting procedure starts. The natural choice would be the configurations where a second-order rod-GVG edge and a second-order one-tangent edge intersect each other, since they are the nodes of the rod-HGVG.

The linking is achieved in two steps. From a configuration $q \in CF_{klm}|_{RC_{ij}} \cap R_{kl}|_{RC_{ij}}$, the rod performs a gradient descent to C_k , while staying on RC_{ij} , until it becomes three-way equidistant to C_i , C_j , and C_k . The rod is guaranteed to terminate on a three-way equidistant configuration from the continuity of

the distance function. Let this three-way equidistant configuration be denoted by q' . From q' the rod aligns itself to the point-GVG edge defined by C_i , C_j , and C_k by following the solution of the curve

$$\dot{c}(t) = \pi_{CF_{ijk} \cap RC_{ij}} v(c(t))$$

where π is a projection operator and $v(q)$ is defined as $v(q) = (\pi_{F_{ij}}(-\nabla d_k(r_i(q))), 0)$. In a sense, we move the contact point between the rod and F_{ij} towards the point-GVG edge F_{ijk} while keeping the rod on $CF_{ijk} \cap RC_{ij}$. Figures 37 and 38 show the same environment as in Figure 37, but with the links to the inner one-tangent edge cycle constructed. Also note that there are some redundant links.

6.6. Rod-occluding Edges

The point-occluding edge for the point-HGVG is the set of points on F_{ij} where there is a discontinuity in the distance to the second closest obstacle. The motivation for accessing and tracing the point-occluding edge is to look for the point-HGVG components that are not visible from the “current” point-HGVG component. It is assumed that these invisible point-HGVG components are connected to the point-occluding edge. Thus, by tracing the point-occluding edge, the planner can access and start tracing the disconnected point-HGVG components. Recall that the components of the point-HGVG are the boundary components of the second-order Voronoi regions, which is defined on an individual F_{ij} , and thus if the point-occluding edge is not an isolated component of the point-HGVG, it must intersect some other components of the point-HGVG.

We could define the rod-occluding edge as the set of configurations where the distance to the second closest obstacle changes discontinuously, which is analogous to the definition of the point-occluding edge. This, in turn, would imply that the rod-occluding edge is a boundary component of the second-order generalized Voronoi region (which could be defined on the rod two-way equidistant face CF_{ij} , i.e., the set of double equidistant configurations) in the configuration space. However, it should be noted that the other components of the rod-HGVG are not necessarily the boundary components of the Voronoi region or any higher-order Voronoi region, which could be defined recursively on the boundary of the Voronoi region. Thus, there is no guarantee that the rod-occluding edge defined as the boundary component of the second-order generalized Voronoi region intersects any other components of the rod-HGVG.

Instead, we define the rod-occluding edge in such a way that the rod “traces” or “tracks” the point-occluding edge. By tracing, we mean that a rod-occluding edge $RV_{kl}|_{RC_{ij}}$ is defined such that the equation

$$V_{kl}|_{F_{ij}} = \cup_{q \in RV_{kl}|_{RC_{ij}}} r_i(q) \quad (23)$$

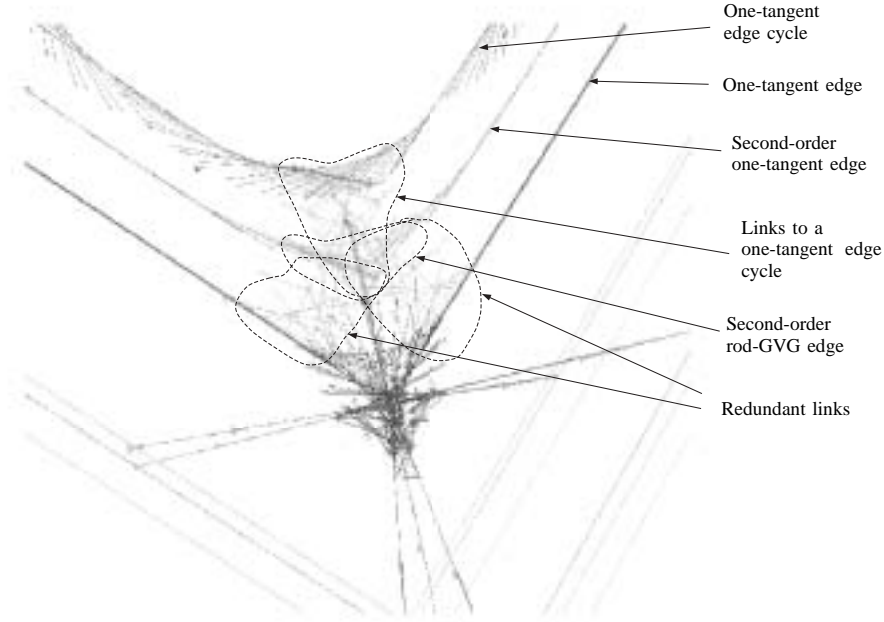


Fig. 38. This figure shows part of the rod-HGVG in the environment shown in Figure 37 to illustrate, in more detail, the links from the second-order connecting configurations to the inner one-tangent edge cycle. Note also that there are redundant links to the one-tangent edges which do not form a cycle.

is satisfied, where $V_{kl}|_{F_{ij}}$ is a point-occluding edge. This implies that for any point x in $V_{kl}|_{F_{ij}}$, there is a rod configuration q in $RV_{kl}|_{CF_{ij}}$ such that $r_i(q) = r_j(q) = x$. Now, assume that a second-order point-GVG edge $F_{ij}|_{F_{lm}}$ intersects the point-occluding edge $V_{kl}|_{F_{ij}}$ at a point x' . Then, if eq. (23) is satisfied, there is a configuration $q' \in RV_{kl}|_{RC_{ij}}$, such that $r_i(q') = r_j(q') = V_{kl}|_{F_{ij}} \cap F_{ij}|_{F_{lm}}$. The configuration q' is not necessarily an element of the second-order one-tangent edge RC_{ij} since q' may not be equidistant to C_k and C_l . However, from q' , we could reach a configuration on $RV_{kl}|_{RC_{ij}}$ by sliding and rotating the rod around the point $x' = V_{kl}|_{F_{ij}} \cap F_{ij}|_{F_{lm}}$, which is not difficult since the rod is already in the tangent space of F_{ij} (because the rod-occluding edge is defined on RC_{ij}) and from the point $r_i(q)$, the tangent direction of $F_{ij}|_{F_{lm}}$ can be readily computed. Similar statements can be made about the point-GVG edge intersecting the point-occluding edge and the one-tangent edge associated with it. This means that if a point-HGVG component is connected to the point-occluding edge, the rod-HGVG structure associated with that point-HGVG component can also be easily detected and reached from $RV_{kl}|_{RC_{ij}}$.

With this in mind, we define the rod-occluding edge as follows:

$$RV_{kl}|_{RC_{ij}} = \{q \in RC_{ij} : r_i(q) \in V_{kl}|_{F_{ij}} \text{ and } R(q) \text{ normal to } V_{kl}|_{F_{ij}}\}. \quad (24)$$

The second condition, i.e., the condition that $R(q)$ is normal to the point-occluding edge, is in some sense arbitrary, and the rod-occluding edge can be defined in different ways as long as it satisfies eq. (23). We use this definition because, from the simulation results of the point-HGVG in various workspaces, it is observed that, quite often, but not always, the point-HGVG components intersect the point-occluding edge at an angle of $\pi/2$. Thus, this definition of the rod-occluding edge could make it easier to connect the rod-occluding edge and the rod-HGVG components that intersect the rod-occluding edge.

The rod-occluding edge can be accessed from a configuration in the one-tangent edge through a gradient descent restricted to RC_{ij} . The planner starts the linking procedure on the configuration in the one-tangent edge where the distance to the closest obstacles attains a local minima. The planner terminates tracing the rod-occluding edge when (i) a rod-occluding edge cycle is detected, and (ii) the rod-occluding edge intersects another rod-occluding edge. Recall that for the point-HGVG, it was not possible to determine the tangent direction of the point-occluding edge precisely, and the planner in fact traces the point-occluding edge in a zigzag manner. We can assume that a similar kind of phenomenon would happen in the case of rod-occluding edges defined using the rod-distance function. Then, it would not be easy to determine when the rod should terminate tracing an occluding edge cycle, because it is not generally possible to align the rod precisely along the

point-occluding edge. However, with this definition, the rod can terminate tracing the occluding-edge when the point $r_i(q)$ becomes sufficiently close to the point $r_i(q_s)$ of the starting configuration q_s , even if there is some error in the orientation.

6.7. Tracing the Rod-occluding Edge

The second-order one-tangent edges and the second-order rod-GVG edges can be constructed exactly the same way as the rod-HGVG edges are constructed, as described in Lee, Choset, and Rizzi (2001). However, we cannot construct the rod-occluding edge using the same technique, since the rod-occluding edge is defined using the discontinuity of a function.

Recall that, even for the point-HGVG, it is not possible to trace the point-occluding edge precisely since the planner cannot determine the precise tangent direction of the occluding edge. Likewise, we cannot expect the planner to trace the rod-occluding edge precisely either. Therefore, we present an approximate method to trace the rod-occluding edges.

First we make some observations. We define the point-occluding face V_{kl} as the set of points in the free workspace, where the distance to the second closest obstacle changes discontinuously. Then the point-occluding edge $V_{kl}|_{F_{ij}}$ can be defined as the intersection of V_{kl} and F_{ij} . Here, we assume that given a rod configuration q (not necessarily on a rod-occluding edge), if $R(q)$ intersects V_{kl} , we can find the point of the intersection, denoted $o_{kl}(q)$. We also assume that we can find the point $c_k(o_{kl}(q))$, i.e., the closest point on the obstacle C_k from the point $o_{kl}(q)$. Since we assume that we have a series of range sensors along the length of the rod, it will not be difficult in practice to find the point where the distance to the second closest obstacle changes discontinuously. Then, by definition of the point-occluding face, the line passing through $o_{kl}(q)$ and $c_k(o_{kl}(q))$, denoted by $l_{occ}^{kl}(q)$, is tangent to the boundary of the obstacle C_i (assuming, without loss of generality, C_i occludes C_k), and also lies on V_{kl} . This means that there is a plane $T_{occ}^{kl}(q)$ tangent to V_{kl} along $l_{occ}^{kl}(q)$. Finally, if we consider the plane $N_{occ}^{kl}(q)$ that intersects $T_{occ}^{kl}(q)$ at $l_{occ}^{kl}(q)$ and is normal to $T_{occ}^{kl}(q)$, it is not difficult to see that $N_{occ}^{kl}(q)$ is also normal to V_{kl} , and more specifically, $N_{occ}^{kl}(q)$ is normal to $V_{kl}|_{F_{ij}}$ at the point $p = V_{kl}|_{F_{ij}} \cap N_{occ}^{kl}(q)$. This means that a configuration q' such that $R(q') \subset N_{occ}^{kl}(q)$, can easily access the rod-occluding edge by sliding on $N_{occ}^{kl}(q)$.

Now we describe a tracing method for the rod-occluding edge, which consists of two steps: (i) a prediction step; (ii) a correcting step.

The prediction step from a rod configuration q on the occluding edge $RV_{kl}|_{RC_{ij}}$, is a translation of the rod on $T_{r_i(q)}F_{ij}$ (i.e., the plane tangent to F_{ij} at $r_i(q)$), in a direction normal to the vector $PQ(q)$. After the prediction step, the rod would not be on the rod-occluding edge in general. More specifically, the rod might not be on RC_{ij} , and even if it is on RC_{ij} , it might not be normal to the point-occluding edge.

Let q' be the configuration after the prediction step. The correction step works in two steps. First it brings the rod onto

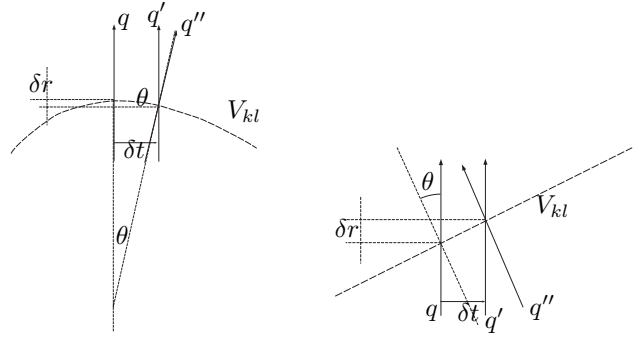


Fig. 39. First correction step. After making a prediction step by translating by δt (from q to q'), the rod is in general not normal either to the occluding edge or the occluding face V_{kl} . Left: the curved occluding edge. If δt is small so that the occluding edge can be approximated by a circle, we have $\theta = \tan^{-1}(\delta t / \delta o_{kl})$. Right: the initial angle between the rod and the occluding is not $\pi/2$. The correcting θ is computed by $\theta = \tan^{-1}(\delta t / \delta o_{kl})$, where δo_{kl} is the change of the o_{kl} on the rod. Note that we have the same equation for both cases, and can make a correction by rotating the rod by θ , resulting in the configuration q'' .

$N_{occ}^{kl}(q')$, i.e., after the first correcting step, $R(q') \subset N_{occ}^{kl}(q')$. Then while keeping the rod on $N_{occ}^{kl}(q')$, the second correction step brings the rod back on a configuration in RC_{ij} , which according to the discussion above, is an element of $RV_{kl}|_{RC_{ij}}$ also.

The first step can be carried out as follows. Assume that initially the angle between $R(q)$ and $V_{kl}|_{F_{ij}}$ is $\pi/2 + \theta$. Then, as shown in Figure 39, unless $\theta = 0$, the point $o_{kl}(q)$ changes its location on the rod, and we can approximately compute the correcting term as $\theta = \tan^{-1}(\delta t / \delta o_{kl})$, where δt is the translational step size and δo_{kl} is the change in $o_{kl}(q)$ on the rod. Then, by rotating the rod by θ around $o_{kl}(q)$ on the plane defined by $PQ(q)$ and $PQ(q')$, we can bring the rod on the $N_{occ}^{kl}(q')$.

Let q'' denote the configuration after the first correction. In general, q'' will not be an element of the rod-occluding edge yet and we need a second correcting step that brings the rod onto RC_{ij} . For this, the rod performs a gradient descent of the function $\{D_i - D_j, \langle PQ, c_i - c_j \rangle\}(q)$, while keeping the rod on the plane $N_{occ}^{kl}(q)$, which can be computed using the vectors $PQ(q)$ and $c_i(q) - o_{kl}(q)$ (Figure 40).

This is the description of the tracing methods for the rod-occluding edge. Note that for the first correction step, we assume that after taking a prediction step, the rod still intersects the point-occluding face. However, since the point-occluding edge and the point-occluding face can have sharp corners, it is possible that the rod may not intersect the point-occluding

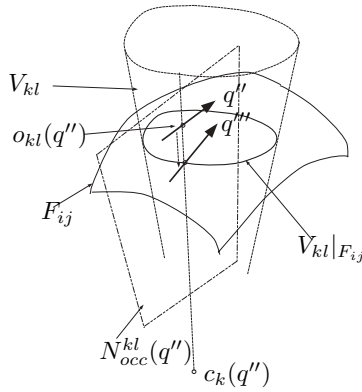


Fig. 40. Second correction step: correcting onto RC_{ij} . From the configuration q'' , the rod corrects to q''' which is in RC_{ij} by gradient descent. During this correction, the rod maintains tangency to the plane $N_{occ}^{kl}(q'')$.

face after the prediction step. Also, if initially the rod is tangent to the point-occluding edge, the rod will not intersect the point-occluding face after the prediction step. Our current work involves development of additional methods to solve these problems.

7. Conclusion

In this paper we introduce a new roadmap, called the rod-HGVG, for a rod-shaped robot operating in a three-dimensional workspace. This roadmap is defined in terms of workspace distance and therefore can be constructed using only range-sensor information and without ever constructing the configuration space.

Although the definition of the rod-HGVG and its incremental construction procedure are contributions unto themselves, we feel that there are some deeper conceptual contributions. The first is the piecewise retract. The configuration space for the rod-HGVG is five-dimensional, and, according to homotopy theory, a one-dimensional deformation retract of the space with dimension greater than two cannot be defined. Therefore, instead of defining a deformation retract for the entire free configuration space, the free configuration space is decomposed into cells in which deformation retracts can be defined. First, the rod four-way equidistant face defines an exact cellular decomposition of the free configuration space, where each cell is called a junction region and the deformation retract of a junction region is a rod four-way equidistant face. However, this deformation retract is two-dimensional, and thus we define another decomposition on it. That is, the two-tangent edges and the rod-GVG edges define another cellular decomposition of a rod four-way equidistant face, where

the deformation retract of a cell (called a subjunction region) is a two-tangent edge or a rod-GVG edge. The two-tangent edges and the rod-GVG edges in a single connected subjunction region form a connected set, making the planning in a subjunction region trivial. In actuality, in this work, we are defining a hierarchical piecewise retract: at the high level, the rod four-way equidistant faces form one piecewise retract connected by point-GVG edges and, at the lower level, the two-tangent edges also form a deformation retract, which we show form a connected set on the rod four-way equidistant faces.

The second contribution of this work is that it uses the connectivity of the workspace to infer connectivity properties of the robot's configuration space. The one-tangent edges are used to connect the deformation retracts we defined, and thus guarantee the connectivity of the roadmap in configuration space. However, the one-tangent edges are defined using point-GVG edge, which represent the connectivity of the workspace. In some sense, the one-tangent edges form the backbone of the rod-HGVG, rather than the deformation retracts, and the deformation retracts can be viewed as the structures that link up the disconnected one-tangent edges.

The fact that we can use structures based on the workspace topology as the backbone of the configuration space is not surprising given the fact that the configuration space we are considering is not just an arbitrary five-dimensional space, but has some special structure, i.e., it is diffeomorphic to $\mathbb{R}^3 \times S^2$. This observation is related to the fact that we used the two-dimensional rod four-way equidistant faces as the deformation retracts instead of the five-way equidistant sets, i.e., the rod-GVG edges. One of the reasons why we use the four-way equidistant faces is that they always exist for rod robots operating in bounded three-dimensional workspaces. Moreover, a deformation retraction to four-way equidistant faces can be easily defined using fixed-orientation gradient ascent, since the configuration space for a robot with a fixed orientation is essentially the three-dimensional Euclidean space. From this observation, we believe that even for highly articulated robots operating in two- or three-dimensional workspace, the three- and four-way equidistant faces (respectively) would be important components of the roadmap. These three- or four-way equidistant faces (respectively) would not be one-dimensional, but the one-dimensional edges could be defined on them using additional constraints such as the tangency condition.

In this paper, we assumed that range sensors along the rod have an infinite range. If the range sensors have only a finite range, and the environment is sparse, the rod-HGVG, as represented in this paper, could not be constructed in a sensor-based way, since the distance to the closest obstacle(s) from some of the edges may exceed the sensor range. In such cases, to explore the environment, some form of coverage would be needed to find obstacles that are out of sensor range from the current position of the robot. One solution would

be to adopt a scheme similar to that used in Acar, Choset, and Atkar (2001), in which they used a simple back-and-forth coverage motion together with the point-GVG to efficiently cover a two-dimensional unknown space with range sensors with a finite range. In a three-dimensional space, we first need to define lower-dimensional subsets of the space, and then perform the coverage on lower-dimensional subsets.

Finally, as we mentioned before, this work is a step towards the motion planning of highly articulated robots. The next step is planning for a convex body. Then we will consider motion planning of a two-body robot operating in two- or three-dimensional workspace. We believe these problems can give us some insight about the issues relating to more general multibody problems.

Appendix A: Rod Gradient

Here, we derive the rod distance gradient. In Figure A1, X , Y , and Z denote the world coordinate frame, and X_r , Y_r , and Z_r denote the body fixed coordinate frame on R (the rod). Let $(x, y, z)^T$ be the origin of the body fixed coordinate frame, and let θ , φ be the orientation of the body fixed coordinate frame with respect to the world coordinate frame. Let c be the closest point on the obstacle C_i to the robot and let r be the closest point to C_i on the robot. Finally, let $(a, b, c)^T$ be the coordinates of r in the body fixed coordinate frame. Then the world coordinate of r is

$$r = \begin{bmatrix} x + a \cos \theta \cos \varphi - b \sin \theta + c \cos \theta \sin \varphi \\ y + a \sin \theta \cos \varphi + b \cos \theta + c \sin \theta \sin \varphi \\ z - a \sin \varphi + c \cos \varphi \end{bmatrix}.$$

Then, following similar steps to the two-dimensional case (Choset and Burdick 1996), the first three components of the distance gradient are

$$\left[\frac{\partial D}{\partial x}, \frac{\partial D}{\partial y}, \frac{\partial D}{\partial z} \right] = \frac{1}{D_i(q)} [(r_x - c_x), (r_y - c_y), (r_z - c_z)].$$

The remaining two rotational components are

$$\frac{\partial D}{\partial \theta} = \frac{1}{D_i(q)} \left\langle \begin{bmatrix} c_x - r_x \\ c_y - r_y \\ c_z - r_z \end{bmatrix}, \begin{bmatrix} aS\theta C\varphi + bC\theta + cS\theta S\varphi \\ -aC\theta C\varphi + bS\theta - cC\theta S\varphi \\ 0 \end{bmatrix} \right\rangle$$

$$\frac{\partial D}{\partial \varphi} = \frac{1}{D_i(q)} \left\langle \begin{bmatrix} c_x - r_x \\ c_y - r_y \\ c_z - r_z \end{bmatrix}, \begin{bmatrix} aC\theta S\varphi - cC\theta C\varphi \\ aS\theta S\varphi + cS\theta C\varphi \\ aC\varphi + cC\varphi \end{bmatrix} \right\rangle$$

where $C\theta$ and $S\theta$ denote $\cos \theta$ and $\sin \theta$, respectively.

Appendix B: Accessibility Proof (Section 4.1)

In this appendix, we demonstrate that a rod starting at a four-way equidistant configuration will access either (i) a rod-GVG edge or (ii) a two-tangent edge via full gradient ascent of distance to the four closest obstacles. Assume that the rod is

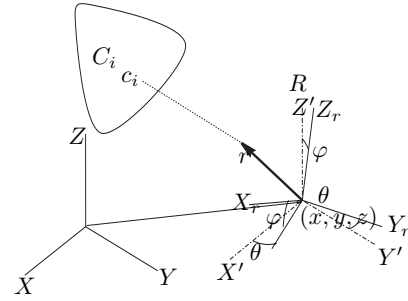


Fig. A1. World and body coordinate system for the rod.

four-way equidistant to C_i , C_j , C_k , and C_l , i.e., $q \in CF_{ijkl}$. Proving case (i) is trivial. Now, we prove case (ii), i.e., the gradient ascent will eventually direct the rod onto the $R_{ij/kl}$ when there are no five-way equidistant configurations. Let $SS_{kl} = \{x \in \mathbb{R}^3 | d_k(k) = d_l, \nabla d_k \neq \nabla d_l\}$, i.e., SS_{kl} is the two-way equidistant surface in the workspace. Then, since, by assumption, the rod has same distance to C_k and C_l , the set $R(q)$ must intersect SS_{kl} . Figure B1 shows a rod configuration which intersects SS_{kl} . Consider the plane formed by the rod vector PQ and the vector $r_k c_k$. Then let the global coordinate frame be located such that (i) the origin is located on P , (ii) the X - and Y -axes are on the plane formed by PQ and $r_k c_k$. Then the Z -axis of the global coordinate frame is perpendicular to that plane. In that frame, the rod configuration is at $(0, 0, 0, 0)$ and the body fixed frame coordinate of r is $(a, 0, 0)$ with some positive value a . Note that in this coordinate system, the θ component of the gradient rotates the rod “in” the plane, and the φ component of the gradient rotates the rod out of the plane. We are interested in the θ component, which, for the obstacle C_k , is

$$\frac{\partial D}{\partial \theta} = \frac{1}{D_i(q)} \left\langle [c_k^x - r_k^x, c_k^y - r_k^y, 0]^T, [a_k \sin \theta, -a_k \cos \theta, 0]^T \right\rangle.$$

Then, the two vectors $(c_k^x - r_k^x, c_k^y - r_k^y, 0)^T$ and $(a_k \sin \theta, -a_k \cos \theta, 0)^T$ are parallel. Thus, $\partial D_k / \partial \theta$ has a positive value, and this means that the angle between the tangent plane on SS_{kl} and the rod increases as a result of gradient ascent. Now, we perform the same analysis with $r_l c_l$; the vector $r_l c_l$ is in the “opposite” direction of $(a_l \sin \theta, -a_l \cos \theta, 0)^T$ and the coordinate value of a_l is larger since r_l is on the “other side” of SS_{kl} . This means that the gradient for C_l has a negative component of $\partial D_l / \partial \theta$ on the plane defined by PQ and $r_l c_l$, with a larger value than $\partial D_k / \partial \theta$. This decreases the angle between the tangent plane and the rod. So, the gradient ascent decreases the angle between the tangent plane and the rod, thus forcing the rod to become “tangent” to the tangent plane.

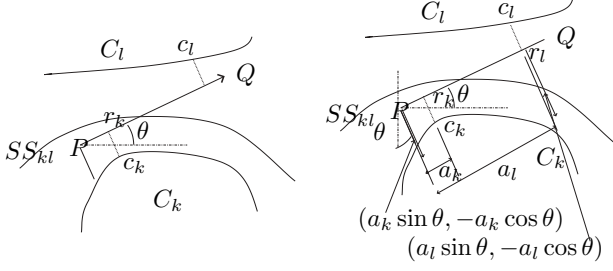


Fig. B1. The rod is equidistant to obstacles C_k and C_l . The closest points on the rod and each obstacles are shown. The rod intersects SS_{kl} transversally. The rod is shown on the plane defined by PQ and $r_k c_k$. In this figure $r_l c_l$ is on the same plane, but in general it may be on a different plane.

Appendix C: Continuity of the Mappings H and HJ (Section 4.1)

In this appendix, we prove that the mappings H and HJ , defined in Section 4.1, are continuous mappings. We do this by showing that the general gradient ascent operation from a fixed set of obstacles is continuous. Then, since H and HJ are both gradient operations from fixed sets of obstacles, they are continuous.

Given two points x_1 and $x_2 \in \mathbb{R}^m$ with $|x_1 - x_2| = \lambda$ and a convex obstacle C , let c_1 and c_2 be the closest points on the obstacle to x_1 and x_2 , respectively. Also, let d_1 and d_2 be their respective distances to the obstacle. Without loss of generality, we assume that $d_1 \leq d_2$. If $d_2 - d_1 > \lambda$, then $d_2 > d_1 + \lambda = |c_1 - x_1| + |x_1 - x_2| > |c_1 - x_2|$, which is a contradiction. Therefore,

$$|d_1 - d_2| \leq \lambda.$$

Also, for c_i , let S_1 and S_2 be the spheres centered on x_1 and x_2 with radii d_1 and d_2 , respectively, and let $c_1 c_2$ be the line segment connecting c_1 and c_2 . Consider a line segment whose endpoints are on each sphere such that the segment itself does not intersect the interior of either sphere. Since the centers of the sphere are λ apart, the length of this line segment is at most $\lambda = |x_1 - x_2|$. Therefore,

$$|c_1 - c_2| \leq \lambda. \quad (25)$$

Given two configurations of the rod, q_1 and q_2 , let q_m be the configuration such that $\Theta(q_m) = \Theta(q_1)$ and $P(q_m) = P(q_2)$. Then, $d(q_1, q_m) \leq d(q_1, q_2)$ and $d(q_2, q_m) \leq d(q_1, q_2)$ (Figure C1). Then,

$$|r_1 - r_m| \leq |P(q_1) - P(q_m)| \leq d(q_1, q_m) \leq d(q_1, q_2)$$

where r_1 and r_m are the closest points on the rod to the obstacle at each configuration.

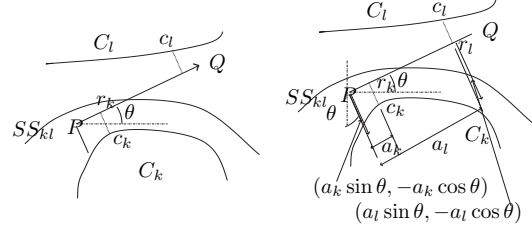


Fig. C1. Given two points, x_1 and x_2 , the distance between the closest points on the obstacle, c_1 and c_2 , from each point cannot be larger than L , which is smaller than $|x_1 - x_2|$.

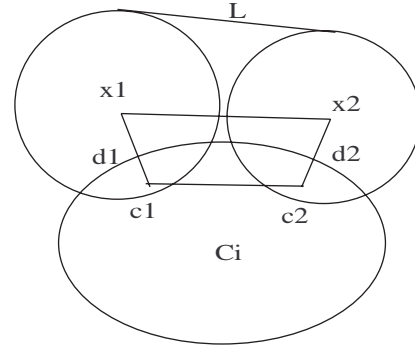


Fig. C2. When we rotate q_1 to q'_1 , the distance $D_i(q)$ and the closest point on the rod $r(q_1)$ do not change.

Now we consider q_m and q_2 . Let $c_i r_i$ be the vector defined by two points, c_i and r_i , and let $PQ(q_i)$ be the vector defined by P and Q , the two endpoints of the rod at configuration q_i . Given q_i , if $\angle(PQ(q_i))(c_i r_i) \neq \pi/2$, then r_i is on either P or Q . For these configurations, we can find a rod configuration q'_i such that $P(q_i) = P(q'_i)$, $r_i = r'_i$, and $\angle(PQ(q'_i))(c_i r_i) = \pi/2$ ¹² (see Figure C2). So, given q_m and q_2 , let q'_m and q'_2 be such configurations for each q_m and q_2 . Then, $|r_2 - r_m| = |r'_2 - r'_m|$, so, without loss of generality, we can assume that $\angle(PQ(q_m))(c_m r_m) = \angle(PQ(q_2))(c_2 r_2) = \pi/2$.

Let ρ_i be the radius of curvature of the wall of the obstacle at c_i , and L be the length of the rod. Then

$$\begin{aligned} |r_m - r_2| &\leq M|(D(q_m) + \rho(q_m))\Theta(q_m) \\ &\quad - (D(q_2) + \rho(q_2))\Theta(q_2)| \\ &\leq M(\max(D(q_m), D(q_2)) + \rho)d(q_m, q_2) \\ &\leq M(\max(D(q_m), D(q_2)) + \rho)d(q_1, q_2) \end{aligned}$$

for some constant M (see Figure C3). Then, assuming that there is no “flat” wall, $\rho < \rho_{max}$ for some constant ρ_{max} , and since the environment is bounded, i.e., $D(q) < D_{max}$, for some D_{max} . Thus,

$$|r_m - r_2| \leq K'd(q_1, q_2)$$

12. $c'_i = c_i$, $r'_i = r_i$.

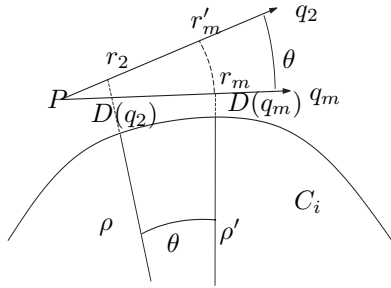


Fig. C3. Here, r_2 and r_m are the closest points on the rod at configurations q_2 and q_m , respectively, and r'_m is the point on the rod at q_2 corresponding to r_m at q_m . Then, $|r_m - r_2| \leq |r_m - r'_m| + |r'_m - r_2| \leq L\theta + (\rho(q_2) + D_i(q_2))\theta$.

where $K' = (D_{max} + \rho_{max})$. Therefore, for any q_1 and q_2

$$|r_1 - r_2| \leq |r_1 - r_m| + |r_m - r_2| \leq d(q_1, q_2) + K'd(q_1, q_2) = Kd(q_1, q_2) \quad (26)$$

for some constant $K = (1 + K')$. Then, from eqs. (25) and (26),

$$|c_1 - c_2| \leq |r_1 - r_2| \leq Kd(q_1, q_2) \quad (27)$$

for some K .

Now, we want to show that $\dot{H}(q, t)$ satisfies the Lipschitz condition with respect to q in free space. First, for gradient ascent from the closest obstacle, $\dot{H}(q, t) = \dot{H}(q) = D_1(\underline{H}(q, t))\nabla(D_1(\underline{H}(q, t)))$, which is

$$\begin{aligned} \dot{H}(q, t) &= D_1(\underline{H}(q, t))\nabla D_1(\underline{H}(q, t)) \\ &= \begin{bmatrix} \nabla d'_1(r(\underline{H}(q, t))) \\ U(\underline{H}(q, t)) \times \nabla d'_1(r(\underline{H}(q, t))) \end{bmatrix} \quad (28) \end{aligned}$$

where $\nabla d'_1(r) = (r - c)$, and $U(q) = r(q) - P(q)$. We want to show that

$$|\dot{H}(q_1, t) - \dot{H}(q_2, t)| < M|q_1 - q_2|$$

for some constant M .

$$\begin{aligned} |\dot{H}(q_1, t) - \dot{H}(q_2, t)| &= \\ & \left[\begin{array}{c} \nabla d'_1(r(\underline{H}(q_1, t))) \\ U(\underline{H}(q_1, t)) \times \nabla d'_1(r(\underline{H}(q_1, t))) \end{array} \right] \\ & - \left[\begin{array}{c} \nabla d'_1(r(\underline{H}(q_2, t))) \\ U(\underline{H}(q_2, t)) \times \nabla d'_1(r(\underline{H}(q_2, t))) \end{array} \right] \quad (29) \end{aligned}$$

Since

$$\begin{aligned} |\nabla d'_1(r(\underline{H}(q_1, t))) - \nabla d'_1(r(\underline{H}(q_2, t)))| &= \\ |(r_1 - c_1) - (r_2 - c_2)| & \\ \leq |r_1 - r_2| + |c_1 - c_2| & \end{aligned}$$

from eqs. (26) and (27),

$$|\nabla d'_1(r(\underline{H}(q_1, t))) - \nabla d'_1(r(\underline{H}(q_2, t)))| \leq M_1d(q_1, q_2)$$

for some constant M_1 . Since,

$$\begin{aligned} |(r_1 - c_1) - (r_2 - c_2)| &< (|r_1 - r_2| + |c_1 - c_2|) \\ &< 2d(q_1, q_2), \end{aligned}$$

it follows that

$$|\nabla d_j(r_1) - \nabla d_j(r_2)| < 2d(q_1, q_2).$$

Also, for $U(q_1)$ and $U(q_2)$

$$\begin{aligned} |U(\underline{H}(q_1, t)) - U(\underline{H}(q_2, t))| &= |(r_1 - P(\underline{H}(q_1, t))) \\ & \quad - (r_2 - P(\underline{H}(q_2, t)))| \\ &= |(r_1 - r_2) - (P(\underline{H}(q_1, t)) \\ & \quad - P(\underline{H}(q_2, t)))| \\ &< (|r_1 - r_2| + |P(\underline{H}(q_1, t)) \\ & \quad - P(\underline{H}(q_2, t))|). \end{aligned}$$

Therefore,

$$|U(\underline{H}(q_1, t)) - U(\underline{H}(q_2, t))| \leq M_2d(q_1, q_2)$$

for some constant M_2 .

Hence,

$$\begin{aligned} &|U(\underline{H}(q_1, t)) \times \nabla d'_1(r(\underline{H}(q_1, t))) \\ & \quad - U(\underline{H}(q_2, t)) \times \nabla d'_2(r(\underline{H}(q_2, t)))| \\ &= |U(\underline{H}(q_1, t)) \times (\nabla d'_1(r(\underline{H}(q_1, t))) - \nabla d'_2(r(\underline{H}(q_2, t)))) \\ & \quad + (U(\underline{H}(q_1, t)) - U(\underline{H}(q_2, t))) \times \nabla d'_2(r(\underline{H}(q_2, t)))| \\ &\leq |U(\underline{H}(q_1, t)) \times (\nabla d'_1(r(\underline{H}(q_1, t))) - \nabla d'_2(r(\underline{H}(q_2, t))))| \\ & \quad + |(U(\underline{H}(q_1, t)) - U(\underline{H}(q_2, t))) \times \nabla d'_2(r(\underline{H}(q_2, t)))| \\ &\leq |U(\underline{H}(q_1, t))| |\nabla d'_1(r(\underline{H}(q_1, t))) - \nabla d'_2(r(\underline{H}(q_2, t)))| \\ & \quad + |(U(\underline{H}(q_1, t)) - U(\underline{H}(q_2, t)))| |\nabla d'_2(r(\underline{H}(q_2, t)))| \\ &\leq M'd(q_1, q_2)|U(\underline{H}(q_1, t))| + M''d(q_1, q_2)| \\ & \quad \nabla d'_2(r(\underline{H}(q_2, t)))| \end{aligned}$$

for some constants M' and M'' . Since $|U| \leq L$ and $|\nabla d'_2(r(\underline{H}(q_2, t)))| = |r(\underline{H}(q_2, t)) - c(\underline{H}(q_2, t))| \leq M'''$ for some M''' from the boundedness of the environment,

$$\begin{aligned} &|U(\underline{H}(q_1, t)) \times \nabla d'_1(r(\underline{H}(q_1, t))) \\ & \quad - U(\underline{H}(q_2, t)) \times \nabla d'_2(r(\underline{H}(q_2, t)))| \\ &\leq Nd(q_1, q_2) \end{aligned}$$

for some N .

So, $\dot{H}(q, t)$ also satisfies Lipschitz condition, i.e.,

$$|\dot{H}(q_1, t) - \dot{H}(q_2, t)| < Md(q_1, q_2)$$

for some constant M for any q_1 and q_2 . Therefore, there exists $\underline{H}(q, t)$ which satisfies the above condition and is also continuous on t and the initial condition, i.e., q (Brand 1966).

For gradient ascent with double or triple equidistance, since $\underline{H}(q, t) = \pi_T \nabla(D_1)$ or $\underline{H}(q, t) = \nabla(D_1 - D_2)$, etc., it also satisfies the condition.

At this point, we could use \underline{H} as our accessibility criterion and our deformation retraction. From here we can conclude that CF_{ijk} is a deformation retraction of a junction region J_{ijk} using \underline{H} . In implementation we use H , which is defined as $H = \underline{H}(q, t)/D(\underline{H}(q, t))$.

Appendix D: Proof of Lemma 1 (Section 4.4)

Here we prove Lemma 1 in Section 4.4, which states that for two adjacent junction regions, J_{ijkl} and J_{ijkm} , if the one-tangent edge $R_{ijk} = \emptyset$, then CF_{ijkl} and CF_{ijkm} intersect each other.

Proof. First, we define

$$\begin{aligned} SR_{ijk} &= \{q : 0 < D_i(q) = D_j(q) = D_k(q), \\ &R(q) \text{ is tangent to } F_{ijk}\}. \end{aligned} \quad (30)$$

Note that SR_{ijk} does not have the condition $D_k(q) < D_l(q)$, $l \neq i, j, k$, and SR_{li} always exists even if R_{li} does not. Now SR_{ijk} is a subset of the union of two adjacent junction regions J_{ijkl} and J_{ijkm} , and thus can be viewed as the structure which connects the two junction regions J_{ijkl} and J_{ijkm} .

Recall the definition of $CF_{ijkl/m}$, introduced in Section 4.5:

$$\begin{aligned} CF_{ijkl/m} &= \{q \in FS \mid 0 < D_i(q) = D_j(q) = \\ &D_k(q) = D_l(q) \leq D_o(q), \\ &o \neq m, i, j, k, l\}. \end{aligned}$$

Clearly, $CF_{ijkl} \subset CF_{ijkl/m}$, and if CF_{ijkl} intersects another four-way equidistant face CF_{ijkm} , forming a rod-GVG edge CF_{ijklm} , then one can say CF_{ijklm} decomposes CF_{ijkl} into two sets: CF_{ijkl} and the set $V_{ijkl} = CF_{ijkl/m} \setminus CF_{ijkl} = \{q : 0 < D_m(q) < D_i(q) = D_j(q) = D_k(q) = D_l(q)\}$. Note that V_{ijkl} may not exist at all, if CF_{ijkl} does contain CF_{ijklm} . On the other hand, CF_{ijkl} may not exist while V_{ijkl} exists. Finally, if both CF_{ijkl} and V_{ijkl} exist, then CF_{ijklm} exists, since CF_{ijklm} is a boundary between CF_{ijkl} and V_{ijkl} .

Now consider a configuration q in SR_{ijk} such that the contact point of the rod to F_{ijk} is F_{ijk} , a point-GVG meetpoint. At configuration q , $D_m(q) \leq D_i(q)$. As the rod travels along SR_{ijk} away from q “towards” the obstacle C_l , there must be a configuration q' where $D_m = D_i$, i.e., $q' \in CF_{ijkl}^*$, and there is a configuration q'' in the neighborhood of q' (on SR_{ijk}) such that $D_m(q'') > D_i(q'')$. Since we assume that R_{ijk} does not exist, at q'' , $D_i > D_l$. From the continuity of the distance, we have $D_m(q') = D_i(q') \geq D_l(q')$. If equality holds, then q' is an element of CF_{ijklm} . If inequality holds, this implies that $D_m(q') = D_i(q') = D_j(q') = D_l(q') < D_l(q)$. This, in turn, means that $q' \in V_{ijlm}$ and, from the comment above, this implies that CF_{ijklm} is not an empty set. Thus, in both cases, CF_{ijkl} and CF_{ijkm} must intersect each other; that is, CF_{ijklm} is not an empty set. \square

Appendix E: Proof of Lemma 2 (Section 4.5)

Here we prove Lemma 2, which states that two adjacent rod four-way equidistant faces are connected either by a one-tangent edge or a rod-GVG edge, but not by both.

Proof. First we define some notation. Given a set of configurations SQ , let $D_{min}(S)$ be

$$D_{min}(SQ) = \min_{q \in SQ} D(q),$$

and, similarly, given a set of points SP in \mathbb{R} , let $d_{min}(SP)$ be

$$d_{min}(SP) = \min_{x \in SP} d(x).$$

Recall that for a given configuration q in R_{ijk} , $D(q) = d(x_q)$, where x_q is the “contact point” between the rod and the point-GVG edge F_{ijk} . Let F_{ijk}^R be the set of “contact points” for R_{ijk} . Then $F_{ijk}^R \subset F_{ijk}$. Therefore, we have

$$d_{min}(F_{ijk}) \leq d_{min}(F_{ijk}^R) = D_{min}(R_{ijk}). \quad (31)$$

Now, consider the configuration space for a rod with a fixed orientation, operating in the same environment, but without rotation. Then the configuration space for this robot is a three-dimensional Euclidean space, populated by convex obstacles. Therefore, we can define a point-GVG-like structure in this space. Let $F_{ijk}^{(\theta, \phi)}$ be the point-GVG edge in a configuration space for a rod, with the fixed orientation (θ, ϕ) , operating in the given workspace without rotation. Also we define $F_{ijkl}^{(\theta, \phi)}$ and $F_{ijkm}^{(\theta, \phi)}$ similarly. Then we have

$$d_{min}(F_{ijk}^{(\theta, \phi)}) \leq d_{min}(F_{ijk}). \quad (32)$$

Now we prove the lemma. The proof is by contradiction. Let us assume that both R_{ijk} and CF_{ijklm} are not empty sets. Consider a configuration q_g in a rod-GVG edge CF_{ijklm} . Then $(x(q_g), y(q_g), z(q_g))$ is a five-way equidistant point $F_{ijklm}^{(\theta(q_g), \phi(q_g))}$ in a three-dimensional fixed-orientation configuration space for a rod with the orientation $(\theta(q_g), \phi(q_g))$. By definition, this point is also in $F_{ijkl}^{(\theta(q_g), \phi(q_g))}$ and $F_{ijkm}^{(\theta(q_g), \phi(q_g))}$, which are zero-dimensional. This means $F_{ijkl}^{(\theta(q_g), \phi(q_g))} = F_{ijkm}^{(\theta(q_g), \phi(q_g))}$. Since $F_{ijkl}^{(\theta(q_g), \phi(q_g))}$ and $F_{ijkm}^{(\theta(q_g), \phi(q_g))}$ are the endpoints of the point-GVG edge $F_{ijk}^{(\theta(q_g), \phi(q_g))}$, such that $F_{ijkl}^{(\theta(q_g), \phi(q_g))}$ and $F_{ijkm}^{(\theta(q_g), \phi(q_g))}$ are the same point, means that the point-GVG edge $F_{ijk}^{(\theta(q_g), \phi(q_g))}$ itself consists of only one point, i.e., $(x(q_g), y(q_g), z(q_g))$.

In other words, the point $(x(q_g), y(q_g), z(q_g))$ is the only point of $F_{ijk}^{(\theta(q_g), \phi(q_g))}$. Using eqs. (31) and (32), we have

$$\begin{aligned} D(q_g) &= d(x(q_g), y(q_g), z(q_g)) \\ &= d_{min}(F_{ijk}^{(\theta(q_g), \phi(q_g))}) \\ &\leq d_{min}(F_{ijk}) \leq D_{min}(R_{ijk}), \end{aligned} \quad (33)$$

i.e.,

$$D(q_g) \leq D_{\min}(R_{ijk}). \quad (34)$$

This is true for all q_g in CF_{ijklm} . Now let us consider the configuration q_r in R_{ijk} , $D(q_r) > D_{\min}(R_{ijk})$. Recall that accessibility implies that there is a configuration $H(q_r, 1)$ in CF_{ijklm} such that $D(H(q_r, 1)) > D(q_r)$, but this is impossible from eq. (34). Therefore, it is not possible that both R_{ijk} and CF_{ijklm} are not empty sets. \square

Appendix F: Proof of Lemma 4 (Section 4.5)

Here we prove Lemma 4, which is that a two-tangent edge $R_{ij/kl}$ is a one-dimensional manifold. The proof is by showing the gradient of $g_{ij/kl}$, which defines the two-tangent edge implicitly, is full rank, and concluding that the two-tangent edge is a one-dimensional manifold by the pre-image theorem (Abraham, Marsden, and Raitu 1988).

Proof. Recall that the two-tangent edge $R_{ij/kl}$ can be considered as the roots of

$$g_{ij/kl} = \begin{bmatrix} D_i - D_j \\ D_i - D_k \\ D_i - D_l \\ PQ \cdot (c_i - c_j) \end{bmatrix}. \quad (35)$$

We show that $R_{ij/kl}$ is a one-dimensional manifold by showing that the differential of $g_{ij/kl}$, $dg_{ij/kl}$, has a full rank (Canny 1988). Note that the first three rows are just the differences between the distance function; thus, the differentials of these rows are just the differences between the distance gradient of each object. The last row, however, requires a careful consideration.

To derive the differential of $PQ \cdot (c_i - c_j)$, first, we derive dPQ . Since

$$PQ = \begin{bmatrix} l \cos \theta \cos \phi \\ l \sin \theta \cos \phi \\ -l \sin \phi \end{bmatrix},$$

we have

$$dPQ = \begin{bmatrix} 0 & 0 & 0 & -l \sin \theta \cos \phi & -l \cos \theta \sin \phi \\ 0 & 0 & 0 & l \cos \theta \cos \phi & -l \sin \theta \sin \phi \\ 0 & 0 & 0 & 0 & -l \cos \phi \end{bmatrix}.$$

Let $\mathbf{s} = [-\sin \theta \cos \phi \quad \cos \theta \cos \phi \quad 0]^T$ and $\mathbf{t} = [-\cos \theta \sin \phi \quad -\sin \theta \sin \phi \quad -\cos \phi]^T$ (Figure F1). Then we have

$$dPQ = [\mathbf{0} \quad \mathbf{0} \quad \mathbf{0} \quad ls \quad lt].$$

Note that both \mathbf{s} and \mathbf{t} are normal to PQ . Now, we derive the equation for dc_i , which we denote

$$dc_i = [c_{ix} \quad c_{iy} \quad c_{iz} \quad c_{i\theta} \quad c_{i\phi}] \in \mathbb{R}^{3 \times 5}, \quad c_{ix}, c_{iy}, c_{iz}, c_{i\theta}, c_{i\phi} \in \mathbb{R}^3. \quad (36)$$

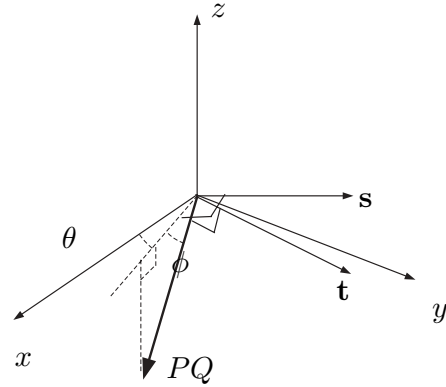


Fig. F1. Rod configuration is represented using ZYZ-Euler angles. The vector \mathbf{s} is a vector on the xy -plane, normal to the projection of PQ onto the xy -plane (\mathbf{s} is also normal to PQ), and \mathbf{t} is a unit vector normal to PQ and \mathbf{s} . Therefore, we have the following relationships: $(PQ/l) \times \mathbf{t} = \mathbf{s}$, $\mathbf{t} \times \mathbf{s} = PQ/l$ and $\mathbf{s} \times (PQ/l) = \mathbf{t}$.

First note that PQ and the line defined by $c_i + u\mathbf{n}_i(c)$ ($u \in \mathbb{R}$) must intersect always (Figure F2¹³). Therefore, using the expression for the distance between two lines, we have

$$(PQ \times \mathbf{n}_i) \cdot (P - c_i) = 0. \quad (37)$$

This should be satisfied as the rod makes a differential motion, and we have

$$d((PQ \times \mathbf{n}_i) \cdot (P - c_i)) = 0$$

by taking the differential of eq. (37).

Thus we have

$$(\mathbf{n}_i \times PQ)^T ((-D_i L_{c_i} + I)(c_{ix})) + (PQ \times \mathbf{n}_i)^T \begin{pmatrix} 1 \\ 0 \\ 0 \end{pmatrix} = 0 \quad (38)$$

$$(\mathbf{n}_i \times PQ)^T ((-D_i L_{c_i} + I)(c_{iy})) + (PQ \times \mathbf{n}_i)^T \begin{pmatrix} 0 \\ 1 \\ 0 \end{pmatrix} = 0 \quad (39)$$

$$(\mathbf{n}_i \times PQ)^T ((-D_i L_{c_i} + I)(c_{iz})) + (PQ \times \mathbf{n}_i)^T \begin{pmatrix} 0 \\ 0 \\ 1 \end{pmatrix} = 0 \quad (40)$$

13. In the figure, the notation is a little sloppy. To be more precise, $PQ + dPQ$ should be written $PQ + dPQ dq$ where $PQ \in \mathbb{R}^3$, $dPQ \in \mathbb{R}^{3 \times 5}$ and $dq = (dx \ dy \ dz \ d\theta \ d\phi)^T \in \mathbb{R}^5$ and so on.

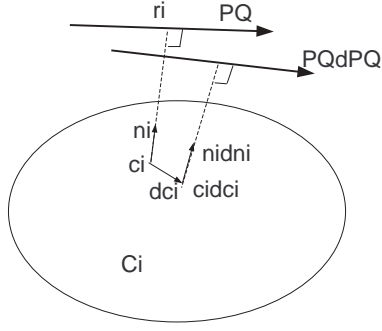


Fig. F2. PQ and the line defined by $c_i + u\mathbf{n}$ ($u \in \mathbb{R}$) must intersect, i.e., $(PQ \times \mathbf{n}_i) \cdot (P - c_i) = 0$, and thus $d((PQ \times \mathbf{n}_i) \cdot (P - c_i)) = 0$. Also note that, when r_i is an interior point of PQ , as shown in this figure, PQ must be normal to \mathbf{n}_i , thus $PQ \cdot \mathbf{n}_i = 0$ and $d(PQ \cdot \mathbf{n}_i) = 0$.

$$(\mathbf{n}_i \times PQ)^T ((-D_i L_{c_i} + I)(c_{i\theta})) + (l\mathbf{s} \times \mathbf{n}_i) \cdot (P - c_i) = 0 \quad (41)$$

$$(\mathbf{n}_i \times PQ)^T ((-D_i L_{c_i} + I)(c_{i\phi})) + (l\mathbf{t} \times \mathbf{n}_i) \cdot (P - c_i) = 0 \quad (42)$$

where L_p denotes the Weingarten map (Thorpe 1979) of C_i at point p , i.e.,

$$L_p(\mathbf{v}) = -\nabla_{\mathbf{v}}\mathbf{n}.$$

Now, we derive the differential of $g_{ij/kl}$:

$$dg_{ij/kl} = \begin{bmatrix} dD_i - dD_j \\ dD_i - dD_k \\ dD_i - dD_l \\ d(PQ \cdot (c_i - c_j)) \end{bmatrix} \in \mathbb{R}^{4 \times 5}. \quad (43)$$

Recall that

$$(dD_i)^T = \frac{1}{D_i} \begin{bmatrix} r_i - c_i \\ (r_i - c_i) \cdot (-u\mathbf{S}\theta\mathbf{C}\phi \quad u\mathbf{C}\theta\mathbf{C}\phi \quad 0) \\ (r_i - c_i) \cdot (-u\mathbf{C}\theta\mathbf{S}\phi \quad -u\mathbf{S}\theta\mathbf{S}\phi \quad -u\mathbf{C}\phi) \end{bmatrix} \in \mathbb{R}^5 \quad (44)$$

where $u = |P - r_i|$. Using \mathbf{s} and \mathbf{t} defined above, we have

$$(dD_i)^T = \frac{1}{D_i} \begin{bmatrix} r_i - c_i \\ (r_i - c_i) \cdot (u\mathbf{s}) \\ (r_i - c_i) \cdot (u\mathbf{t}) \end{bmatrix} \quad (45)$$

$$= \begin{bmatrix} \mathbf{n}_i \\ \mathbf{n}_i \cdot (u\mathbf{s}) \\ \mathbf{n}_i \cdot (u\mathbf{t}) \end{bmatrix} \in \mathbb{R}^5, \text{ where } \mathbf{n}_i \in \mathbb{R}^3, \quad (46)$$

since $\mathbf{n}_i = (r_i - c_i)/|r_i - c_i| = (r_i - c_i)/D_i$. Therefore, the first row of $dg_{ij/kl}$ is

$$(dD_i - dD_j)^T = \begin{bmatrix} \mathbf{n}_i - \mathbf{n}_j \\ u(\mathbf{n}_i - \mathbf{n}_j) \cdot \mathbf{s} \\ u(\mathbf{n}_i - \mathbf{n}_j) \cdot \mathbf{t} \end{bmatrix} \in \mathbb{R}^5$$

where $\mathbf{n}_i - \mathbf{n}_j \in \mathbb{R}^3$, (47)

and the second and third rows have similar forms. The fourth row of $dg_{ij/kl}$ is

$$(d(PQ \cdot (c_i - c_j)))^T = (dPQ)^T(c_i - c_j) + d(c_i - c_j)^T PQ \quad (48)$$

$$= dPQ^T(c_i - r_i + r_j - c_j) + d(c_i - r_i + r_j - c_j)^T PQ \quad (49)$$

$$= D_i dPQ^T(-\mathbf{n}_i + \mathbf{n}_j) + d(-\mathbf{n}_i + \mathbf{n}_j)^T PQ. \quad (50)$$

So, our goal now is to show that the last row of eq. (43) is linearly independent of the other rows of eq. (43). We do this in three cases, depending on the location of r_i and r_j on the rod.

Case 1 ($r_i = r_j = P$). In this case, we have $u = 0$, and therefore

$$(dD_i - dD_j)^T = \begin{bmatrix} \mathbf{n}_i - \mathbf{n}_j \\ 0 \\ 0 \end{bmatrix}. \quad (51)$$

Note that in this case $c_{i\theta} = 0$ and $c_{i\phi} = 0$, so eq. (48) becomes

$$(d(PQ \cdot (c_i - c_j)))^T = (dPQ)^T(c_i - c_j) + d(c_i - c_j)^T PQ \quad (52)$$

$$= \begin{bmatrix} (c_{ix} - c_{jx}) \cdot PQ \\ (c_{iy} - c_{jy}) \cdot PQ \\ (c_{iz} - c_{jz}) \cdot PQ \\ l\mathbf{s} \cdot (c_i - c_j) \\ l\mathbf{t} \cdot (c_i - c_j) \end{bmatrix}. \quad (53)$$

Recall that \mathbf{s} and \mathbf{t} are the last two columns of dPQ . Since both $l\mathbf{s} \cdot (c_i - c_j)$ and $l\mathbf{t} \cdot (c_i - c_j)$ cannot be zero at the same time (if so, that would imply $(c_i - c_j)$ is normal to \mathbf{t} and \mathbf{s} , and then this implies that $(c_i - c_j)$ is parallel to PQ , which is not possible), so the fourth row is linearly independent of the first row.

Case 2 (r_i is an interior point of PQ). In this case, PQ must be normal to $r_i - c_i = D_i(\mathbf{n}_i)$, i.e., $PQ \cdot (r_i - c_i) = 0$, and after a small movement of the rod, this condition must also be satisfied and thus $d(PQ \cdot (r_i - c_i)) = 0$ also (Figure F2).

So, using $(r_i - c_i) = D_i \mathbf{n}_i$, we have

$$0 = dPQ^T(r_i - c_i) + d(r_i - c_i)^T PQ \quad (54)$$

$$= dPQ^T(r_i - c_i) + D_i d(\mathbf{n}_i)^T PQ \quad (55)$$

$$= dPQ^T(r_i - c_i) - D_i \begin{bmatrix} L_{c_i} c_{ix} \\ L_{c_i} c_{iy} \\ L_{c_i} c_{iz} \\ L_{c_i} c_{i\theta} \\ L_{c_i} c_{i\phi} \end{bmatrix} PQ. \quad (56)$$

Therefore, we have

$$dPQ^T(r_i - c_i) = D_i \begin{bmatrix} L_{c_i} c_{ix} \\ L_{c_i} c_{iy} \\ L_{c_i} c_{iz} \\ L_{c_i} c_{i\theta} \\ L_{c_i} c_{i\phi} \end{bmatrix} PQ. \quad (57)$$

Substituting eq. (57) into eq. (49), we have (see Figure F3)

$$\begin{aligned} (d(PQ \cdot (c_i - c_j)))^T &= \begin{bmatrix} ((I - D_i L_{c_i}) c_{ix}) \cdot PQ \\ ((I - D_i L_{c_i}) c_{iy}) \cdot PQ \\ ((I - D_i L_{c_i}) c_{iz}) \cdot PQ \\ ((I - D_i L_{c_i}) c_{i\theta}) \cdot PQ \\ ((I - D_i L_{c_i}) c_{i\phi}) \cdot PQ \end{bmatrix} \\ &- \begin{bmatrix} ((I - D_j L_{c_j}) c_{jx}) \cdot PQ \\ ((I - D_j L_{c_j}) c_{jy}) \cdot PQ \\ ((I - D_j L_{c_j}) c_{jz}) \cdot PQ \\ ((I - D_j L_{c_j}) c_{j\theta}) \cdot PQ \\ ((I - D_j L_{c_j}) c_{j\phi}) \cdot PQ \end{bmatrix}. \end{aligned} \quad (58)$$

Since r_i can be represented as

$$r_i = c_i + D_i \mathbf{n}_i,$$

we have

$$r_{i\theta} = c_{i\theta} + D_{i\theta} \mathbf{n}_i + D_i \mathbf{n}_{i\theta} \quad (59)$$

$$= c_{i\theta} + u(\mathbf{s} \cdot \mathbf{n}_i) \mathbf{n}_i - D_i L_i(c_{i\theta}) \quad (60)$$

$$= (I - D_i L_{c_i}) c_{i\theta} + u(\mathbf{s} \cdot \mathbf{n}_i) \mathbf{n}_i, \quad (61)$$

using $D_{i\theta} = u\mathbf{s} \cdot \mathbf{n}_i$ ¹⁴ and $\mathbf{n}_{i\theta} = -L_i(c_{i\theta})$, or we can write

$$(I - D_i L_{c_i}) c_{i\theta} = r_{i\theta} - u(\mathbf{s} \cdot \mathbf{n}_i) \mathbf{n}_i. \quad (62)$$

We can derive similar equations for the other coordinates. Substituting eq. (62) and similar equations for the other coordinates into eq. (58), we have

$$(d(PQ \cdot (c_i - c_j)))^T = \begin{bmatrix} PQ \cdot (r_{ix} - r_{jx}) \\ PQ \cdot (r_{iy} - r_{jy}) \\ PQ \cdot (r_{iz} - r_{jz}) \\ PQ \cdot (r_{i\theta} - r_{j\theta}) \\ PQ \cdot (r_{i\phi} - r_{j\phi}) \end{bmatrix}. \quad (63)$$

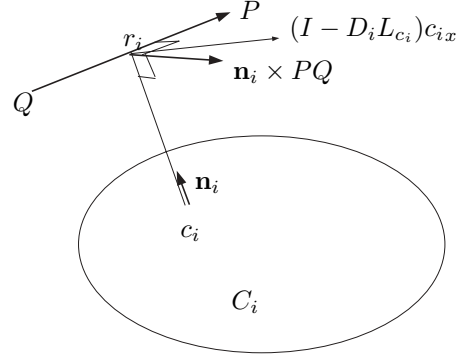


Fig. F3. When r_i is an interior point of PQ , PQ , and \mathbf{n}_i are normal to each other. Also note that the vector $(I - D_i L_{c_i}) c_{ix}$ lies on the plane defined by PQ and $\mathbf{n}_i \times PQ$, since c_{ix} lies on the tangent space of C_i at c_i , and $L_{c_i}(c_{ix})$, which is the change of the normal vector along the direction of c_{ix} , also lies on the tangent space of C_i at c_i . Finally, note that eqs. (38)–(42) involve the expression of the form $(\mathbf{n}_i \times PQ)^T ((-D_i L_{c_i} + I)(c_{ix}))$ and eq. (58) involves the expression of the form $(\mathbf{n}_i \times PQ) \cdot ((-D_i L_{c_i} + I)(c_{ix}))$. That is, those equations have the expression for the PQ and $\mathbf{n}_i \times PQ$ components of the vector $(-D_i L_{c_i} + I)(c_{ix})$. The same can be said of c_{iy} , c_{iz} , etc.

Now, we show that this vector is linearly independent of eq. (47) and, for this, it is enough to show that the three-vector whose components are the first three elements of eq. (63) is linearly independent of the three-vector whose components are the first elements of eq. (47), which is, in fact, parallel to

$$\mathbf{n}_i - \mathbf{n}_j. \quad (64)$$

Note that eq. (64) is also parallel to $c_i - c_j$.

Now, we only need to consider the translational motion of the rod since the first three components of eq. (63) represent the differential in translational coordinates. A translational differential motion of the rod can be decomposed into \mathbf{n}_i , PQ , and $\mathbf{n}_i \times PQ$ components, which we can write as

$$dh = dh_{\mathbf{n}_i} + dh_{PQ} + dh_{\mathbf{n}_i \times PQ}. \quad (65)$$

For this motion, the differential change in r_i can be written as

$$dr_i = dr_{i\mathbf{n}_i} + dr_{iPQ} + dr_{i\mathbf{n}_i \times PQ}. \quad (66)$$

Note that for the motion in the \mathbf{n}_i direction, $dh_{\mathbf{n}_i}$, the change in r_i is exactly the same as $dh_{\mathbf{n}_i}$. For motion in the PQ direction, r_i does not change. For $dh_{\mathbf{n}_i \times PQ}$, the change in r_i is parallel to the tangent space of C_i at c_i (and not necessarily parallel to $dh_{\mathbf{n}_i \times PQ}$). So we can rewrite eq. (66) as (Figure F4)

$$dr_i = dr_{i\mathbf{n}_i} + dr_{iPQ} + dr_{i\mathbf{n}_i \times PQ} \quad (67)$$

$$= dh_{\mathbf{n}_i} + 0 + (dh_{\mathbf{n}_i \times PQ} + dv_{PQ}), \quad (68)$$

14. As in eq. (36), $D_{i\theta}$ denotes the differential of D_i in θ coordinates, etc.

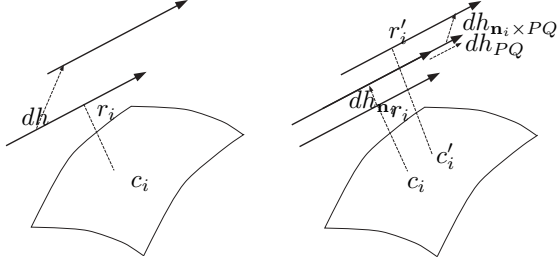


Fig. F4. Translational motion of the rod can be decomposed into three directions: \mathbf{n}_i , PQ , and $\mathbf{n}_i \times PQ$.

Here, dv_{PQ} is the change of r_i in the PQ direction, whose magnitude is linear on the magnitude of $dh_{\mathbf{n}_i \times PQ}$, i.e.,

$$dv_{PQ} = a_i |dh_{\mathbf{n}_i \times PQ}| \mathbf{u}_{PQ}. \quad (69)$$

where \mathbf{u}_{PQ} is a unit vector parallel to PQ . Then, we have

$$PQ \cdot r_{ix} = PQ \cdot (dh_{\mathbf{n}_i} + 0 + dh_{\mathbf{n}_i \times PQ} + a_i |dh_{\mathbf{n}_i \times PQ}| \mathbf{u}_{PQ}) \quad (70)$$

$$= a_i |PQ| |dh_{\mathbf{n}_i \times PQ}| \quad (71)$$

where a_i is a proportional constant.

Therefore, for the first three components of eq. (63) we have

$$\begin{bmatrix} c_i \mathbf{u}_{\mathbf{n}_i \times PQ} - c_j \mathbf{u}_{\mathbf{n}_j \times PQ} \end{bmatrix} \quad (72)$$

which cannot be parallel to $\mathbf{n}_i - \mathbf{n}_j$.

Case 3 ($r_i = r_j = Q$). In this case, $dr_i = dQ$, i.e.

$$dr_i = dQ = \begin{bmatrix} 1 & 0 & 0 \\ 0 & 1 & 0 \\ 0 & 0 & 1 \end{bmatrix} \begin{bmatrix} ls \\ lt \\ 1 \end{bmatrix}, \quad (73)$$

where \mathbf{s} and \mathbf{t} are three-dimensional column vectors as defined above. Since

$$c_i = r_i - D_i \mathbf{n}_i, \quad (74)$$

we have

$$dc_i = dr_i - dD_i \mathbf{n}_i - D_i d\mathbf{n}_i \quad (75)$$

$$= dr_i - \mathbf{n}_i \begin{bmatrix} \mathbf{n}_i^T & ls \cdot \mathbf{n}_i & lt \cdot \mathbf{n}_i \end{bmatrix} + D_i L_{c_i} (dc_i). \quad (76)$$

Since C_i is convex and \mathbf{n}_i is defined to be the normal vector pointing away from the obstacle C_i , the curvatures are negative. Then, $(I - D_i L_{c_i})$ is non-singular since the eigenvalues of $(I - D_i L_{c_i})$ are the principal curvatures, and $D_i > 0$. Thus,

rearranging eq. (76), we obtain

$$dc_i = (I - D_i L_{c_i})^{-1} (dr_i - \mathbf{n}_i \begin{bmatrix} \mathbf{n}_i^T & ls \cdot \mathbf{n}_i & lt \cdot \mathbf{n}_i \end{bmatrix}) \quad (77)$$

$$= (I - D_i L_{c_i})^{-1} \begin{bmatrix} I_{3 \times 3} - \mathbf{n}_i \mathbf{n}_i^T \\ l(\mathbf{s} - (\mathbf{s} \cdot \mathbf{n}_i) \mathbf{n}_i) \\ l(\mathbf{t} - (\mathbf{t} \cdot \mathbf{n}_i) \mathbf{n}_i) \end{bmatrix}^T. \quad (78)$$

Note that $\mathbf{s} - (\mathbf{s} \cdot \mathbf{n}_i) \mathbf{n}_i$ and $\mathbf{t} - (\mathbf{t} \cdot \mathbf{n}_i) \mathbf{n}_i$ are the respective components of \mathbf{s} and \mathbf{t} , which are parallel to the tangent space of C_i . Let $U_i = (I_{3 \times 3} - \mathbf{n}_i \mathbf{n}_i^T)$. Essentially, U_i projects a vector onto the tangent space of C_i at c_i . Then, eq. (78) can be rewritten as

$$dc_i = (I - D_i L_{c_i})^{-1} U_i \begin{bmatrix} I_{3 \times 3} & ls & lt \end{bmatrix}. \quad (79)$$

Now, let $W_i = (I - D_i L_{c_i})^{-1} U_i$, and substituting eq. (79) into eq. (48), we have

$$\begin{aligned} (d(PQ \cdot (c_i - c_j)))^T &= (dPQ)^T (c_i - c_j) + d(c_i - c_j)^T PQ \\ &= D_i \begin{bmatrix} 0_{3 \times 3} & ls & lt \end{bmatrix}^T (-\mathbf{n}_i + \mathbf{n}_j) \\ &\quad + (W_i \begin{bmatrix} I_{3 \times 3} & ls & lt \end{bmatrix} \\ &\quad - W_j \begin{bmatrix} I_{3 \times 3} & ls & lt \end{bmatrix})^T PQ \quad (80) \\ &= \begin{bmatrix} \mathbf{0} \\ lD_i \mathbf{s} \cdot (-\mathbf{n}_i + \mathbf{n}_j) \\ lD_i \mathbf{t} \cdot (-\mathbf{n}_i + \mathbf{n}_j) \end{bmatrix} \\ &\quad + \begin{bmatrix} (W_i - W_j)^T PQ \\ ls_j^T (W_i - W_j)^T PQ \\ lt_j^T (W_i - W_j)^T PQ \end{bmatrix}. \quad (81) \end{aligned}$$

If $(W_i - W_j)^T PQ$ is not linearly dependent of $\mathbf{n}_i - \mathbf{n}_j$, which are the first three components of $d(D_i - D_j)$, $d(PQ \cdot (c_i - c_j))$ is linearly independent of $d(D_i - D_j)$. If $(W_i - W_j)^T PQ$ is linearly dependent on $\mathbf{n}_i - \mathbf{n}_j$, one can write $(W_i - W_j)^T PQ = K(\mathbf{n}_i - \mathbf{n}_j)$. Then, eq. (81) becomes

$$\begin{aligned} (d(PQ \cdot (c_i - c_j)))^T &= \\ &= \begin{bmatrix} K(\mathbf{n}_i - \mathbf{n}_j) \\ lD_i \mathbf{s} \cdot (\mathbf{n}_j - \mathbf{n}_i) + lK \mathbf{s}_j^T (\mathbf{n}_i - \mathbf{n}_j) \\ lD_i \mathbf{t} \cdot (\mathbf{n}_j - \mathbf{n}_i) + lK \mathbf{t}_j^T (\mathbf{n}_i - \mathbf{n}_j) \end{bmatrix}, \quad (82) \end{aligned}$$

which cannot be parallel to $d(D_i - D_j)$ for $D_i > 0$. Thus, we conclude that for each of the three cases, a two-tangent-edge is a one-dimensional manifold. \square

Appendix G. Proof of Lemma 5 (Section 4.5)

Here we prove Lemma 5, which states that a two-tangent edge has one connected component on a rod four-way equidistant face CF_{ijkl} homeomorphic to S^2 .

Proof. First, let us consider a rod with zero length, denoted l_o . In other words, l_o is a point with direction. For l_o , each

$R_{ij/kl}$ has one component homeomorphic to S^1 . This is true because if any configuration q_o belongs to $R_{ij/kl}$, then all of the configurations with endpoints located at the same point as the endpoint of q_o , and having the direction such that they are tangent to F_{ij} , also belong to $R_{ij/kl}$. This is because all such configurations occupy the same workspace volume as q_o , and hence all such configurations are four-way equidistant to C_i , C_j , C_k , and C_l , and do not intersect any of the obstacles. Now, imagine the change in $R_{ij/kl}$ as the length of the rod increases in the same environment. (We still assume that $CF_{ij/kl}$ is homeomorphic to S^2 in this process.) Now assume that for some value of the length, we have a $R_{ij/kl}$ with two or more components. Since $R_{ij/kl}$ changes “continuously” as the length of the rod changes, this means that there must be some “critical” length of the rod at which either one component shrinks to a point or two components intersect each other transversally. However, this means that at this “critical” length, $R_{ij/kl}$ is not a manifold. This is contradictory to Lemma 4, which does not depend on the length of the rod. Therefore, $R_{ij/kl}$ can have only one component. \square

Appendix H: Index to Multimedia Extensions

We have included some animations of the rod tracing the rod-HGVG in three dimensional spaces (see below). The multimedia extension page can be found at <http://www.ijrr.org>.

Extension 1 shows the rod exploring a rectangular enclosure shown in Figures 20 and 21. In this example, there is no rod-GVG edges since the rod is “short”. Therefore, the rod-HGVG forms a connected set with only the one-tangent edges (shown in sky blue) and the two-tangent edges (shown in yellow).

Extension 2 shows the rod exploring the space shown in Figure 22, a rectangular enclosure with a wall in the middle. In this example, there are the rod-GVG edges (shown in pink) near the both ends of the room.

Table of Multimedia Extensions

Extension	Type	Description
1	Video	The rod-HGVG in a rectangular environment, without the rod-GVG edges
2	Video	The rod-HGVG in a large rectangular environment, with the rod-GVG edges

References

Abraham, R., Marsden, J. E., and Raitu, T. 1988. *Manifolds, Tensor Analysis and Applications*, 2nd edition, Springer-Verlag, New York.

Acar, E. U., Choset, H., and Atkar, P. N. 2001. Complete sensor-based coverage with extended-range detectors: a

hierarchical decomposition in terms of critical points and Voronoi diagrams. *Proceedings of the 2001 IEEE/RSJ International Conference on Intelligent Robots and Systems (IROS)*, Maui, HI, October.

Aurenhammer, F. 1991. Voronoi diagrams—a survey of a fundamental geometric data structure. *ACM Computing Surveys* 23(3):345–405.

Aurenhammer, F. and Klein, R. 2000. Voronoi diagrams. *Handbook of Computational Geometry*, J. Sack and G. Urrutia, editors, Elsevier, Amsterdam, Chapter V, pp. 201–290.

Borenstein, J. and Koren, Y. 1998. Real-time obstacle avoidance for fast mobile robots. *IEEE Transactions on Systems, Man and Cybernetics* 19(5):1179–1187.

Brand, L. 1966. *Differential and Difference Equations*, Wiley, New York.

Bredon, G. 1995. *Topology and Geometry*, 3rd edition, Springer-Verlag, Berlin.

Brooks, R. A. 1983. Solving the find-path problem by good representation of free space. *IEEE Transaction on Systems, Man and Cybernetics* 13(3):190–197.

Brooks, R. A. and Lozano-Pérez, T. 1983. A subdivision algorithm in configuration space for Findpath with rotation. *Proceedings of the International Joint Conference on Artificial Intelligence*, Karlsruhe, Germany, August, pp. 799–806.

Canny, J. F. 1988. *The Complexity of Robot Motion Planning*, MIT Press, Cambridge, MA.

Choset, H. and Burdick, J. 2000a. Sensor-based motion planning: the hierarchical generalized Voronoi graph. *International Journal of Robotics Research* 19(2):96–125.

Choset, H. and Burdick, J. 2000b. Sensor-based motion planning: incremental construction of the hierarchical generalized Voronoi graph. *International Journal of Robotics Research* 19(2):126–148.

Choset, H. and Burdick, J. W. 1996. Sensor-based planning for a planar rod robot. *Proceedings of the IEEE International Conference on Robotics and Automation (ICRA)*, Minneapolis, MN.

Choset, H. and Lee, J. Y. 2001. Sensor-based construction of a retract-like structure for a planar rod robot. *IEEE Transaction of Robotics and Automation* 17(4):435–449.

Chuang, J. H. and Ahuja, N. 1998. An analytically tractable potential fidel model of free space and its application in obstacle avoidance. *IEEE Transactions on Systems, Man and Cybernetics – Part B: Cybernetics* 28(5):729–736.

Cox, J. and Yap, C. K. 1991. On-line motion planning: case of a planar rod. *Annals of Mathematics and Artificial Intelligence* 3:1–20.

Dattasharma, A. and Sathiyar Keerthi, S. 1995. An augmented Voronoi roadmap for 3D translational motion planning for a convex polyhedron moving amidst convex polyhedral obstacles. *Theoretical Computer Science* 140(2):205–230.

- Foskey, M., Garber, M., Lin, M., and Monocha, D. 2000. A Voronoi-based hybrid motion planner for rigid bodies. Technical Report TR00-025, UNC Chapel Hill Computer Science.
- Kavraki, L. 1997. Part orientation with programmable vector fields: two stable equilibria for most parts. *Proceedings of the IEEE International Conference on Robotics and Automation (ICRA)*, Albuquerque, NM, April.
- Kavraki, L. and Latombe, J.-C. 1994. Randomized preprocessing of configuration space for path planning: articulated robots. *Proceedings of the IEEE/RSJ International Conference on Intelligent Robots and Systems (IROS)*, Munich, Germany, pp. 1764–1771.
- Kavraki, L., Svestka, P., Latombe, J.-C., and Overmars, M. 1996. Probabilistic roadmaps for path planning in high-dimensional configuration spaces. *IEEE Transactions on Robotics and Automation* 12(4):566–580.
- Khatib, O. 1986. Real-time obstacle avoidance for manipulators and mobile robots. *International Journal of Robotics Research* 5:90–98.
- Khosla, P. and Volpe, R. 1988. Superquadric artificial potential for obstacle avoidance and approach. *Proceedings of the IEEE Conference on Robotics and Automation (ICRA)*, Philadelphia, PA, pp. 1778–1784.
- Koren, Y. and Borenstein, J. 1991. Potential field methods and their inherent limitations for mobile robot navigation. *Proceedings of the IEEE Conference on Robotics and Automation (ICRA)*, Sacramento, CA, pp. 1398–1404.
- Kuan, D. T., Zamiska, J. C., and Brooks, R. A. 1985. Natural decomposition of free space for path planning. *Proceedings of the IEEE International Conference on Robotics and Automation (ICRA)*, St. Louis, MO, pp. 168–173.
- Kuffner, J. J. and LaValle, S. M. 2000. RRT-connect: an efficient approach to single-query path planning. *Proceedings of the IEEE International Conference on Robotics and Automation (ICRA)*, San Francisco, CA, April 24–28, pp. 995–1001.
- Latombe, J.-C. 1991. *Robot Motion Planning*, Kluwer Academic, Boston, MA.
- Latombe, J.-C., Kavraki, L. E., Svestka, P., and Overmars, M. 1996. Probabilistic roadmaps for path planning in high-dimensional configuration spaces. *IEEE Transactions on Robotics and Automation* 12(4):566–580.
- LaValle, S. M. 1998. Rapidly-exploring random trees: a new tool for path planning. Technical Report TR 98-11, Computer Science Department, Iowa State University, October.
- Lee, J. Y., Choset, H., and Rizzi, A. A. 2001. Sensor-based planning for rod-shaped robots in three dimensions: piecewise retracts of $\mathbb{R}^3 \times S^2$. *Proceedings of the IEEE International Conference on Robotics and Automation (ICRA)*, Seoul, Korea, May 21–26, pp. 991–999.
- Munkres, J. R. 2000. *Topology*, Prentice-Hall, Englewood Cliffs, NJ.
- Nilsson, N. J. 1969. A mobile automation: an application of artificial intelligence techniques. *Proceedings of 1st International Joint Conference on Artificial Intelligence*, Washington, DC.
- Noborio, H., Haniwa, T., and Arimoto, S. 1989. A feasible motion planning algorithm for a mobile robot on a quadtree representation. *Proceedings of IEEE International Conference on Robotics and Automation (ICRA)*, Scottsdale, AZ, May, pp. 327–332.
- Ó'Dúnlaing, C., Sharir, M., and Yap, C. K. 1986. Generalized Voronoi diagrams for moving a ladder. I: topological analysis. *Communications on Pure and Applied Mathematics* 39:423–483.
- Ó'Dúnlaing, C. and Yap, C. K. 1985. A “retraction” method for planning the motion of a disc. *Journal of Algorithms* 6:104–111.
- Overmars, M. H. 1992. A random approach to motion planning. Technical Report RUU-CS-92-32, Department of Computational Science, Utrecht University, Utrecht, the Netherlands, October.
- Pisula, C., Hoff, K., Lin, M., and Manocha, D. 2000. Randomized path planning for a rigid body based on hardware accelerated Voronoi sampling. *Proceedings of the 4th Workshop on Algorithmic Foundations of Robotics (WAFR)*, Hanover, NH, March 16–18.
- Press, W. H., Teukolsky, S. A., Vetterling, W. T., and Flannery, B. P. 2002. *Numerical Recipes in C++: The Art of Scientific Computing*, 2nd edition, Cambridge University Press, Cambridge.
- Rimon, E. 1997. Construction of C-space roadmaps from local sensory data. What should the sensors look for? *Algorithmica* 17(4):357–379.
- Sharir, M. 1997. Algorithmic motion planning. *Handbook of Discrete and Computational Geometry*, J. E. Goodman and J. O'Rourke, editors, CRC Press, Boca Raton, FL, pp. 733–754.
- Thorpe, J. A. 1979. *Elementary Topics in Differential Geometry*, Springer-Verlag, Berlin.
- Wilmarth, S. A., Amato, N. M., and Stiller, P. F. 1999. Motion planning for a rigid body using random networks on the medial axis of the free space. *Proceedings of the 15th Annual ACM Symposium on Computational Geometry*, Miami Beach, FL, June, pp. 173–180.
- Yu, Y. and Gupta, K. 1999. On sensor-based roadmap: a framework for motion planning for a manipulator arm in unknown environment. *Proceedings of the IEEE/RSJ International Conference on Intelligent Robotics and Systems*, Kyongju, Korea, pp. 1919–1924.